

Instabilities in crystal growth by atomic or molecular beams

Paolo Politi ^{a,b,c,d,*}, Geneviève Grenet^{e,†}, Alain Marty ^{d,‡}, Anne Ponchet ^{f,§}, Jacques Villain ^{b,c,g,**}

^a *Fachbereich Physik, Universität GH Essen, 45117 Essen, Germany*

^b *Dipartimento di Fisica dell'Università degli Studi di Firenze and Sezione INFN, L.go E. Fermi 2, 50125 Florence, Italy*

^c *Centre de Recherches sur les Très Basses Températures, CRTBT-CNRS, BP-166 38042 Grenoble Cedex 9, France*

^d *CEA, Département de Recherche Fondamentale sur la Matière Condensée, SPMM/NM, 38054 Grenoble Cedex 9, France*

^e *LEAME, Ecole Centrale de Lyon, 36 avenue Guy-de-Collongue. B.P. 163 - F69131 Ecully Cedex, France*

^f *CEMES-CNRS 29 rue Jeanne Marvig BP 4347 31055 Toulouse-Cedex 04, France*

^g *CEA, Département de Recherche Fondamentale sur la Matière Condensée, SPSMS, 38054 Grenoble Cedex 9, France*

(November 26, 2024)

When growing a crystal, a planar front is desired for most of the applications. This plane shape is often destroyed by instabilities of various types. In the case of growth from a condensed phase, the most frequent instabilities are *diffusion instabilities*, which have been studied in detail by many authors and will be but briefly discussed in simple terms in chapter II. The present review is mainly devoted to instabilities which arise in ballistic growth, especially Molecular Beam Epitaxy (MBE). The reasons of the instabilities can be geometric, but they are mostly *kinetic* (when the desired state cannot be reached because of a lack of time) or *thermodynamic* (when the desired state is unstable). The kinetic instabilities which will be studied in detail in chapters IV and V result from the fact that adatoms diffusing on a surface do not easily cross steps (Ehrlich-Schwoebel or ES effect). When the growth front is a high symmetry surface, the ES effect produces mounds which often coarsen in time according to power laws. When the growth front is a stepped surface, the ES effect initially produces a meandering of the steps, which eventually may also give rise to mounds. Kinetic instabilities can usually be avoided by raising the temperature, but this favours thermodynamic instabilities of the thermodynamically unstable materials (quantum wells, multilayers ...) which are usually prepared by MBE or similar techniques. The attention will be focussed on thermodynamic instabilities which result from slightly different lattice constants a and $a + \delta a$ of the substrate and the adsorbate. They can take the following forms. i) Formation of misfit dislocations, whose geometry, mechanics and kinetics are analyzed in detail in chapter VIII. ii) Formation of isolated epitaxial clusters which, at least in their earliest form, are 'coherent' with the substrate, i.e. dislocation-free (chapter X). iii) Wavy deformation of the surface, which is presumably the incipient stage of (ii) (chapter IX). The theories and the experiments are critically reviewed and their comparison is qualitatively satisfactory although some important questions have not yet received a complete answer. Short chapters are devoted to shadowing instabilities, twinning and stacking faults, as well as the effect of surfactants.

PACS codes:

81.15.Hi Molecular, atomic, ion, and chemical beam epitaxy.

81.10.Aj Theory and models of crystal growth.

Keywords: MBE (Molecular Beam Epitaxy); Instability; Crystal growth.

*Corresponding author. E-mail: politip@fi.infn.it

†E-mail: genevieve.grenet@ec-lyon.fr

‡E-mail: amarty@cea.fr

§E-mail: ponchet@cemes.fr

**E-mail: villain@drfmc.ceng.cea.fr

Contents

I	Growth, surface roughness and instabilities	4
A	Growth instabilities	4
B	Thermal roughness and roughening transition	5
II	Snowflakes, diffusion instabilities and DLA	6
III	Growth from diluted vapour and MBE	7
A	MBE, what is that?	7
B	MBE of metals	8
C	III-V compounds	8
D	MBE, why?	9
E	Instabilities	9
IV	The Ehrlich-Schwoebel instability on a high symmetry surface	10
A	Introduction	10
B	Continuum description of the surface	10
C	Different sources of noise	11
D	The surface current \vec{j}	12
1	The Ehrlich-Schwoebel current	13
2	Mullins-type current	15
3	Symmetry breaking current	17
E	Experimental results	18
F	Continuum theory of the instability	19
1	One dimensional models	19
2	Two-dimensional models	22
3	Symmetry-breaking terms	24
4	Constantly increasing slope	25
5	The Zeno model and the need of a nonlocal evolution equation	25
G	Monte Carlo simulations	25
V	Kinetic instabilities of vicinal surfaces	26
A	Introduction	26
B	Single step: linear stability analysis	27
C	Linear analysis for a train of steps	30
D	Single step: weakly nonlinear analysis	31
E	Nonlinear analysis for a train of steps	32
F	Continuum description and step flow	33
G	Step flow and nucleation	34
VI	Shadowing instabilities	35
VII	Wetting and non-wetting	35
VIII	Coherent and incoherent epitaxy: misfit dislocations and critical thickness	36
A	Misfit dislocations	37
B	Critical thickness	38
C	Nucleation of a dislocation at the growing surface	40
D	Relaxation by an array of dislocations	41
E	Blocking mechanism	43
IX	The Asaro-Tiller-Grinfeld instability and related phenomena	44
A	Three-dimensional clusters as an alternative to misfit dislocations	44
1	Experimental facts	44
2	Energetics	45
3	Kinetics	45
4	Singular and non-singular orientations	46

B	The Asaro-Tiller-Grinfeld instability: thermodynamics	46
C	The Asaro-Tiller-Grinfeld instability: kinetics	48
1	Classical theory near equilibrium	48
2	High symmetry surfaces and MBE growth	50
D	Experiments	52
E	Effect of the adsorbate thickness	53
F	Solid-solid interfaces and other generalizations	54
X	Thermodynamics of an epitaxial, coherent cluster	55
A	Energy of a cluster	55
B	Capillary energy of a cluster	55
C	Scaling laws for the elastic free energy of a cluster	56
D	Case of a thin cluster: Tersoff approximation	57
E	Equilibrium shape of a coherent cluster: 2d-3d transition	58
F	More ambitious treatments	59
G	Experiments	60
XI	Formation and evolution of a population of clusters	60
A	The three stages	60
B	When a monolayer starts growing	61
C	Elasticity and the 2d-3d transition	62
D	Annealing of a population of incoherent clusters in the absence of growth: the Lifshitz-Slyozov mechanism	62
E	Experiments	63
F	Open questions	64
XII	Stacking faults and twins	65
XIII	Effect of additives (surfactants)	66
XIV	Conclusion	67
	APPENDIXES	69
A	List of Symbols	69
B	The diffusion length and the nucleation lengths	69
C	Qualitative considerations on the coarsening exponent	71
D	Nonlinear analysis of the dynamics of a single step, in the presence of step-edge barriers	72
1	Dimensionless equation	72
2	Differential equation and boundary conditions at different orders	73
E	Scaling laws for coherent epitaxial clusters	74
1	Scaling of the elastic free energy of a cluster with respect to the misfit	74
2	Scaling of the elastic free energy of a cluster with respect to its volume V	75
3	Scaling of the strain at long distance \vec{r} of a cluster as a function of its volume V	75
4	Scaling of the strain at long distance \vec{r} a cluster as a function of r	76
5	Elastic interactions at long distance \vec{r} between clusters or adatoms	76

I. GROWTH, SURFACE ROUGHNESS AND INSTABILITIES

A. Growth instabilities

Crystals are known to be the stable form at low temperature of all materials, except helium under moderate pressure.

Nevertheless, most of the natural materials which surround us are not crystals or are made of very small crystals. This fact shows that crystals do not easily grow. The reason is that growing crystals are subject to *instabilities* which introduce crystal defects and eventually result in the formation of polycrystals or even amorphous materials.

On the other hand, crystals are of great technological interest, because they have reproducible properties. Semiconductor technology uses large quantities of big crystals of silicon which are artificially pulled from the liquid phase and which are perfect. This has only been possible because the mechanism of instabilities in this type of growth was well understood. Even so, in the case of *metals*, it is impossible to avoid the formation of a few dislocations in a macroscopic crystal. The case of semiconducting elements (e.g. Si), which can be prepared as ideal crystals, is exceptional. These elements, even though they can be modified by implantation of appropriately chosen impurities, are not sufficient for all technological requirements. Quantum wells, for instance, are made of a slice of a material *A*, of well-defined thickness, sandwiched between two slices of a material *S*. A usual case is $A=\text{GaAs}$ and $S=\text{GaAlAs}$. One of the standard techniques to do that is Molecular Beam Epitaxy (MBE) [1].

The word *epitaxy* designates the adsorption of a crystal on another crystal, with a well-defined relative orientation of the two crystals. In most of the examples cited in the present review, both crystals are cubic and their principal axes are parallel.

In MBE, the atoms are ballistically deposited by a beam of molecules or atoms. The required thickness is obtained by switching the beam of material *S* during an appropriate time. If the atoms do not stick at once, they are sucked out by a vacuum pump, so that one can for instance deposit n layers of AlAs, then m layers of GaAs and avoid the formation of a GaAlAs mixture.

MBE is a very slow technique, which has the advantage to permit the production of artificial devices which could not be produced by other methods. Other examples are *multilayers* (Fig. 1) or ‘superlattices’ which are appropriate for fundamental research because they are periodic and therefore have, for instance, a simple diffraction spectrum. These materials are generally not thermodynamically stable but can be metastable during a very long time once they have been prepared.

Growth by ballistic deposition, as well as from the melt or a solution, is subject to instabilities. These instabilities generally appear at the place where the dynamics is fastest, i.e. the surface. The initial stage of the instability is a deformation of the growing surface (or ‘front’) which ceases to be planar and starts forming bumps or holes. Growth instabilities may be classified as follows (Fig. 2):

i) Diffusion instabilities (Fig. 2a) are typical of growth from the melt or from a solution. In a supersaturated solution, dendrites can form because diffusing atoms or molecules tend to go to the nearest point of the solid, and therefore to tips which unavoidably form at the growth front.

ii) Kinetic instabilities (Fig. 2b) which take place because the growth is too fast and the surface has no time to find its equilibrium shape, which in the simplest case is a chemically homogeneous plane.

iii) Thermodynamic instabilities (Fig. 2c) which take place when one tries to make a thermodynamically unstable material.

iv) Geometric instabilities. A typical example is the shadowing instability which occurs in oblique deposition (Fig. 2d).

Diffusion instabilities have been studied in many articles and review papers. For this reason, only a few words will be said about them in chapter II, and the present review will mainly be devoted to the other types of instabilities. One might think that diffusion instabilities do not arise in ballistic deposition and in particular in MBE. However, diffusion does occur *on* the surface and is responsible for instabilities as will be seen in chapter V.

A special type of kinetic instability will be investigated in great detail in chapters IV and V. It occurs when atoms diffusing on the surface have difficulties to cross steps. Presumably, the reason of its popularity among theorists is that this instability is consistent with the so-called S.O.S. model, a model in which the topology of the solid is fixed, atoms are assumed to pile up on preexisting lattice sites. Other instabilities, e.g. stacking faults, are not so easy to describe by a simple model.

Thermodynamic instabilities often result from a difference in the lattice constants of different materials which one tries to assemble in a single crystal. If the lattice constants of the substrate and the adsorbate are a and $a + \delta a$, then $\delta a/a$ is called (relative) ‘misfit’ or ‘mismatch’. It will play an important role in chapters VIII, IX and X where this instability will be studied. Another cause of thermodynamic instability may be of chemical nature. A typical example is the solidification of an eutectic solution, which by definition leads to coexisting clusters of two chemically different

alloys. The cluster size is determined by atomic motion on and near the growth front, and is related to the shape of a front, which becomes more or less complex and typical of a growth instability [2].

Strictly speaking, thermodynamic instabilities do not appear only during growth. However, in practice, they mainly appear at high enough temperature, and in particular, during growth, while the evolution of a solid toward equilibrium at room temperature is often geologically slow.

The shadowing instability will be much more briefly addressed in chapter VI, as well as kinetic instabilities resulting from stacking faults and polymorphism, which will be treated in chapter XII. The very unequal length of the various chapters corresponds partly to the unequal competence of the authors, partly to a different state of the art. In cases which are still poorly understood, we shall mainly give references, essentially experimental ones.

In the case of non-crystalline materials, the bumps and holes which are formed at the surface are macroscopic. In the case of crystals, which is of interest in this review, the modulation of the surface may be microscopic. It is generally the case, for instance, when dislocations are formed. Dislocation formation, which may be in competition with other types of instabilities, will be addressed in chapter VIII.

Instabilities are often characterized by a sudden burst. Before the instability takes place, the surface is smooth. Then, suddenly, an instability develops and its amplitude increases dramatically for short times, for instance exponentially with time. This fast initial increase gives no information on the final state of the system, which may be a spatially periodic modulation, or a general collapse, or chaotic. Only in the case of a sharp initial increase of the perturbation the word ‘instability’ will be used. It will not be used for instance if the fluctuation amplitude $\delta h(t)$ of the surface increases as a power of the time t , $\delta h(t) \simeq t^{1/z}$. In the latter case, we will just say that the surface is ‘rough’.

B. Thermal roughness and roughening transition

A rough surface, with a roughness which increases in time, is frequently predicted for a growing object [3–5] when the growth rate undergoes stochastic fluctuations, as is usually the case. But even at thermal equilibrium, i.e. in the absence of growth, the surface of a crystal can be rough. Although the minimization of the surface (or ‘capillary’) energy corresponds to a plane surface, thermal fluctuations can produce some ‘roughness’. At low temperature, this roughness has only a microscopic scale, and the surface is said to be ‘smooth’. The roughness becomes macroscopic, and the surface is then said to be ‘rough’, above the so-called roughening temperature T_R which depends very much on the surface orientation [3–5]. High symmetry surfaces, (001) or (111), of fcc metals are smooth until very near the melting temperature, while high index surfaces, e.g. (1,1,11), have very low roughening temperatures which cannot be observed because thermodynamic equilibrium cannot be reached [4]. But thermal roughening can be observed on (113) or (110) metal surfaces. High symmetry surfaces of semiconductors are also believed to be smooth at equilibrium until very high temperatures, higher than those used for MBE.

Elasticity is generally ignored in theoretical treatments of the roughening transitions which have been reviewed for instance by Nozières [3], Pimpinelli & Villain [4], Barabási & Stanley [5]. Some properties of crystal surfaces above and below T_R are summarized in table I. An important property, which will be of interest in chapter IX, is that the energy of a plane surface, which above T_R is an analytic function of its orientation, becomes non analytic below T_R . In the case of a high symmetry surface, this is a consequence of the positive step free energy per unit length γ : if the surface is disoriented by an angle θ , the energy cost is the product of γ by the number of steps, which is proportional to $|\theta|$, which is a non analytic function for $\theta = 0$. Such a surface with a non-analytic dependence on the orientation is called *singular*. Similarly, a height modulation of wavelength $2\pi/q$ (see chapter IX) is an analytic function of q for $T > T_R$ and non-analytic for $T < T_R$.

Another property of a smooth, infinite, high symmetry crystal surface at equilibrium is that its height cannot change continuously. Indeed a continuous change requires the creation of an infinitely long step which has an infinite energy. On the contrary, the height of a rough surface can change continuously without paying any free energy through a motion of the steps. A precise, renormalisation group description has been given by Tang & Nattermann [6].

The experimental determination of T_R is not always easy [4]. The safest method uses the equilibrium shape of crystals. The presence of facets of a particular orientation at a temperature T indicates that $T_R > T$ for this orientation. Unfortunately, this method is only applicable if T_R is pretty close to the melting temperature T_M . For instance, for Si, where $T_M = 1413^\circ\text{C}$ Heyraud et al. [7] have very recently found $T_R = 1370^\circ\text{C}$ for the {110} face, $T_R = 1340^\circ\text{C}$ for the {113} face, and $T_R > 1400^\circ\text{C}$ for the {111} face and add: “The case of {001} is much less clear, and is left to a future paper ...”. This sentence which reflects the hope of a better future also reflects our present ignorance of thermodynamic properties of the most common surfaces.

To conclude this paragraph on roughness, one can say that a ‘rough’ surface, as the man in the street would call it, can originate i) either from stochastic fluctuations or ii) from an instability. In the latter case, the mathematical

description is provided by deterministic equations of motion. In the first case, the stochastic fluctuations can be either thermal fluctuations at equilibrium, or for instance the fluctuations of the beam in MBE (the so-called ‘shot noise’). The mathematical description of beam fluctuations requires the introduction of a stochastic term in the equations, while thermal fluctuations are just taken into account by the Boltzmann factor in Gibbs’s canonical distribution. We prefer to restrict the use of the word ‘roughness’ to that which arises from stochastic effects, and to use the expression ‘instability’ when the roughness arises from a deterministic mechanism. Some references to stochastic effects will be made in the next chapters, but most of the present review will be devoted to instabilities.

II. SNOWFLAKES, DIFFUSION INSTABILITIES AND DLA

The goal of this chapter is to give an intuitive introduction to diffusion instabilities. The mathematical treatment will be found in review papers and books [9–13].

A crystal growing from a dense phase often forms ‘dendrites’. Snowflakes (Fig. 3b) are the most familiar example. However, their formation in clouds is a complicated process [8], since clouds are made of supercooled liquid droplets coexisting with solid particles and water molecules which travel from the former to the latter. It is simpler to consider growth from a homogeneous phase, e.g. a solution. As an example, Fig. 4b shows a pattern which has a resemblance to a snowflake. It is not a crystal, but similar instabilities arise in crystals growth as well. Diffusion instabilities arise (Fig. 3a) because, for some reason (e.g. thermal fluctuations) small protruding parts appear. If there are protruding parts, the molecules which diffuse through the solution to the solid surface go preferably to those parts (Fig. 3a) because paths leading to protruding parts are on the average shorter. Thus, protruding parts become more protruding and form dendrites.

This mechanism can be implemented by simulations. In the simplest model (‘Diffusion limited aggregation’ or DLA [14,15]) molecules are assumed to be independent in the fluid phase. They diffuse randomly from a very large distance, and stop moving as soon as they meet the solid. This model gives rise to very irregular shapes (Fig. 4).

The striking difference between the irregular cluster of Fig. 4 and the fairly regular shape of snowflakes is partly due to the hexagonal symmetry of ice crystals. Another factor which favours order is the possibility of atom diffusion along the solid surface, which is ignored in DLA. It is important in the case of snow, and according to Mason [16] surface diffusion is the reason of certain shape transitions of snow with temperature. Finally, interactions between atoms, which are neglected in the DLA model, make growth more deterministic. An extreme case is growth from the melt. Since the fluid is almost incompressible, the above picture, based on matter diffusion, is not valid. Actually, the quantity which diffuses, at least in a pure melt, is not matter, but energy. The equation which represents energy diffusion in the liquid, or matter diffusion in a vapour (or in a solution) is the diffusion equation

$$\partial\rho/\partial t = D\nabla^2\rho \quad (1)$$

where $\rho(\vec{r}, t)$ is the density of energy in one case, of matter in the other case. A third case of interest is solidification from an impure melt. Then the relevant diffusing quantity is the density of impurities, whose diffusion is much slower than energy diffusion. The relevant process is the slowest one.

Equation (1) must be coupled with appropriate boundary conditions at the interface, which is assumed to be a continuous surface [11–13,17,18]. If one wishes to model ‘directional solidification’ (the usual way to pull a crystal from the melt, e.g. silicon) the initial condition is a plane surface. If the pulling velocity is low enough, the surface remains a plane. For a given temperature gradient, the instability sets in [17] if the pulling velocity v is larger than a critical value v_c . It is called the *Mullins-Sekerka instability*. If v is not too large, the ultimate state of the surface is a periodic modulation [11–13,17] (Fig. 3c). The contrast between this smooth pattern and the DLA pattern of Fig. 4 is striking.

The DLA cluster is indeed a *fractal* [19]. This means that the relation between its radius R and its mass M is not $M = \text{Const} \times R^d$, where $d = 3$ is the dimension of the space, but (for large R)

$$M = \text{Const} \times R^{d_f} \quad (2)$$

where d_f is called an ‘effective fractal dimension’ [20]. Usually, it is not an integer and is smaller than the space dimension d , which is generally $d = 3$ in real materials although simulations are often made in $d = 2$ since they are easier. In two-dimensional DLA [20], d_f is close to 1.7. The radius R can be defined at any time as the distance from the center such that a diffusing atom has a probability lower than a certain value (e.g. 0.1) to reach it.

One can wonder whether continuous theories based on (1) can also produce a fractal. To our knowledge, there is no clear theoretical answer, but Arneodo et al. [21] performed experiments which can reasonably be described by continuous models and were able to produce fractal objects quite analogous to DLA clusters [21].

The various patterns which arise from diffusive instabilities result from differences in the details. For instance, in directional solidification there is a temperature gradient which has an important stabilizing effect and has no equivalent in the experiments of Arneodo et al. [21] which, as reported above, yield fractal objects. However, the onset of the instability results from equations which, for a given initial condition (e.g. a plane front $z = vt$) are very similar in all the cases. At the beginning of the instability, the deviation $\delta z(x, y, t)$ from the planar shape is indeed very small and the equations can be linearized with respect to $\delta z(x, y, t)$. A Fourier transformation in the (x, y) space yields $dz_k(t)/dt = \omega_k z_k$, where the coefficients ω_k depend on the model, and there is an instability if at least one of them is positive. This method is called a ‘*linear stability analysis*’. It is sufficient to prove that a plane front is unstable, but does not predict the shape of the resulting dendrites which can only be deduced from a nonlinear treatment.

Before leaving diffusion instabilities, we come back to snow. The formation of snow crystals in clouds proceeds in three steps [8]: i) Heterogeneous nucleation of an ice particle by deposition from the vapour phase on an impurity called ‘ice nucleus’ or by nucleation in a supercooled water droplet by an ice nucleus. ii) Growth of the ice particle by deposition of water molecules evaporated from liquid droplets and diffusing through the vapour phase, until the diameter reaches about 0.2 mm. iii) Growth by sticking of supercooled liquid water droplets on the ice particle or by aggregation of ice particles. Examples of ice nuclei are small crystals of AgI. The typical diameter of a water droplet in a cloud is between 10 and 100 μm . Although diffusion plays a part in these processes, the simple scheme of a diffusion instability is not applicable.

In view of the considerable amount of work devoted to diffusion instabilities, nothing more will be said about this topic in the present review. Instead, we shall describe instabilities which arise when the atoms do not diffuse toward the crystal, but travel ‘ballistically’, i.e. without collisions, from a source, and then form epitaxial layers.

We have nevertheless devoted this short chapter to diffusion instabilities for several reasons. First, for the completeness of this review on growth instabilities. Second, instabilities which arise from diffusion on the moving front will be encountered in chapter V. Third, the methods which are useful to investigate diffusion instabilities can often be used also for other instabilities. For instance, linear stability analysis will be used in parts IV, V and IX B.

III. GROWTH FROM DILUTED VAPOUR AND MBE

A. MBE, what is that?

The remainder of this review is devoted to techniques where the deposition is ballistic rather than diffusive, so that no instability can arise from diffusion in the fluid phase. Apart from the short chapter VI, the attention will be concentrated on Molecular Beam Epitaxy (MBE) and similar techniques.

Among all the advanced semiconductor growth techniques, Molecular Beam Epitaxy provides the greatest ease of growing complex semiconductor multilayer structures with a precise control of the thickness (up to the monolayer scale accuracy), the composition and the doping of the involved layers [22]. In this technique, growth proceeds under ultrahigh vacuum conditions (pressures $\leq 10^{-8}$ Pascals) by the condensation of thermal energy molecular beams on an underlying single crystal substrate. The substrate has a strong influence on the growth. Generally, the deposited film adopts as far as possible the orientation and crystallographic characteristics of the substrate. As a matter of fact, when thermal atoms or molecules arrive on a substrate, they diffuse until they reach an adequate crystallographic site where they can be incorporated (see Fig. 5). One can distinguish two main cases. i) On singular surfaces, atoms or molecules can meet each other and aggregate to form two-dimensional nuclei. Then, these two-dimensional nuclei grow by incorporating further atoms or molecules and finally coalesce to form new epilayers. This growth mode called ‘two-dimensional nucleation growth mode’ can be monitored in-situ on an atomic scale by Reflection High Energy Electron Diffraction (RHEED) intensity oscillations. A RHEED intensity maximum corresponds to a single atomic or molecular layer completion because it is the surface roughness minimum. ii) On vicinal surfaces (see definition in chapter V), this growth mode can only exist if the terraces are large enough with respect to the diffusion length ℓ_D (see App. B). Otherwise, atoms and molecules are incorporated at existing steps, whose forward motion results in the growth of the crystal. This second growth mode is called ‘step flow’. In both cases, most of the incorporation sites are supplied by steps which result either from two-dimensional nuclei edges or from vicinal surface steps and their number and distribution are important features of the growth front.

MBE growth can be influenced by many parameters, e.g. the incident beam rates which determine the relative concentration of adatoms at the growth front, the adatom re-evaporation rates, the substrate temperature which determines the adatom migration velocity but also the surface chemical and/or structural properties such as roughness, composition or surface reconstruction.

B. MBE of metals

The case of metals is conceptually the simplest. The naive representation of atoms as hard spheres is not too bad, and the surface is in many cases not reconstructed.

Thin metallic layers and multilayers of pure elements or alloys are interesting in several respects: magnetic properties, mechanical and elastic anomalous behaviour [23], enhanced catalytic properties [24]. A great deal of attention has been devoted in recent years to magnetic properties of metallic thin layers and multilayers. Among them, Giant Magneto-Resistance and Perpendicular Magnetic Anisotropy may lead to technological improvement of the magnetic recording techniques. The possibility of a Perpendicular Magnetic Anisotropy as a consequence of the reduced symmetry, was first pointed out by Néel. Strong experimental evidence for this anisotropy was found by Gradmann's group [25]. In multilayers, composed of magnetic and non-magnetic metals, interface anisotropy is expected, too [26]. The magneto-elastic effect, which involves the same fundamental energy, i.e. the spin-orbit coupling, may be the leading factor [27]. Strong magneto-crystalline anisotropy has also been observed in metallic alloys layers grown by sputtering or Molecular Beam Epitaxy when an anisotropic structure is obtained with the easy magnetic axis perpendicular to the layer (hexagonal, tetragonal, etc.) [28,29]. It has also been shown that antiferromagnetic coupling may occur between magnetic layers through non-magnetic layers, and the magnitude of this effect oscillates with the non-magnetic layer thickness [30]. This magnetic coupling gives rise to Giant Magneto-Resistance [31]. The occurrence and magnitude of these properties depend dramatically on the quality (roughness, etc.) of the layer. The instability of the growing front may alter this quality.

C. III-V compounds

In the remainder of this chapter, attention will be focussed on III-V semiconductors which have been most extensively studied because of their technological interest. In this case, the substrate temperature and the V-III ratio are chosen in such a way that the growth rate is controlled by the group-III element incorporation rate (close to one), the group-V element being incorporated only if chemically reacting with group III-elements. Thus, increasing the group-III element deposition rate increases the growth velocity. On the other hand an increase of the V-element beam rate decreases the surface diffusion constant. In this case, the choice of a particular V/III ratio associated with a particular substrate temperature corresponds to the choice of particular growth kinetics. Since the group V element evaporates when it is not at once incorporated, the MBE growth of III-V compounds can be described with a reasonable approximation by models in which a atoms of a single species are considered [22,32–34]. This species is the group III element, whose deposition and diffusion on the surface determines the growth rate and the type of growth. Such models will be used in the following chapters and are applicable to GaAs, for instance, if the word ‘atom’ is everywhere replaced by ‘Ga atom’. However, one has to be careful when using this approximation. For instance, as noted by Tersoff et al. [35] the temperature dependence of the Ga adatom density ρ_0 at equilibrium is not given, as it would be in a one-component system, by

$$\rho_0 = a^{-2} e^{-\beta W_0} \quad (3)$$

where a^2 is the area per atom and W_0 a constant. The reason is the following: terraces contain an equal number of Ga and As atoms, while Ga adatoms move presumably alone, without the company of an As atom. Therefore, if a Ga adatom is released from a terrace, a consequence is (apart from the energy cost) the release of an As atom from the same terrace into the vapour. Therefore, there is an entropy gain which modifies W_0 by a temperature-dependent amount. Treating the As vapour as an ideal gas, Tersoff et al. [35] obtain

$$\rho_0 = a^{-2} (P/P_0)^{-1/m} e^{-\beta W'_0} \quad (4)$$

where W'_0 is a constant, P is the As pressure, $m = 2$ for the diatomic vapour As_2 , and [4]

$$P_0(T) = \sqrt{\frac{M^3 (k_B T)^5}{2\pi^3 \hbar^6}} \quad (5)$$

where M is the mass of the molecules of the vapour (150 times the proton mass in the case of As_2). Thus, if (4) is replaced by (3) in a single component model, W_0 depends on temperature. For the values used by Tersoff et al. ($T = 850$ K and $P = 10^{-4}$ Pascals) formula (5) yields $(P/P_0)^{-1/m} \approx 10^9$, a remarkably large value. If, instead of being at equilibrium, the system is subject to MBE growth, an effective pressure can be defined [35] as “that pressure which would give the same As desorption rate in equilibrium as actually occurs”. Experimentally, Tersoff et al. find a factor 10^{15} unfortunately far from the above mentioned factor 10^9 .

D. MBE, why?

The merit of MBE is the possibility to prepare a wide range of III-V semiconductor materials¹, with tailor-made lattice constants or electronic properties. For instance, in a ternary compound $A_xB_{1-x}C$, the choice of x allows for tuning the lattice constant so as to make possible epitaxy on a given substrate. Instead of the lattice constant, one can tune the electronic band-gap in order to obtain the desired optic or electronic properties. Examples are provided by the ternary compounds with $A=As$, $B=P$ and $C=Ga$. Pure GaAs ($x = 1$) has a direct band gap in the infrared, while GaP an indirect band gap in the green, and their mixture $GaAs_{0.6}P_{0.4}$ has a direct band gap emitting in the red. This film growth technique provides thus a flexible and powerful tool to select a particular wavelength by choosing the alloy composition (see Fig. 6) and/or to engineer the band structure by growing layers of predetermined and well controlled alloy composition.

These materials (binary compounds or alloys) can be combined in single or multilayer ‘heterostructures’ made of different semi-conductors which have different electronic properties (e.g. band gap energy) but closely matching lattice parameters.

The simplest heterostructures are quantum wells, which are used in optoelectronics and constitute the active zone of optoelectronic devices (lasers or optical amplifiers). In a quantum well, the charge carriers (electrons and holes) are confined between two planes (see Fig. 9a). Examples of materials appropriate to make a quantum well are $Ga_{1-x}In_xAs$ and $Al_{1-x}In_xAs$. These two alloys are lattice-matched on an InP substrate for $x = 0.53$ and $x = 0.52$, respectively, but their band gap energy varies from 0.76eV ($1.65\mu m$) for GaInAs to 1.46eV ($0.85\mu m$) for AlInAs.

These quantum wells themselves can be organized in complex superlattices. It should be noted that band discontinuity resulting from the alignment of different band structures can induce another kind of interesting carrier confinement: the junction often includes a step and a notch in the valence or the conduction bands. A typical example is the heterojunction between highly n-type AlGaAs and lightly doped GaAs (Fig. 9b). For most technological applications, the important point is to make perfect interfaces between materials free of structural or chemical defects. However, it is actually a difficult task because of the surface segregation [36] of the binary with the lower surface energy which acts against the chemical abruptness of the interface.

E. Instabilities

MBE allows to make chemically unstable alloys. This challenge to chemistry is not free from any danger. The most usual danger is a ‘chemical instability’, i.e. composition modulations (alternating AC rich and BC rich domains) appear during the growth, either parallel or perpendicular to the growth plane. As an example, Fig. 7 shows the surface of unstable alloys of composition close to $Al_{0.5}In_{0.5}As$, which are unstable and tend to decompose into two phases of composition close to AlAs and InAs.

From a technological point of view, a chemical instability leads to a non-uniformity of the band-gap and thus induces an undesirable broadening of the photoluminescence line width and a lowering of the electron mobility. But, on the other hand, the chemical instability of the alloy can be used to obtain spontaneous nanoscale strained structures (wires or dots) if correctly controlled. The deviation from randomness can also take the form of an ordered phase. Both composition modulation (Fig. 7) and long range ordering (Fig. 8), have been observed and sometimes they coexist in the same sample.

Once it has been grown, the bulk material can survive during centuries at room temperature, because bulk diffusion is very slow. In contrast, surface diffusion is pretty fast at the growth temperature, and must be so to ensure a good crystal quality.

Even in the absence of any chemical instability, a multilayer or a double layer can be unstable if the lattice constants of the pure materials are too different. When a semi-conductor is grown lattice-mismatched with the substrate, a thin pseudomorphic layer is expected to grow first uniformly and commensurably with the strain energy increasing linearly with thickness up to a critical threshold. Below this critical threshold which drastically depends on the growth conditions, a compressed or stretched pseudomorphic layer is obtained, with a modified band structure which can be useful for a wide range of practical applications. Beyond the threshold, dislocations or other types of instabilities usually appear.

¹II-VI semiconductors can also be prepared and are currently studied in laboratories, but their industrial use is not so wide as that of III-V materials.

While chemical instabilities will not be addressed in the remainder of this review, elastic instabilities will be studied in detail in chapters VIII and following.

IV. THE EHRLICH-SCHWOEBEL INSTABILITY ON A HIGH SYMMETRY SURFACE

A. Introduction

In the present chapter and in the next one we will give a description of kinetic instabilities occurring in homoepitaxial growth, due to the so-called Ehrlich-Schwoebel (ES) effect which makes the sticking process of an adatom to a step asymmetric. This effect was discovered thirty years ago by Ehrlich and Hudda [37], who observed –through a field ion microscopy technique– that tungsten atoms diffusing on a terrace were repelled by a descending step. It was shown by Schwobel and Shipsey [38] that this effect is stabilizing on a vicinal surface, while its destabilizing character for a high symmetry surface was pointed out by Villain only a few years ago [39].

For a quantitative analysis of this mechanism, microscopic details are extremely important: lattice structure, surface orientation, step orientation, sticking process. For example, Stoltze [40] has performed a detailed study of the surface energetics of several fcc metals, based on the effective medium theory. According to this work, an ES barrier exists for any surface and step orientation. The extra energy barrier is of the order of 100/300 meV (a fraction of the diffusion barrier on a flat surface) and it depends on the sticking process, which may take place through a hopping over the edge or through an exchange mechanism with an edge atom. The former is almost always favorable for the (100) and (111) surface orientations, while the latter prevails in several cases for the (110) orientation.

Ab initio calculations show that the ‘real’ picture may be even more complicated. For Al(111) –which has an extremely low diffusion barrier: 40 meV– Stumpf and Scheffler [41] have shown that the exchange process is favorable, but the extra energy barrier is very small, and perhaps smaller than the ‘long-range’ attraction energy between step and adatom. For Au(111) [42] the static barriers (at $T = 0\text{K}$) are fairly large and almost equal for the two mechanisms, but simulations at $T > 450\text{K}$ show that exchange does not require an extra energy.

The experimental picture is not universal. Field ion microscopy studies by Ehrlich and collaborators (see the paper [43] by Kyuno and Ehrlich and references therein) show that an adatom approaching a descending step may feel a step-edge trap rather than a step-edge barrier, which may reduce the diffusion bias (the up-hill current induced by the ES effect: see below).

Several authors [44] have proposed and/or performed an indirect evaluation of the additional step-edge barrier through the study of the nucleation rate on top of islands. The method is applied to metal epitaxy (Fe, Ag, Pt) and the results generally attest the existence of such a barrier. For instance, Morgenstern et al. [45] find a Schwobel barrier equal to $0.13 \pm 0.04\text{ eV}$ for Ag(111).

In contrast, the existence and the importance of step-edge barriers in semiconductor materials is a much more debated question. These barriers have been invoked to explain the roughening of Si(100) [46] before the crystal-amorphous transition; on the other side a recent and detailed study [47] of the growth of Si(111) shows a morphology which does not agree with the unstable evolution due to ES barriers. Nevertheless, some calculations [48] based on empirical potentials [49] do give a finite barrier even for the (111) orientation.

A surface evolution in agreement with step-edge barriers is found for Ge(001) [50,51], even if the barriers are evaluated to be fairly weak. Also for GaAs there is some evidence [32,52,53] supporting their existence.

The efficiency of the ES barrier clearly depends on the temperature: the ES instability –which hinders the attainment of the equilibrium– manifests itself at low T .

The name Ehrlich-Schwobel instability is generally used in relation to growth of a high symmetry surface: in this case it gives rise to the formation of three-dimensional structures rather than to a layer-by-layer growth. This instability is studied in the present chapter.

On a vicinal surface, where growth proceeds via step flow, the same microscopic mechanism (the ES effect) determines meandering of the steps, usually referred to as Bales-Zangwill (BZ) instability [54], which resembles the fingering instabilities discussed in chapter II. It will be studied in the next chapter.

B. Continuum description of the surface

The evolution of the surface shape may be attributed to two types of mechanisms. i) Deterministic ones, which tend for instance to reduce the free energy and to restore thermal equilibrium. ii) Stochastic processes related to the randomness of the deposition, of atom diffusion, of nucleation The stochastic part is usually called ‘noise’, in analogy with noise in electric circuits for instance, which is caused by a stochastic motion of electrons. Thus, if $z(\vec{x}, t)$

denotes the local height of the surface profile in $\vec{x} = (x, y)$, its temporal variation is expected to satisfy an equation of the form:

$$\partial_t z(\vec{x}, t) = \mathcal{A}(\{z\}) + \text{noise} \quad (6)$$

where $\mathcal{A}(\{z\})$ is a deterministic functional of $z(\vec{x}, t)$ and $\partial_t \equiv \partial/\partial t$.

If volume diffusion is neglected, the dynamics of the surface is governed by three microscopic processes: deposition, surface diffusion and desorption. By definition, surface diffusion conserves matter on the surface; deposition from the vapour phase is the source of new matter, but generally it is a process which does not depend on the surface profile: it contributes to the local velocity $\partial_t z$ through a term $F(\vec{x}, t) = F_0 + \delta F(\vec{x}, t)$. We can get rid of the average value F_0 by simply redefining the local height: $z(\vec{x}, t) \rightarrow (z(\vec{x}, t) - F_0 t)$, while $\delta F(\vec{x}, t)$ contributes to the noise. In some cases the deposition rate does depend on the surface profile, for example when the average flux impinges sideways upon the surface. This may give rise to shadowing instabilities, which will be discussed in Chap. VI. Another possibility is a rate of attachment of the impinging atom which depends on the local environment.

Finally, desorption can be important, especially in semiconductors, whose typical growth temperatures are higher than for metals. The description of a high symmetry surface will be worked out mainly under assumption that evaporation is negligible.

Once that matter is conserved on the surface, the next step is to assume that overhangs, voids and interstitials are not relevant, so that volume as well is conserved. If it is so, the functional $\mathcal{A}(\{z\})$ must be the divergence of the surface current and therefore:

$$\partial_t z(\vec{x}, t) = -\nabla \cdot \vec{j} + \text{noise} \quad (7)$$

where the current \vec{j} is a functional of the surface profile $z(\vec{x}, t)$, similarly to $\mathcal{A}(\{z\})$ in Eq. (6). An important question is whether \vec{j} is a local or nonlocal functional. In other words, is it sufficient to know the surface profile in \vec{x} ($z(\vec{x}, t), \nabla z, \nabla^2 z, \dots$) to determine the growth velocity $\partial_t z$, or is it determined by the surface profile in a finite space around \vec{x} ? In principle, epitaxial growth is not a local process, mainly because diffusion is not. In this sense, Eq. (7) must be understood as an equation which is valid on large space and time scales: space scales larger than the typical distance between steps and time scales larger than the filling time of one monolayer ($= 1/F_0$). Nevertheless, even so a nonlocal description may be necessary: we will come across one case later on.

Because of the translational invariance in the z -direction, the current \vec{j} as well as the quantity \mathcal{A} in the general case of non conserved volume, does not depend explicitly on $z(\vec{x}, t)$, but only on its derivatives. So, it may be useful to think of \vec{j} (or \mathcal{A}) as a functional of the local slope $\vec{m} = \nabla z$. By taking the gradient of (7), we obtain:

$$\partial_t \vec{m} = -\nabla(\nabla \cdot \vec{j}) + \nabla(\text{noise}) \quad (8)$$

$$= -\nabla^2 \vec{j} - \nabla \wedge (\nabla \wedge \vec{j}) + \nabla(\text{noise}) \quad (9)$$

In 1+1 dimensions the current and the slopes are scalar quantities and therefore the curl term in the right-hand-side disappears ($\partial_x \equiv \partial/\partial x$):

$$\partial_t m(x, t) = -\partial_x^2 j + \partial_x(\text{noise}) \quad (1 + 1 \text{ dim}) \quad (10)$$

If the current is derivable from some effective free energy \mathcal{F}

$$j(x, t) = -\frac{\delta \mathcal{F}}{\delta m} \quad (11)$$

the evolution equation for m may take or not the form of the Cahn-Hilliard [55] equation, depending on \mathcal{F} .

In 2+1 dimensions the curl term vanishes if the current is nonrotational: $\nabla \wedge \vec{j} = 0$. Since \vec{j} is a functional of \vec{m} and $\nabla \wedge \vec{m} = \nabla \wedge (\nabla z) \equiv 0$, the current is expected to be nonrotational only if it is linear in the slope, but this is generally true only in the earliest stages of growth, when $|\vec{m}| \ll 1$. Therefore $\nabla \wedge \vec{j} \neq 0$ as a rule. All the same, the evolution of the surface may have many similarities with a phase separation process (see chapter IV F 2).

C. Different sources of noise

Till now the possible sources of noise have not been indicated explicitly. In Molecular Beam Epitaxy there are three: i) Fluctuations in the incoming flux (the so-called shot noise); ii) Fluctuations in the diffusion current (conserved noise); iii) Fluctuations in the nucleation process of new islands.

The first two have been well studied in the context of several different models [4,5]: generally speaking, their effect is to roughen a surface which would be flat in the absence of noise. Here the typical situation we want to study is different: the surface is deterministically unstable and therefore the ‘deterministic roughness’ may overcome the stochastic one, induced by noise. Furthermore, if the dynamics resembles a phase separation process, noise is known to be an irrelevant parameter, at least in 2+1 dimensions. A second remark on shot noise is in order: roughness induced by shot noise is in part healed by surface diffusion. It is therefore important to understand on which time and length scales roughness is relevant. Here we report a qualitative argument due to Villain [39], which will also be used in the context of unstable growth of a high symmetry surface (see App. C).

The average number of atoms falling on a region of size ℓ during time t is: $\bar{N} = F_0 t \ell^d$ and its fluctuation due to a Gaussian shot noise is: $\Delta N \approx \sqrt{\bar{N}} = \sqrt{F_0 t \ell^d}$. Such ‘volume’ fluctuations determine a ‘height’ fluctuation $\Delta h = \Delta N / \ell^d \approx \sqrt{h / \ell^d}$, where $\bar{h} = F_0 t$ is the average number of deposited layers. The central question is: What is ℓ ? In the context of a surface which is deterministically stable, ℓ is the diffusion length ℓ_D (see App. B): diffusion is supposed to heal shot noise just on this scale. If $\ell_D \approx 10^2 \div 10^3$, in two dimensions we will have $\Delta h \approx 1$ after the deposition of $10^4 \div 10^6$ layers, which is quite a large value.

The contributions of shot noise and diffusion noise to Eq. (7) are generally written as $\delta F(\vec{x}, t)$ and $\eta_D(\vec{x}, t)$ respectively, with:

$$\langle \delta F(\vec{x}, t) \rangle = 0 \quad \langle \delta F(\vec{x}, t) \delta F(\vec{x}', t') \rangle = 2F_0 \delta(\vec{x} - \vec{x}') \delta(t - t') \quad (12)$$

$$\langle \eta_D(\vec{x}, t) \rangle = 0 \quad \langle \eta_D(\vec{x}, t) \eta_D(\vec{x}', t') \rangle = -2D \nabla^2 \delta(\vec{x} - \vec{x}') \delta(t - t') \quad (13)$$

where D is the surface diffusion constant.

Concerning nucleation, it is due to an encounter of two (or more) adatoms during the diffusion process. So, we might ask why nucleation noise is something different from diffusion noise. It is indeed possible to separate the two contributions in the following way: on a region of high slope, nucleation is almost negligible (see App. B), but diffusion noise still exists; conversely, in the continuum limit $a \rightarrow 0$ we will see that diffusion noise is negligible while nucleation noise survives.

A further feature which characterizes nucleation noise with respect to shot and diffusion noise is that for the latter ones it is clear the meaning of ‘absence of noise’. In other words, it is obvious which is the corresponding deterministic model: $\delta F(\vec{x}, t) \equiv 0$ and $\eta_D(\vec{x}, t) \equiv 0$. But which is the deterministic model of nucleation? We will show that even if a model can be proposed, it may give rise to a nonanalytic profile in the nucleation sites.

An important question is whether nucleation noise is enough to roughen the surface by itself. The answer, according to the works by Elkinani and Villain [56] and Wolf et al. [57], is ‘no’. Even more important, there is numerical evidence [58] that nucleation noise is able to heal surface defects at small length scales. However, a deeper analytical comprehension of nucleation noise would be necessary. Preliminary studies will be found in Refs. [57,59].

D. The surface current \vec{j}

This chapter addresses a problem which is common to several branches of physics: How to derive a continuum equation, valid at large length scales, starting from a microscopic and discrete point of view? Here the situation is particularly difficult because the surface is made up of two different microscopic objects –steps and adatoms– whose characteristic time scales are fairly different: if τ_{ad} is the typical diffusion time to a neighbouring site and τ_{step} is the time necessary to advance the step of one lattice constant, it is easily found that $\tau_{ad} \approx a^2/D$ and $\tau_{step} \approx 1/(F_0 \ell a^{d-1})$, where ℓ is the typical distance between steps. The condition $\tau_{step} \gg \tau_{ad}$ reads (we put $a = 1$) $\ell \ll (D/F_0) = \ell_D^{1/\delta}$, with $1/\delta > 2$ (see App. B). Since ℓ must be smaller than ℓ_D and $\ell_D \gg 1$, the above condition is certainly fulfilled. Therefore adatoms see stationary steps during their motion and steps feel adatoms only as an ‘average’ current: the Burton, Cabrera and Frank theory [60] of crystal growth is indeed based on this quasi-stationary hypothesis.

A possible approach to the problem of determining a continuum Langevin equation is to start from the microscopic rates for the single processes (deposition, diffusion, evaporation ...) in a solid-on-solid model and write down a master equation for the discrete variables h_i (the height of the i -th column in the SOS model). This procedure generally requires the truncation of an infinite hierarchy of equations to arrive to a set of discrete Langevin equations, one for each h_i ; afterwards, it is necessary to find a continuum limit in the space variables and this requires a regularization scheme for step functions. This method has been used by several authors: Plischke et al. [61] for Metropolis dynamics, Zangwill et al. [33], Vvedensky et al. [62] and more recently by Předota and Kotrla [63] for Arrhenius dynamics.

As pointed out by the same authors this approach suffers from important problems, the major one regarding the regularization scheme for the step function: no rigorous procedure exists, different schemes give different results and in the final results some coefficients entering in the regularization procedure which should depend on the flux F_0

remain undetermined. A critical discussion of the master equation approach in the case of equilibrium relaxational dynamics can be found in Ref. [64].

A completely different approach uses the method of Burton, Cabrera and Frank [60]: one writes the diffusion equation for adatoms on a given terrace and solves it with suitable boundary conditions at steps: this gives rise to a current of adatoms, from which step velocities can be evaluated. Once they are known, one can study numerically the evolution of the surface or one can try to obtain a continuum evolution equation through some ‘coarse graining’ procedure. This method is generally restricted to sufficiently large slopes: in fact it is not easy to introduce nucleation in this kind of approach.

Instead of giving further details on the different methods which can be employed to obtain some expression for \vec{j} , we prefer to introduce the different terms phenomenologically and justify them.

1. The Ehrlich-Schwoebel current

The first place clearly deserves the term which is responsible for the instability treated in the present chapter: the current induced by the Ehrlich-Schwoebel effect. Let us imagine a surface which has a pyramidal structure and therefore top, bottom and vicinal terraces (see Fig. 10).

Such a ‘three levels’ structure exists even in the *absence* of any step-edge barrier (see, for example, the simulations reported in Fig. 7a of Ref. [56]). If an ES barrier exists, it has a double effect: i) on a top terrace, since atoms are hindered from descending, the probability of nucleation is increased and this makes pyramids higher; ii) on a vicinal terrace, adatoms prefer sticking to the ascending step and therefore existing holes are not filled. Both effects destabilize the flat surface, giving rise to three-dimensional growth. From a continuum point of view, the above mechanisms give rise to a nonequilibrium current \vec{j}_{ES} which depends on the slope of the surface. This is of extreme importance, because all the other terms in the current will be seen to vanish on a surface of constant slope.

Let us start by considering a 1+1 dimensional surface, which is supposed to have a positive slope. On a terrace of size ℓ we solve the diffusion equation: $\partial_t \rho = F_0 + D \partial_x^2 \rho$ in the quasi-static approximation ($\partial_t \rho = 0$), which is justified by the relation $\tau_{step} \gg \tau_{ad}$. This gives $\rho(x) = A + Bx - (F_0/2D)x^2$, where constants A and B are determined through boundary conditions at steps in $x = \pm \ell/2$. Here, the sticking coefficients k_+ and k_- (respectively from the upper and lower terrace) are introduced: an infinite coefficient means that the adatom is automatically incorporated as it reaches the step, while a vanishing one means the adatom is unable to stick. The existence of a current \vec{j}_{ES} is due to an asymmetry between k_+ and k_- : in fact, such an asymmetry makes asymmetric the density of adatoms with respect to the center $x = 0$ of the terrace, i.e. $B \neq 0$. Since the microscopic current on the terrace is: $j_{mic} = -D \partial_x \rho = -D[B - (F_0/D)x]$, its average value is simply: $j_{ES} = \langle j_{mic} \rangle_{ter} = -DB$.

If the equilibrium density is neglected with respect to the density due to the external flux, boundary conditions read: $D \rho'(\pm \ell/2) = \pm k_{\mp} \rho(\pm \ell/2)$. In the simplifying hypothesis that $k_- = \infty$ we can introduce a single parameter, the so-called ES length: $\ell_{ES} = D/k_+$, and the boundary conditions read $\rho(\ell/2) = 0$ for the ascending step and $\rho'(-\ell/2) = -\rho(-\ell/2)/\ell_{ES}$ for the descending one. Under these conditions it is found that $B = -F_0 \ell_{ES} \ell / [2D(\ell_{ES} + \ell)]$ and therefore²

$$j_{ES} = \frac{F_0 \ell_{ES} m}{2(1 + |m| \ell_{ES})|m|} \quad (14)$$

The previous relation can be easily read in the two limiting cases of a strong ES effect ($\ell_{ES} \gg \ell$) and a weak one ($\ell_{ES} \ll \ell$). In the former case all the atoms falling on the terrace contribute to the current and therefore j_{ES} is proportional to ℓ and independent of ℓ_{ES} ; in the latter one, only the atoms falling within a distance ℓ_{ES} from the ascending step contribute to the current and j_{ES} is now proportional to ℓ_{ES} .

Eq. (14) is clearly not applicable in the limit $m \rightarrow 0$, because the relation $|m| = 1/\ell$ is valid as far as no nucleation takes place on the terrace itself. The simplest way to obtain the correct expression for any value of m is to observe that the current must vanish on the high symmetry orientation $m = 0$; so, it is expected to be linear at small slopes: $j_{ES} = \alpha m$ and the constant α is determined by matching the two expressions for $|m| \simeq 1/\ell_D$. This gives $\alpha = F_0 \ell_{ES} \ell_D / [2(1 + \ell_{ES}/\ell_D)]$. The simplest function interpolating between the two limiting expressions is:

$$j_{ES} = \frac{F_0 \ell_{ES} \ell_D m}{2(1 + \ell_{ES}/\ell_D + |m| \ell_{ES})(1 + |m| \ell_D)} \quad (15)$$

²In this chapter and in the following, z is the height divided by the monolayer thickness c , so that the slope m has the dimension of the reciprocal of a length.

which reads, for weak and strong step-edge barriers:

$$j_{ES} = \frac{F_0 \ell_{ES} \ell_D m}{2(1 + |m| \ell_{ES})(1 + |m| \ell_D)} \quad \ell_{ES} \ll \ell_D \quad (16)$$

$$j_{ES} = \frac{F_0 \ell_D^2 m}{2(1 + |m| \ell_D)^2} \quad \ell_{ES} \gg \ell_D \quad (17)$$

A more rigorous derivation of j_{ES} at small slopes is given in Ref. [58]: for $|m| < 1/\ell_D$ the surface is made up of a ‘sequence’ of top, bottom and vicinal terraces of typical width ℓ_D , whose average slope is just m : since vicinal terraces are the only ones to contribute both to the (average) slope and to the ES current, and both quantities are linear in the number of vicinal terraces in the ‘sequence’ under study, we conclude that the ES current and the slope must be proportional. This method gives the same expression as before for the constant α .

Before going on, let us comment on different methods for determining j_{ES} . In the spirit of the procedure just explained, we could modify the starting differential equation for the density ρ in order to take into account nucleation at *that* level. This procedure has been used by Myers-Beaghton and Vvedensky [34], who have introduced a term proportional to ρ^2 to simulate the formation of a dimer. In this case the diffusion equation reads: $F_0 + D\rho''(x) - \varsigma\rho^2(x) = 0$. This equation is not solvable in closed form, but in the limiting cases $\ell \rightarrow 0$ and $\ell \rightarrow \infty$ it displays [65] the same behaviour as before. In the limit $\ell \rightarrow 0$ this is obvious, since in such a limit the quadratic term is negligible.

We want to emphasize that two different lengths are relevant for the problem: the ES length ℓ_{ES} and the diffusion length ℓ_D . The latter one is generally defined as the typical distance between nucleation centers on a high symmetry surface (see App. B), and the value of ℓ_{ES} does not enter in ℓ_D . Nevertheless, when nucleation can take place on vicinal and/or top terraces, the ES barrier affects the adatom density and therefore the typical size of a vicinal or top terrace. It is possible [56,66] to introduce a ‘nucleation’ length ℓ_n for a vicinal terrace (ℓ_n^V) and for a top one (ℓ_n^T) (for a bottom one we simply have $\ell_n^B = \ell_D$): a new terrace nucleates on an old one when ℓ becomes of the order of ℓ_n . When $\ell_{ES} = 0$, $\ell_n^V = \ell_n^T = \ell_D$ and for a finite ES effect the nucleation lengths decrease (because the adatom density increases): ℓ_n^V has a weak dependence on ℓ_{ES} and $\ell_n^V(\ell_{ES} = \infty) = \ell_D/\sqrt{2}$ [66], while ℓ_n^T goes to zero when $\ell_{ES} \rightarrow \infty$ (see Fig. 44). Strictly speaking, the quantity ℓ_D in Eq. (15) should be replaced by ℓ_n^V , but we have just seen that $\ell_n^V \simeq \ell_D$ for any value of ℓ_{ES} . Because of this, the nucleation term (proportional to $\rho^2(x)$) in the diffusion equation can be neglected if $\ell \ll \ell_D$ whatever is the value of ℓ_{ES} : in this limit, Eq. (14) should be recovered.

Finally, we will mention the previously discussed ‘microscopic’ approach which makes use of the master equation: in the presence of step-edge barriers it gives [62] an ES current proportional to the slope, but no expression beyond the linear approximation is known so far. Nevertheless the expression for the proportionality coefficient α found by Vvedensky et al. [62] has the merit to clearly show that the ES current vanishes when detailed balance is satisfied. Our expression (15) trivially satisfies the detailed balance: since thermal detachment from step has been neglected there, it is sufficient that j_{ES} vanishes for $F_0 = 0$.

The expression we have found for j_{ES} has two main limits: it is valid in 1+1 dimensions and it does not take into account possible discrete effects in the z direction. For example, if we are still in one dimension and $m = 0$ means the high symmetry (10) orientation of a square lattice, then $m = 1/a$ necessarily means the (11) orientation, which is also of high symmetry. Does the ES current vanish as well on this orientation? If so, Eq. (15) is wrong because it only vanishes for $m = 0, \pm\infty$. The fact that $j_{ES}(\pm 1/a)$ should vanish is not obvious since flux could break the symmetry.³

Concerning real, 2+1 dimensional surfaces, we can observe that here as well as for other terms in the current we must accept some reasonable generalizations of the expression found in 1+1 dimensions and nothing more. Microscopic approaches can not help here, because they give expressions at the lowest order (for example, the linear one for the ES current), in which case the generalization is generally trivial.

Nevertheless, since the evolution of the surface depends only on some very general features of the current, we should not be worried too much about this. We will see in the following that the only relevant features of \vec{j}_{ES} are: i) A linear behaviour at small slopes: $\vec{j}_{ES} = \alpha \vec{m}$, with a positive α , so that the surface will be linearly unstable. ii) The existence or the absence of finite zeros in the current. iii) Possibly, the behaviour of the current at large slopes, if such zeros do not exist. iv) The in-plane symmetry of the current.

The simplest expression for the ES current in the absence of the above mentioned zeros is the one proposed by Johnson et al. [53]:

³Siegert and Plischke (see note [11] of Ref. [67]) have pointed out that it should not be relevant. Indeed, the problem is equivalent to have an incoming flux forming an angle of 45° with the surface (10): the ES current vanishes anyhow, since shadowing effects are completely negligible.

$$\vec{j}_{ES} = \frac{\alpha \vec{m}}{1 + m^2 \ell_D^2} \quad (18)$$

We observe that this expression may be valid only for $\ell_{ES} \gg \ell_D$. To take into account discrete effects in the z -direction and therefore possible zeros in the current, Siegert and Plischke [67] have replaced \vec{m} with $\vec{m}/(1 - m^2 a^2)$: this corresponds to the substitution of $\tan \theta \equiv ma$ by $(1/2) \tan 2\theta = \tan \theta / (1 - \tan^2 \theta)$, i.e. a function of period π by a function of period $\pi/2$. The resulting current is [67]:

$$\vec{j}_{ES} = \frac{\alpha \vec{m}(1 - a^2 m^2)}{(1 - a^2 m^2)^2 + m^2 \ell_D^2} \equiv \vec{m} f(m^2) \quad (19)$$

The previous expression vanishes on the ‘circle’ $|m| = 1/a$: there is a continuous in-plane symmetry. Discrete effects in the plane should break this symmetry. For example, for a cubic lattice we could write [67,68]:

$$(j_{ES})_{x,y} = m_{x,y} f(m_{x,y}^2) \quad (20)$$

Now, the number of zeros is finite and equal to four: $\vec{m} = (\pm 1, \pm 1)/a$. On the basis of the ‘relevant features’ of \vec{j}_{ES} discussed above, Eqs. (19) and (20) can be replaced by the following simpler expressions:

$$\vec{j}_{ES} = \alpha \vec{m}(1 - a^2 m^2) \quad \text{Same qualitative properties as (19)} \quad (21)$$

$$(j_{ES})_{x,y} = \alpha m_{x,y}(1 - a^2 m_{x,y}^2) \quad \text{Same qualitative properties as (20)} \quad (22)$$

A model with \vec{j}_{ES} given by Eq. (21) has been studied by Strosio et al. [69].

To conclude this part, we can wonder whether some other mechanisms can contribute to a slope dependent current. It is indeed so: generally these mechanisms are not thermally activated and are due –on one side– to the release of the condensation heat when the adatom lands on the surface, and –on the other hand– to the fact that the adatom does not necessarily land on a hollow site. These processes are called (see Ref. [70]) downward funneling, knock-out, transient mobility, and they are illustrated in Fig. 11.

Their effect is a down-hill current which depends on the density of steps and therefore on the slope of the surface. In the simplest picture they give rise to a current $j_{NT} = -\tilde{\alpha} m$ which must be added to j_{ES} . Now, two possibilities exist: if $\tilde{\alpha} > j'_{ES}(0)$ the total current ($j_{NT} + j_{ES}$) is downhill and no instability takes place; conversely, if $\tilde{\alpha} < j'_{ES}(0)$ the total current is uphill at small slopes but downhill at large slopes: therefore it vanishes at a finite slope m_0 even if j_{ES} does not! For example, if j_{ES} is given by the one dimensional version of Eq. (18) then $m_0 = \sqrt{(\alpha/\tilde{\alpha}) - 1/\ell_D}$.

A final remark is in order: The current j_{NT} and therefore $\tilde{\alpha}$ depend on the crystal structure, but there is no reason to think that the slope m_0 at which it counterbalances j_{ES} has some special value.

2. Mullins-type current

Let us consider a grooved surface in the absence of any external flux, so that it is close to equilibrium. Furthermore, we suppose that the temperature is sufficiently low so that evaporation is negligible and the surface relaxes to equilibrium through surface diffusion. This problem is a ‘classical’ one (see the recent review [71]) and for a non singular surface it has been solved forty years ago by Mullins [72]: atoms thermally detach from steps and feel a surface chemical potential which is larger in the region of negative curvature. This determines a current from the top to the bottom of grooves, which relaxes the surface. More precisely, we have a current: $\vec{j}_M = -\Upsilon \nabla \mu$ where Υ is a kinetic coefficient. The expression given by Mullins is $\Upsilon = \beta \rho_0 D$ where ρ_0 is the equilibrium adatom density and $\beta = 1/(k_B T)$, where k_B is the Boltzmann constant, set equal to one in this chapter and in the following one. The chemical potential μ is the variational derivative of the surface free energy⁴: $\mu = \delta \mathcal{E} / \delta z$, where \mathcal{E} has the general expression:

$$\mathcal{E} = \int dx dy \varphi(z_x, z_y) \quad \text{with} \quad \varphi = \sigma(\nabla z) \sqrt{1 + c^2(z_x^2 + z_y^2)} \quad (23)$$

⁴The correct definition [4] is that μ is the Gibbs free energy per particle. The pressure will be assumed to be low enough to allow the replacement of the Gibbs free energy by the Helmholtz free energy. In the present chapter, the solid is assumed incompressible and the free energy reduces to the surface free energy \mathcal{E} , apart from a constant part, so that $\mu = \delta \mathcal{E} / \delta z$. In other chapters the elastic bulk energy will be taken into account.

where $z_{x,y} \equiv \partial_{x,y}z$, c is the out-of-plane lattice constant and $\sigma(\nabla z)$ is the (slope-dependent) surface tension.

In the limit of small slopes ($|\nabla z| \ll 1/a$) and for in-plane isotropy, $\varphi = (c^2\tilde{\sigma}/2)(z_x^2 + z_y^2)$ and μ is simply proportional to the curvature of the surface: $\mu = -a^2c^2\tilde{\sigma}\nabla^2z$, $\tilde{\sigma} = (\sigma(0) + c^{-2}\sigma''(0))$ being the surface stiffness. Finally, the current reads

$$\vec{j}_M = K\nabla(\nabla^2z) = K\nabla^2\vec{m} \quad K \equiv \Upsilon a^2c^2\tilde{\sigma} = \beta D(\rho_0a^2)(\tilde{\sigma}c^2) \quad (24)$$

where we have used the fact that $\nabla \wedge \vec{m} = 0$.

If we use \vec{j}_M as the surface current inside Eq. (7), we easily find that a sinusoidal profile of wavelength λ relaxes to the flat surface in a time of the order of λ^4 . This current, as previously mentioned, has a *stabilizing* character.

After this digression on the current for a surface which is i) non singular and ii) close to equilibrium, we can ask what all this has got to do with a growing surface, which also may be a high symmetry one. A first answer is that flux is just what makes Mullins' theory applicable even to a singular surface: in fact, the surface is roughened by the flux and therefore behaves as a non singular one, even if T is lower than the roughening transition temperature. Nonetheless, the basic mechanism of Mullins' current is thermal detachment from steps: a process which may be hindered by the flux, if the typical time for detachment is longer than the typical time ($1/F_0a^2$) to fill in one layer. For example, Strosio and Pierce [73] assert that thermal detachment is negligible at room temperature during the homoepitaxial growth of Fe. Because of this, in Ref. [69] they replace \vec{j}_M with a current of the form $\vec{j} = K\nabla^2\nabla^2\vec{m}$. As we shall see, in the presence of a flux the thermal detachment mechanism can be dominated by other ones.

In Ref. [74] two of us have tried to study directly the growing, far from equilibrium surface. We started from the assumption that the relation $\vec{j}_{ne} = -\Upsilon_{ne}\nabla\mu_{ne}$ is still valid, where the subscript *ne* stands for 'non equilibrium'. μ_{ne} must be read as a fictitious 'step chemical potential': steps at distance ℓ exchange atoms because of the existing gradient of μ : $\delta\mu_{ne}/\ell$. The result is $\Upsilon_{ne} = p_0\beta a^{2-d}$, where p_0 is the emission rate for step site. The pseudo surface free energy \mathcal{E} giving rise to μ_{ne} is due both to step energy and to entropy. The result is that Eq. (24) is still valid at small slopes, with $K = K_{ther}$ given by [74]:

$$\begin{aligned} K_{ther} &= p_0a^2\ell_D & 1+1 \text{ dim} \\ K_{ther} &= p_0\beta a^2\gamma\ell_D & 2+1 \text{ dim} \end{aligned} \quad (25)$$

where γ is the step stiffness (equal to the step free energy per unit length in the simplest case, when it is isotropic).

At larger slopes the picture is more complicated because \mathcal{E} is no more quadratic in ∇z . For example, in 1+1 dimensions μ_{ne} is not proportional to the curvature z'' , but rather to $(z''/|z'|)$: the same result has been obtained by Krug et al. [64] for a solid on solid model, close to equilibrium.

The main result of this part is that a current of the form (24) is expected even if the surface is strongly out of equilibrium, provided that thermal detachment is allowed (i.e. $p_0 \neq 0$). We want now to suggest that a Mullins-like current is expected even if thermal detachment is forbidden: in this case, \vec{j}_M is due to nucleation and diffusion noise; Let us start with the latter one.

Randomness in diffusion means that the number of adatoms reaching the step of a terrace of size ℓ per unit time fluctuates around the average value (equal to $F_0\ell/2$ in the absence of step-edge barriers). Nonetheless adatoms feel the curvature only close to a step and once a freshly landed adatom has approached a step it can no more be distinguished from a freshly detached atom from the step: therefore the contribution of diffusion noise to the kinetic coefficient K is entirely similar to K_{ther} provided that p_0 is replaced by $(F_0\ell/2)$:

$$\begin{aligned} K_{dif} &= F_0a^2\ell_D^2/2 & 1+1 \text{ dim} \\ K_{dif} &= F_0a^3\ell_D^2\beta\gamma & 2+1 \text{ dim} \end{aligned} \quad (26)$$

The discussion of nucleation noise starts from the analysis of Eq. (7) in the linear approximation:

$$\partial_t z = -\nabla \cdot (\alpha\vec{m} + K\nabla^2\vec{m}) \quad (27)$$

where the first term in brackets is due to the ES effect. The solution is $z(\vec{x}, t) = z_0 \exp(-i\vec{q} \cdot \vec{x} + \omega t)$, with $\omega = \omega(\vec{q}) = \alpha q^2 - Kq^4$. The flat surface is therefore unstable ($\omega > 0$) if $q < q^* = \sqrt{\alpha/K}$ and the most unstable mode (which maximizes $\omega(q)$) corresponds to $q_u = \sqrt{\alpha/2K}$. In other words, the Mullins-like current stabilizes the surface on scales smaller than $\lambda^* = 2\pi/q^* = 2\pi\sqrt{K/\alpha}$ and the instability develops after a finite time of the order of $t_u = 1/\omega(q_u) \simeq K/\alpha^2$ and with a typical wavelength $\lambda_u = 2\pi/q_u = \sqrt{2}\lambda^*$. This stabilization is evident in the homoepitaxial growth of GaAs(001) as reported by Orme et al. [52]: the substrate is rough at small length scales ($< 0.1\mu\text{m}$) and the preexisting defects are healed before the ES instability develops on larger scales. In the case of

Ge(001) (Ref. [50]) another feature appears: at higher temperatures, larger thicknesses must be attained in order to observe the instability. This is easily explained by the expression of t_u : at higher temperatures the ES barriers are less effective and therefore α decreases, whilst K increases (see Eqs. (25,26) and Eq. (28) here below).

In Ref. [58] we have studied a one dimensional model of growing surface where the only source of noise is nucleation of new islands and thermal detachment from step is forbidden. In such a model, according to the above discussion the K -term should be absent; nevertheless numerical simulations clearly show that a finite λ_u does exist; even more importantly, λ_u does not exist if we adopt a (somewhat artificial) deterministic model for nucleation.⁵ These results prove that nucleation noise is also a source of a Mullins-like current: Which is the relevant value of $K = K_{nuc}$ in this case? If $\ell_{ES} = 0$, the only parameters entering our model are the intensity of the flux F_0 and the diffusion length ℓ_D . Since $[K] = \text{length}^{4-d}/\text{time}$, dimensional analysis suggests that

$$K_{nuc} \approx F_0 \ell_D^4 \quad (28)$$

both in 1+1 and in 2+1 dimensions.

In conclusion, we have found that in a far from equilibrium surface, thermal detachment, diffusion and nucleation noise all contribute to a Mullins-like current:

$$K = K_{ther} + K_{dif} + K_{nuc} \quad (29)$$

In 2+1 dimensions, since $p_0 = (D/a^2) \exp(-\beta W_a)$ where W_a is the energy to transform a kink atom into an adatom, we will have that:

$$K_{nuc} \gg K_{ther} \quad \text{if} \quad \ell_D^3 (\beta \gamma a) \ll a^3 \exp(\beta W_a) \quad (30)$$

$$K_{nuc} \gg K_{dif} \quad \text{if} \quad \ell_D^2 \gg (\beta \gamma a) a^2 \quad (31)$$

Since $\beta \gamma a \approx 1$, expression (31) confirms that in the continuum limit $\ell_D \gg a$, the ‘nucleation noise’ contribution to K prevails over the ‘diffusion noise’ contribution. Conversely, the contribution due to thermal detachment will be negligible at sufficiently low temperatures: $\exp(\beta W_a) \gg (\ell_D/a)^3$.

We conclude by pointing out the main limit of this part: ES barriers have been neglected in the evaluation of the various contributions to K . The reason is that K_{ther} , K_{dif} and K_{nuc} are present even in the limit $\ell_{ES} = 0$ and therefore for a weak ES effect we can neglect it. Conversely it is not certainly guaranteed that the given expressions for K are still valid for a strong ES effect. For instance K_{ther} must vanish in such a limit, because in general adatoms will stick only to the same step they have detached from and therefore there is no exchange of atoms between steps: $K_{ther}(\ell_{ES} = \infty) = 0$. For the same reason we also expect that $K_{dif}(\ell_{ES} = \infty) = 0$.

3. Symmetry breaking current

According to the terms introduced up to now for the surface current \vec{j} , Eq. (7) has two symmetry properties: in-plane reflection symmetry ($\vec{x} \rightarrow -\vec{x}$) and up-down symmetry ($z \rightarrow -z$). The general validity of the former depends on the in-plane symmetry of the surface. In the case of a three-fold symmetry, which is pertinent for epitaxial growth of fcc(111) metals, such symmetry is absent and the relevant current [68] will be given in Eq. (62). Conversely, irrespective of crystal structure and surface orientation, there is no basic reason to expect that the up-down symmetry survives when the surface is subject to an external flux.

The simplest expression for a current which changes sign with \vec{x} but does not change sign with z is: $\vec{j}_{SB} = \nabla G(m^2)$, where G is any even function of the slope \vec{m} and the subscript SB stands for symmetry breaking. Before proceeding we can make some general considerations on \vec{j}_{SB} . If we consider a sinusoidal profile: $z(\vec{x}) = z_0 \sin(\vec{q} \cdot \vec{x})$ it is straightforward to write down:

$$\vec{j}_M = -K q^2 \vec{m} \quad (32)$$

$$\vec{j}_{SB} = 2G'(m^2) [\partial_{xx}^2 z + \partial_{yy}^2 z] \vec{m} \quad (33)$$

The ES current (see Eqs. (18-22)) has the same sign of the slope and for this reason it has a ‘destabilizing’ character. In contrast, the Mullins-like current \vec{j}_M is stabilizing; finally, the symmetry breaking current has a different behaviour

⁵In this model a new terrace is nucleated on an old one as soon as its length equals the nucleation length ℓ_n (see App. B). The artificial character of this model determines a nonanalytical form of the profile in the nucleation sites.

according to the sign of the curvature: $[\partial_x^2 z + \partial_y^2 z]$. We will see that the physically relevant case corresponds to $G'(m^2) > 0$: this means that \vec{j}_{SB} is destabilizing (resp. stabilizing) in a region of positive (resp. negative) curvature and therefore the bottoms of a grooved profile are narrower than the tops and in some models they even look like crevasses.

The first analytical derivation of \vec{j}_{SB} has been done by Politi and Villain [58] in the case of a 1+1 dimensional surface. Afterwards, this result has been confirmed by Krug with a different method [75]. The existence of a curvature-dependent term in the current which has not the form of j_M is easily deduced by the following consideration: a surface profile whose slope is not constant is surely time-dependent, even if $\ell_{ES} = 0$ and all the sources of the Mullins-like term (thermal detachment and noise) are switched off: in this case the velocity of each step –in the BCF theory– is proportional to half of the sum of the lengths of the upper and lower terraces. This means that $\partial_t z \neq 0$ even if $\vec{j}_{ES} = \vec{j}_M = 0$.

A very simple, but not rigorous argument to justify \vec{j}_{SB} is now given: the ‘microscopic’ current on a terrace is $\vec{j}_{mic} = -D\nabla\rho$. In the paragraph on the ES current we have evaluated j_{ES} as an average of j_{mic} on a terrace of size ℓ : step-edge barriers make ρ asymmetric with respect to the center of the terrace and therefore $j_{ES} \neq 0$. Nonetheless, even if $\ell_{ES} = 0$ the density ρ varies from one terrace to another, if there is a curvature in the surface profile: in fact, the solution of the diffusion equation $D\nabla^2\rho + F_0 = 0$ on a terrace of size ℓ with ρ vanishing at steps gives an average value $\bar{\rho} \approx (F_0\ell^2/D)$. The terrace width ℓ is of the order of ℓ_D at small slopes and of the order of $1/|m|$ at high slopes. The simplest function interpolating between these two limiting behaviours [58,75] is: $\ell^2 \approx \ell_D^2/(1 + m^2\ell_D^2)$. Therefore we obtain:

$$\vec{j}_{SB} \approx -D\nabla \left(\frac{F_0}{D} \frac{\ell_D^2}{1 + m^2\ell_D^2} \right) = -\nabla \left(\frac{F_0\ell_D^2}{1 + m^2\ell_D^2} \right) \quad (34)$$

So, the function $G(m^2)$ appears to be:

$$G(m^2) \approx -\frac{F_0\ell_D^2}{1 + m^2\ell_D^2} \quad (35)$$

whose derivative $G'(m^2)$ is always positive. At large slopes: $\vec{j}_{SB} \approx -F_0\nabla(1/m^2)$ which agrees –in its 1+1 dimensional version– with the results of Refs. [58,75]. The numerical prefactor is (1/8) for Politi and Villain and (1/12) for Krug. It is important that both methods give a constant prefactor, not depending on the ES length. If the rough argument given above to justify \vec{j}_{SB} is slightly modified to take into account finite step-edge barriers, the function G appears to be ℓ_{ES} -dependent, but the dependence is extremely weak: the prefactor simply varies between (1/12) and (1/3) for ℓ_{ES} varying from zero to infinity.

Anyway, we should realize that such argument is far from being rigorous, because the diffusion between terraces must be understood as an effective one, since steps capture atoms. In this respect, it is important to point out that Eq. (7) –and so the current \vec{j} – is the result of a spatiotemporal average and therefore \vec{j}_{SB} may appear even if no interlayer diffusion is allowed by the microscopic dynamics. Indeed, more microscopic approaches based on the Master equation [62] confirm that such term is present even if thermal detachment is forbidden.

At small slopes we have

$$\vec{j}_{SB} \approx F_0\ell_D^4\nabla(m^2) \equiv \lambda\nabla(m^2) \quad (36)$$

It is noteworthy that $\lambda \approx K_{nuc}$: this is not surprising because $[\lambda]=[K]$ and since F_0 and ℓ_D are the only parameters entering the model, there is no other way to obtain a quantity which is dimensionally correct. The current (36) appears in the study of the conserved Kardar-Parisi-Zhang equation [76]; in the more specific context of MBE, it was introduced by Villain [39].

We conclude by observing that a rigorous derivation of the surface current should give all the terms we have introduced: the ES current, which depends on the slope \vec{m} ; the symmetry-breaking term, which depends also on the curvature $\nabla \cdot \vec{m}$; the Mullins-like current, which depends on higher order derivatives ($\nabla^2\vec{m}$). Nonetheless, at the moment a systematic derivation is lacking.

E. Experimental results

In this paragraph we want to present and discuss some experimental results concerning unstable MBE growth on a high symmetry surface, which are thought to be due to step-edge barriers. Let us start by describing the main features of the ES instability on a singular surface.

After deposition of a certain thickness of material, which depends on the material itself and on the growth conditions, a three dimensional mound structure sets in. These mounds can be characterized by a typical size L and a typical slope m_0 : it is often the case that L increases with time via a coarsening process, where bigger mounds eat neighbouring smaller ones. Experimental data for $L(t)$ are plotted in a log-log scale in order to obtain the so-called coarsening exponent n : $L(t) \sim t^n$.

In Tab. II we summarize some experimental data, concerning metals (Fe, Cu and Rh) and semiconductors (GaAs and Ge). For any experimental system we give: the growth temperature T in Kelvin; the coarsening exponent n with its error (when indicated); the range of sizes $L_{min} \div L_{max}$ of the mounds over which n is calculated or the typical values of L which are displayed; the slope of the mounds; the range of thicknesses N corresponding to the sizes given in the L column or the maximal thickness reached in the articles referenced here; the intensity of the flux; the experimental techniques.

From the third column we see that n varies between 0.16 ± 0.04 and 0.56 and that three values out of seven are in the range $0.23/0.26$. It is not always possible to know on which range of values of L the exponent refers to; if it is possible, such range ($L_{min} \div L_{max}$) is indicated in column “ L ”. It is therefore seen that the ratio L_{max}/L_{min} varies of a factor from two [79] up to ten [81].

It is important to point out that for all metals a mound structure already appears after the deposition of a very few layers, or even in the submonolayer regime. The case of semiconductors is different: for example let us consider the epitaxial growth of germanium [50]. Here –as well as for silicon– the main problem is that the system undergoes a ‘crystalline/amorphous growth’ phase transition at a critical thickness h_{cr} which strongly depends on temperature: this implies for example that it is difficult to track the ES instability at different thicknesses and it may be necessary to increase T in order to obtain mounds of larger size. In the case of Ge, the size of the first mounds increases with T . Their typical size, much larger than in most of metals, indicates a weaker ES barrier.

A second point we want to stress regards the slope of mounds: Is it constant or does it increase with time? Experimentally, the question puts additional problems for two reasons: slope may increase because the ‘constant slope regime’ has not yet been attained, or slope may look to be constant in the range $L_{min} \div L_{max}$ because the increase rate is too slow. These possibilities should be taken into account for Refs. [79] and [69], because in both cases larger and constant slopes are found in the same [77,78] or similar [80] systems, respectively.⁶

We finally observe that large slopes, corresponding to well defined orientations, are found only for metals, while unstable growth in semiconductors seems to be characterized by fairly small slopes ($< 3^\circ$).

F. Continuum theory of the instability

In chapter IV D we have discussed the surface current \vec{j} which should enter in the evolution equation for the surface profile. Here we will concentrate on the few models for which some well established results exist and we will discuss how ‘robust’ such results are with respect to modifications in the model.

1. One dimensional models

We have said that j is generally made up of three terms:

$$j = j_{ES} + j_M + j_{SB} \quad (37)$$

Concerning the ES current there are two main classes, according to the existence or not of finite zeros in j_{ES} . Anyhow $j_{ES}(m)$ can always be derived from an effective potential energy $U(m)$:

$$j_{ES}(m) = -\frac{\delta}{\delta m} \int dx U(m(x)) \quad \text{with} \quad U'(m) = -j_{ES}(m) \quad (38)$$

The Mullins-like current has the expression $j_M = Km''(x)$ at sufficiently small slopes, which can also be written:

$$j_M = -\frac{\delta}{\delta m} \int dx \frac{K}{2} (m')^2 \quad (39)$$

⁶Clearly we must take care in comparing experimental results obtained at different temperatures (Ref. [69] at room temperature and Ref. [80] at $T \sim 150^\circ\text{C}$).

Nevertheless there is no basic reason to use the small- m expansion for j_M if the surface develops an instability with large slope regions. Starting from Eq. (23) it is easily found that a more general expression is: $j_M = \Upsilon \partial_x [\tilde{\sigma}(m)m']$, where $\tilde{\sigma}(m) = [\sigma(m)/\sqrt{1+c^2m^2} + \sigma'(m)\sqrt{1+c^2m^2}/c^2m]$ is an even function of m . In this case j_M is no more derivable from a free energy: some considerations will be done at this regard in the following.

Finally, the term $j_{SB} = \partial_x G(m^2)$ can not be derived from a free energy either. This is not true for any symmetry breaking terms, but it is necessary to pass to a higher order term [82]. For example:

$$\tilde{j}_{SB} = \tilde{\lambda} \partial_x [(m')^2] = -\frac{\delta}{\delta m} \int dx \mathcal{F}_{SB} \quad (40)$$

with $\mathcal{F}_{SB} = (\tilde{\lambda}/3)(m')^3$.

If we neglect for the moment all the nonpotential terms, we are left with the expression:

$$j = j_{ES}(m) + Km''(x) \quad (41)$$

where j_{ES} may have (model I) or not (model II) zeros at finite m .

Before starting to study dynamics, it is important to consider stationary configurations of Eq. (7), corresponding to a vanishing current: $j \equiv 0$. This equation is immediately recognized as the equation of motion of a particle of mass K moving in the potential $V(m) = -U(m)$. To be definite let us consider the following expressions for the ES current:

$$j_{ES} = \alpha m [1 - m^2/m_0^2] \quad \text{model I} \quad (42)$$

$$j_{ES} = \frac{\alpha m}{[1 + m^2 \ell_D^2]^\gamma} \quad \text{model II} \quad (43)$$

Model II reduces for $\gamma = 1$ to the current introduced by Johnson et al. [53] in 2+1 dimensions (Eq. (18)) and by Hunt et al. [83] in 1+1 dimensions. All microscopic models yield $\gamma = 1$. Nonetheless it is useful to study the generalization to $\gamma > 1$ [84]. The corresponding expressions for $V(m)$ are:

$$V(m) = \frac{\alpha}{2} m^2 - \frac{\alpha}{4m_0^2} m^4 \quad \text{model I} \quad (44)$$

$$V(m) = \left(\frac{\alpha}{2\ell_D^2} \right) \ln(1 + m^2 \ell_D^2) \quad \text{model II, } \gamma = 1 \quad (45)$$

$$V(m) = - \left[\frac{\alpha(\gamma-1)}{2\ell_D^2} \right] \frac{1}{(1 + m^2 \ell_D^2)^{\gamma-1}} \quad \text{model II, } \gamma > 1 \quad (46)$$

In Fig. 12 we plot these functions.

In our mechanical analogy m plays the role of space, x of time and stationary configurations correspond to oscillatory motions around the equilibrium position $m = 0$. Such motions have different behaviours in the three cases: the important feature is how the period of the oscillations (i.e. the wavelength λ of the stationary configuration) depends on the amplitude (i.e. the maximal value m^* of the slope). In the harmonic regime [$V(m) = \alpha m^2/2$] the period does not depend on the amplitude: this corresponds to the linear regime of Eq. (7), with a well defined wavelength and an ‘undefined’ amplitude (depending on the real time, in the dynamical problem). When the amplitude is large enough we enter in the nonlinear regime and the question is: Does λ increase or decrease with m^* ? For both models I and II, as well as for the current given in (15), λ increases with m^* because the ‘force’ j_{ES} decreases with respect to the harmonic regime, i.e. j_{ES}/m decreases with m . This condition can be found by writing:

$$|j_K| = |j_{ES}| \implies K \frac{m^*}{\lambda^2} \approx j_{ES}(m^*) \implies \lambda \approx \sqrt{\frac{K m^*}{j_{ES}(m^*)}} \quad (47)$$

This means that stationary solutions of arbitrarily large wavelength exist and they correspond to increasing values of m^* : this common feature is one of the necessary ingredients to have a coarsening phenomenon. However, important differences exist between the models: in model I, $\lambda \rightarrow \infty$ when $m^* \rightarrow m_0^-$, while in models II, $\lambda \rightarrow \infty$ when m^* also diverges. In model I it is possible to define a stationary solution which corresponds to the boundary conditions: $m(x) \rightarrow \pm m_0$ when $x \rightarrow \pm \infty$. This solution is called ‘domain wall’ or ‘kink’ because $m(x)$ is always constant (and equal to $\pm m_0$) except in a narrow region around $x = 0$. The width of this region is

$$L_{dw} = \frac{2m_0}{|m'(0)|} = \sqrt{\frac{8K}{\alpha}} \quad (48)$$

which (up to a numerical factor of order unity) is nothing but the lower critical wavelength λ^* : The surface is dynamically stable at smaller scales.

In the limit $m^* \rightarrow m_0^-$ stationary configurations are made up of domains of increasing size L where the slope is alternately equal to $\pm m_0$, separated by domain walls. This picture breaks down for model II because now $m^* \rightarrow \infty$ and it is no more possible to define domains of constant slope. Nonetheless a major difference exists between the cases $\gamma = 1$ and $\gamma > 1$: for $\gamma = 1$ there is no stationary solution corresponding to the boundary conditions $m(x) \rightarrow \pm\infty$ when $x \rightarrow \pm\infty$, while this solution does exist if $\gamma > 1$. This also implies that for $\gamma = 1$ (the physically relevant case) the maximal velocity in $m = 0$ diverges when $m^* \rightarrow \infty$: in other words stationary solutions are characterized by a curvature which diverges in the minima and maxima of the profile (i.e. where $m(x) \equiv dz/dx = 0$).

Stationary solutions are important for the dynamics for the following reasons: coarsening means that these stationary configurations are stable with respect to amplitude fluctuations, but unstable with respect to wavelength fluctuations. The evolution of the system is such that the surface profile passes through stationary configurations of increasing wavelength.

Let us now come back to the expression (41). Since our one dimensional current j is derivable from the effective free energy:

$$\mathcal{F} = \int dx \left[\frac{K}{2} (m')^2 + U(m) \right] \quad (49)$$

the evolution equation for the order parameter $m(x)$ is given by Eq. (10):

$$\partial_t m(x, t) = \partial_x^2 \left(\frac{\delta F}{\delta m} \right) + \partial_x (\text{noise}) \quad (50)$$

For model I we exactly obtain the so-called Cahn-Hilliard equation [55], which has been extensively studied. First we give the results and afterwards some qualitative explanations:

$$L(t) \sim \ln t \quad \text{noise} \equiv 0 \quad \text{Ref. [11]} \quad (51)$$

$$L(t) \sim t^{1/3} \quad \text{shot noise} \neq 0 \quad \text{Ref. [85,86]} \quad (52)$$

The best way to explain these results is to recall the kink picture. A system with only one kink corresponds to a surface profile with only one mound: $m(x) \equiv z'(x) \rightarrow \pm m_0$ when $x \rightarrow \mp\infty$. This stationary profile is stable, but if we put more kinks the profile is no more stable because kinks interact through the tails of their profiles. The shape of the tail can be easily determined linearizing the equation $j = 0$ around m_0 : $m(x) = m_0 - \epsilon(x)$. We obtain:

$$j_{ES}(m) + K m''(x) = -j'_{ES}(m_0) \epsilon(x) - K \epsilon''(x) = 0 \quad (53)$$

The function $\epsilon(x)$ has therefore an exponential behaviour: $\epsilon(x) = \epsilon_0 \exp(-\kappa x)$ with $\kappa = \sqrt{|j'_{ES}(m_0)|/K} = \sqrt{2\alpha/K}$. The inverse of κ can be recognized (up to a constant) as the width of the domain wall: $L_{dw} = 1/\kappa$.

It is therefore reasonable to expect that kink interaction and kink velocities (in the absence of noise) decrease exponentially with the interkink distance $L(t)$. Coarsening means that kinks feel an effective *attractive* interaction: if a kink has a velocity $v \sim \exp(-\kappa L)$ where L is the distance with its nearest kink, then the time $t(L)$ necessary for the annihilation of a pair of neighbouring kinks is $t(L) \sim L \exp(\kappa L)$, which gives: $L(t) \sim L_{dw} \ln t$.

The effect of noise is more difficult to take into account, because $m(x, t)$ is a conserved order parameter: $\partial_t \int dx m(x, t) = 0$. On one side noise would make kinks move independently through a sort of random walk; on the other side the constraint of conservation couples the motion of the different kinks. In the absence of conservation we would simply have $L(t) \sim t^{1/2}$. In fact, in a random walk the time necessary to travel a distance L is $t \sim L^2$. If $m(x)$ is conserved the constraint slows down the kink motion and we pass from $t^{1/2}$ to $t^{1/3}$.

Now let us comment on the case $\tilde{\sigma}(m) \neq \text{constant}$. If $\tilde{\sigma}$ depends on the slope m the current reads:

$$j = \Upsilon \partial_x (\tilde{\sigma}(m) m') + j_{ES}(m) \quad (54)$$

What about stationary configurations? We can define the function $M(m) = \int_0^m du \tilde{\sigma}(u)$, so that:

$$j = \Upsilon M''(x) + j_{ES}(m(M)) \quad (55)$$

where $M(m)$ is an odd function which always increases with m , since $M'(m) = \tilde{\sigma}(m) > 0$. We have seen that

$$\frac{j_{ES}(m)}{M} = \frac{j_{ES}(m)}{m} \cdot \frac{m}{M} \quad (56)$$

must be a decreasing function of m , in order to have coarsening. The first ratio on the right hand side is a decreasing function of m , because we suppose that coarsening does exist if $\bar{\sigma}(m)$ is constant (i.e. if $M = m$). On the other side, if $\bar{\sigma}(m)$ decreases with m , the ratio (m/M) increases because M/m is the average value of $\bar{\sigma}(u)$ in the interval $(0, m)$. According to this, the right hand side of Eq. (56) is the product of a decreasing function and of an increasing function of m and therefore no general conclusion can be drawn from it, if a specific form for $\sigma(m)$ [and therefore for $\bar{\sigma}(m)$] is not assumed.

2. Two-dimensional models

In chapter IV B we already remarked that a continuum description of crystal growth in 2+1 dimensions differs from a standard phase separation process even if the current can be derivable from an effective free energy. Let us discuss this point.

The generalization of Eq. (41) is:

$$\vec{j} = \vec{j}_{ES}(\vec{m}) + K \nabla^2 \vec{m} \quad (57)$$

This equation is almost always derivable from a free energy (it is indeed so for Eqs. (18-22)) but not for any form of \vec{j}_{ES} , in opposition to the one dimensional case. The reason is that

$$\vec{j}_M = K \nabla^2 \vec{m} = -\frac{\delta}{\delta \vec{m}} \int d\vec{x} \frac{K}{2} [(\nabla m_x)^2 + (\nabla m_y)^2] \quad (58)$$

while \vec{j}_{ES} can be written as

$$\vec{j}_{ES}(\vec{m}) = -\frac{\delta}{\delta \vec{m}} \int d\vec{x} U(\vec{m}) \quad (59)$$

if and only if:

$$\frac{\partial^2 U}{\partial m_x \partial m_y} = \frac{\partial^2 U}{\partial m_y \partial m_x} \quad \text{i.e.} \quad \frac{\partial}{\partial m_y} [(j_{ES})_x] = \frac{\partial}{\partial m_x} [(j_{ES})_y] \quad (60)$$

Eqs. (18-22) and similar ones have the general form:

$$\vec{j}_{ES} = \vec{m} g(m^2) \quad \text{or} \quad (j_{ES})_{x,y} = m_{x,y} g(m_{x,y}^2) \quad (61)$$

where the first one is valid for in-plane symmetry and the second for a square symmetry. In both cases the relation (60) is fulfilled, as well as for their generalization (71), see below. For a three-fold symmetry, Siegert [68] has suggested the following modification of Eq. (22):

$$\begin{aligned} (j_{ES})_x &= \alpha(1 + 2m_x)[m_x(1 - m_x) - m_y^2] \\ (j_{ES})_y &= \alpha m_y(1 - 2m_x - 2m^2) \end{aligned} \quad (62)$$

Again, this equation fulfills the condition (60). The conclusion of this part is that –in practice– the passage from 1+1 to 2+1 dimensions does not put additional problems for the derivation of \vec{j} from a free energy.

We now state the two major features which are introduced in 2+1 dimensions: i) The constraint $\nabla \wedge \vec{m} = 0$, and ii) The impossibility for the time evolution of \vec{m} to be governed by the Cahn-Hilliard equation. It is important to point out their common origin: the fact that the order parameter \vec{m} derives from the local height $z(\vec{x}, t)$ [$\vec{m} = \nabla z \Rightarrow \nabla \wedge \vec{m} = 0$] and therefore the fact that its evolution equation derives from Eq. (7). So, we have

$$\partial_t \vec{m} = -\nabla(\nabla \cdot \vec{j}) \quad (63)$$

and not

$$\partial_t \vec{m} = -\nabla^2 \vec{j} \quad (64)$$

Conversely, the phase separation process for a conserved order parameter is governed by Eq. (64), in order to implement the conservation law

$$\partial_t \int d\vec{x} m_i = - \int d\vec{x} \nabla^2 j_i \quad (65)$$

which vanishes for the divergence theorem.

Siegert and Plischke [67,68,87] have solved numerically Eq. (7) with $\vec{j} = \vec{j}_{ES} + K \nabla^2 \vec{m}$, where \vec{j}_{ES} is given by Eq. (19) [continuous symmetry in the plane] or Eq. (20) [four fold symmetry in the plane], and in the presence of noise.

For a ‘true’ phase separation process, the two currents give different results for the coarsening law $L(t) \sim t^n$ (see the review [88]): $n = 1/4$ if the potential $U(\vec{m})$ has a continuous infinity of minima [in $|m| = 1/a$, for Eq. (19)] and $n = 1/3$ if $U(\vec{m})$ has a finite number of minima [in $\vec{m} = (\pm 1, \pm 1)/a$, for Eq. (20)]. So, the result by Siegert and Plischke for the surface growth models (Eqs. (19-20)) is surprising: $n \simeq 1/4$ in both cases [67].

A deeper comprehension of the difference between the surface growth evolution and a ‘real’ phase separation process can be gained by comparing the different pictures of Fig. 13.

They refer, respectively, to the following models:

$$\partial_t \vec{m} = \nabla^2 \left(\frac{\delta \mathcal{F}_{ani}}{\delta \vec{m}} \right) + \nabla \eta \left(\begin{array}{c} \text{Four-state} \\ \text{clock model} \end{array} \right) \quad \text{Fig. 13a} \quad (66)$$

$$\partial_t \vec{m} = \nabla \left[\nabla \cdot \left(\frac{\delta \mathcal{F}_{ani}}{\delta \vec{m}} \right) \right] + \nabla \eta \left(\begin{array}{c} \text{Surface growth:} \\ \text{four-fold in-plane symmetry} \end{array} \right) \quad \text{Fig. 13b} \quad (67)$$

$$\partial_t \vec{m} = \nabla \left[\nabla \cdot \left(\frac{\delta \mathcal{F}_{iso}}{\delta \vec{m}} \right) \right] \left(\begin{array}{c} \text{Surface growth:} \\ \text{in-plane invariance} \end{array} \right) \quad \text{Fig. 13c} \quad (68)$$

where:

$$\mathcal{F}_{ani} = \int d\vec{x} \left\{ \frac{K}{2} [(\nabla m_x)^2 + (\nabla m_y)^2] + \alpha \left[-\frac{m^2}{2} + \frac{m_x^4 + m_y^4}{4} \right] \right\} \quad (69)$$

$$\mathcal{F}_{iso} = \int d\vec{x} \left\{ \frac{K}{2} [(\nabla m_x)^2 + (\nabla m_y)^2] + \alpha \left[-\frac{m^2}{2} + \frac{m^4}{4} \right] \right\} \quad (70)$$

We stress that (b) and (c) are both growth models, but with different symmetries of the order parameter while (a) and (b) have the same symmetry for \vec{m} , but the operators ‘gradient’ and ‘divergence’ are interchanged.

A point of basic importance is that in surface growth a domain wall must be straight, because it corresponds to the intersection of two planes.

In this respect Siegert, Plischke and Zia [89] have also proven that domain wall relaxation is much faster than coarsening, so that domain walls look straight on the time scale of coarsening.

More precisely, if \vec{m}_1 and \vec{m}_2 are any two minima of \mathcal{F}_{ani} or \mathcal{F}_{iso} : $\vec{m}_{1,2} = |\vec{m}|(\cos \theta_{1,2}, \sin \theta_{1,2})$, then their intersection takes place along a line forming an angle $\theta = (\theta_1 + \theta_2)/2$ with the horizontal axis.

This means that in principle model (b) allows for only four distinct kinds of domain wall, forming respectively angles $\theta = 0, \pm\pi/4, \pi/2$ with the x -axis, but domain walls parallel to the x, y axes ($\theta = 0, \pi/2$) cost less energy (because one of the two components of the order parameter keeps constant) and therefore dominate the others. On the other hand, while the domain walls parallel to the Cartesian axes can intersect, giving rise to a pyramid, the other two walls cannot intersect. The constraint $\nabla \wedge \vec{m} = 0$ requires that each ‘diagonal’ domain wall ($\theta = \pm\pi/4$) –if present– terminates at the same ending point as a horizontal *and* a vertical domain wall. In Fig. 13b all the possible intersections are visible.

In the isotropic growth model (Fig. 13c) the energy cost of a domain wall does not depend on its orientation, but the constraint deriving from $\vec{m} = \nabla z$ implies a relation between the values of \vec{m} in neighbouring domains and the direction of the separating domain wall. The consequence is a periodic surface profile which is made of a network of square-based or hexagonal-based pyramids. Only in the former case the up-down symmetry is fulfilled. The statistics of the orientations of the different facets/domains indeed show [90] that they are not randomly distributed, but four orientations $\vec{m}_i = (\cos \theta_i, \sin \theta_i)$, with $\theta_{i+1} = \theta_i + \pi/2$ are more likely to take place. We speculate that this phenomenon would be even more evident in the presence of noise (as in Fig. 13b).

In a very recent paper [91], Martin Siegert has proposed a more complex scenario for coarsening in 2+1 dimensions. He stresses the importance of having two classes of domain walls according to the values of θ (see above): parallel to the axes ($\theta = 0, \pi/2$) and diagonal ones ($\theta = \pm\pi/4$). This fact should prevent from the applicability of any theoretical

approach based on the existence of a single length scale, because the densities of the two different classes of kinks ($\rho_0 = \rho(\theta = 0, \pi/2)$ and $\rho_1 = \rho(\theta = \pm\pi/4)$) have different time dependences. Even if diagonal domain walls are more energy-expensive, they play a basic role in the dynamics because the surface would not coarsen in absence of them [89,91].

The two relevant length scales are $R = 1/\rho_0$ and $D = 1/\rho_1$: The latter one has a fast increase: $D(t) \sim t^{1/3}$, while the former one increases more slowly, with an exponent close to $1/4$.

The previous picture can be completed with an expression for the ES current which is more general than Eqs. (21,22):

$$(j_{ES})_x = m_x(1 - m_x^2 - bm_y^2) \quad (j_{ES})_y = m_y(1 - m_y^2 - bm_x^2) \quad (71)$$

Eqs. (21,22) are recovered respectively for $b = 1$ and $b = 0$. The parameter b (whose relevant range of variability for a quadratic symmetry is $-1 < b < 1$) gives the dependence of each component $(j_{ES})_{x,y}$ of the current on the relative perpendicular component of the slope $m_{y,x}$. Such dependence is mainly due to edge diffusion, whose importance has been experimentally shown in metal epitaxy by Jorritsma et al. [78]. The picture given above is applicable for $b > -3/4$, when diagonal domain walls are suppressed by energetics. Conversely for $-1 < b < -3/4$ they are favored over horizontal/vertical domain walls. Since coarsening requires the nucleation of roof tops, for $b = -3/4$ this process does not cost anything and a larger coarsening exponent ($n = 1/3$) is found [91].

The same result should be valid for a triangular symmetry, relevant for (111) surfaces of fcc crystals, where only one type of domain walls is present. This prediction agrees with the experimental results by Tsui et al. [81] on the growth of Rh(111).

We conclude this part with some considerations on different continuous growth models.

3. Symmetry-breaking terms

In 1+1 dimensions it has been recently shown [92] that a current of the form $j_{SB} = \partial_x G(m^2)$ does not change the coarsening laws, at least for the model I. Let us discuss briefly this point.

Kawasaki and Ohta [85] studied the dynamical evolution of model I in one dimension by reformulating the problem of phase separation for the order parameter m as a problem of nonlinear dynamics of kinks. A kink represents a (zero dimensional) domain wall between regions where m takes different constant values, corresponding to the zeros of the ES current ($= \pm m_0$ for the current (42)). The kink profiles $M_{\pm}(x)$ are the solutions of the equation $j = 0$ with $M_{+}(\pm\infty) = \pm m_0$ for the positive kink, and $M_{-}(\pm\infty) = \mp m_0$ for the negative one. Because of the up-down symmetry, $M_{-}(x) = -M_{+}(x)$ and it is easily found that

$$M_{\pm}(x) = \pm m_0 \tanh(\kappa_0 x/2) \quad \text{with} \quad \kappa_0 = \sqrt{2\alpha/K} \quad (72)$$

Because of kink interaction, kink dynamics has a deterministic component governed by the minimization of the pseudo surface free-energy, and a random component due to shot-noise.

Since the kink picture does not depend on the derivability of the surface current from any free-energy, it has been applied [92] to the case of symmetry breaking induced by $j_{SB} = \lambda \partial_x(m^2)$. We can summarize the main results as follows: (i) The functional form of the kink profiles does *not* change. (ii) It is no more true that $M_{-}(x) = -M_{+}(x)$. In fact now:

$$M_{\pm}(x) = \pm m_0 \tanh(\kappa_{\pm} x/2) \quad (73)$$

with $\kappa_{+} > \kappa_{-}$ (positive kinks are narrower than negative kinks) and $\kappa_{+}\kappa_{-} = \kappa_0^2$ (the product of their widths is constant). (iii) The total effective interaction between kinks is *not* qualitatively modified. (iv) The coarsening laws are the same, but the crossover time between the logarithmic one (at short times) and the power-law one (at longer times) may be significantly increased. (v) Positive kinks may be so narrow that their width is comparable to the lattice constant. In this case the positive kink should be replaced by an angular point, with a discontinuity of the surface slope.

Concerning the symmetry-breaking in 2+1 dimensions, the only study of a surface growth model in the presence of such term is a numerical analysis due to Strosio et al. [69], who do not use the Mullins term: $\vec{j}_M = K \nabla^2 \vec{m}$, but a higher order one: $\vec{j} = K \nabla^2 (\nabla^2 \vec{m})$. Their numerical integration gives a coarsening exponent $n = 0.18 \pm 0.02$ which is told to be insensitive to the presence or the absence of \vec{j}_{SB} .

4. Constantly increasing slope

At the moment there is no rigorous study –not even in 1+1 dimensions– for a model where the ES current has not zeros at finite slope. Hunt et al. [83] have studied numerically model II with $\gamma = 1$ (see Eq. (43)) in 1+1 dimensions, and found $n \approx 0.22$ in the presence of a weak shot noise: therefore, a result well different from the values obtained for model I: $n = 1/3$ in presence of noise and $n = 0$ (logarithmic coarsening) in absence of noise. The qualitative argument based on noise effects and given in App. C, if applied to the case $\gamma = 1$ gives [93,94] $n = 1/5$ in 1+1 dimensions.

The kink picture is manifestly not applicable for model II, since the current has no zeros at finite m and therefore regions of constant slope cannot exist. Even more important, the equation $j = 0$ has no solution with $M(\pm\infty) = \pm\infty$ as boundary condition: this means that periodic stationary solutions do not converge to a self-similar limit.

Preliminary results [84] on models II (with $\gamma = 1$ and $\gamma > 1$) in 1+1 dimensions show that steepening makes coarsening faster in absence of noise and slower in presence of it. The reason of the deterministic “acceleration” is the following: even if a kink picture is not suitable to describe the interface, at least for $\gamma > 1$ the kink can be replaced by the wave function of the ground state of a potential well, whose profile depends on the exact form of the unstable current. Since the kink profile has an exponential tail while the wave function decays algebraically for models II, potential wells interact more strongly than kinks, and as a consequence of this coarsening is faster. The reason of the noisy “slowing down” has not a simple explanation, but it is probably due to the competition between steepening and coarsening (see also the next paragraph on Monte Carlo simulations).

5. The Zeno model and the need of a nonlocal evolution equation

The ‘Zeno model’ [58] deserves some attention. it is a one-dimensional model for a high-symmetry surface which evolves through instantaneous attachment of adatoms to preexisting steps and creation of new steps via nucleation of new terraces (a process which is intrinsically random). In this model only fluctuations in the nucleation process contribute to the Mullins-like term ($K = K_{nuc}$); since nucleation is unlikely on small terraces, the K -term is expected to decrease when the slope increases. This explains the strong up-down asymmetry displayed by the model (see Fig. 14): nucleation is not effective to counterbalance the ES current in a region of high slope and the SB term is destabilizing in a region of positive curvature. In the Zeno model the asymmetry has a striking consequence: the regions of positive curvature are replaced by angular points. Because of the discontinuity of the slope m in an angular point, the SB term in the current ($j_{SB} = \partial_x G(m^2)$) gives a divergent contribution to the velocity of the interface, if a local evolution equation is assumed: $\partial_t z = -\partial_x j_{SB}$.⁷ The solution [58] is to replace $\partial_t z(x, t) = -\partial_x j$ with the following nonlocal evolution equation:

$$\partial_t z(x, t) = -\partial_x \int dx' \chi(x - x') j(x', t) \quad (74)$$

where $j(x', t)$ is the local current evaluated in the point x' and the kernel $\chi(x - x')$ has the form: $\chi(x) = \exp(-|x|/x_0)$.

The Zeno model has a second major feature: the existence of an upper critical wavelength λ_c^{sup} at which coarsening stops. The reason is that stationary configurations ($\partial_t z \equiv 0$) exist only for $\lambda < \lambda_c^{sup}$. At larger scales mounds are unstable even for height fluctuations, and therefore deeper and deeper crevasses form in between.

G. Monte Carlo simulations

This final paragraph is devoted to kinetic Monte Carlo (MC) simulations of a singular surface, in the presence of step-edge barriers. We will limit ourselves to some representative works in 2+1 dimensions.

An important preliminary statement concerns the implementation of a constant slope in a simulation where crystal structure effects are difficult to take into account. The adopted solutions may differ: In a simple cubic SOS model, the simplest way is to allow the freshly landed adatom to hop to a neighbouring lower site (see Refs. [87,95]). For more realistic cubic lattices (bcc/fcc) the typical solution is a downward funneling mechanism [96,97] according to which a higher coordination site has a larger ‘capture area’.

⁷The Mullins term gives an even more divergent contribution (because of the higher derivative), but nucleation (and therefore K_{nuc}) is completely negligible in a large slope region.

Šmilauer and Vvedensky [95] obtain different time dependences for the slope by varying the intensity of the down-hill current. Two limiting cases are noteworthy: constant slope and absence of the down-hill current. In the former case, the relevant model should give a coarsening exponent $n \simeq 1/4$. Simulations give a value varying between 0.21 and 0.26. The latter case (absence of a down-hill current) is interesting because slope is certainly expected not to saturate (slope $\sim t^{\vartheta'}$), and a naïve application of the condition $|\vec{j}_{ES}| \sim |\vec{j}_M|$, with $|\vec{j}_{ES}| \sim 1/|m|$ would give $\vartheta' = n$. Simulations [95], in one case out of two, give a result which agrees: $n = 0.19, \vartheta' = 0.21$. An important feature which emerges from their simulations is that size growth is slowed down by an existing slope increase, that is to say steepening and coarsening of mounds are two competitive processes. This fact is supported by the qualitative analyses of Refs. [93,94], discussed in App. C: the exponent n decreases, if the slope passes from being constant to increase with the mound size.

Siebert and Plischke [87] consider, in addition to isotropic ES barriers, anisotropic ones for which $(j_{ES})_y \equiv 0$ and the resulting mound structure has a one dimensional profile ($m_y = 0$). Nonetheless the anisotropic 2+1 dimensional model differs from the same model in one dimension (at least if noise is present) because the latter does not order at finite temperature. So, while the isotropic case gives $n = 0.26$ (very close to $1/4$) the anisotropic case does not give $n = 1/3$ –as expected for the noisy one dimensional model– but a much smaller value: $n \approx 0.18$.

Finally, we want to comment on the works by Thürmer et al. [97] and by Amar and Family [96] on bcc/fcc(100) lattices. The models seem to be fairly similar, but the results differ substantially: Thürmer et al. find constant slopes –corresponding to the facets (012)– and a coarsening exponent $n \approx 0.24/0.26$. On the other side Amar and Family find a much broad range of variability for n ($n \approx 0.16/0.25$ for weak barriers and $n \simeq 1/3$ for strong ones) and the slope has various behaviors. A possible explanation is that even minimal differences in the model may influence step-edge diffusion, and –after Refs. [78,91]– the coarsening behaviour.⁸

V. KINETIC INSTABILITIES OF VICINAL SURFACES

A. Introduction

A vicinal surface is a surface which is cut along an orientation close to a high symmetry one. It is made up of low index terraces (e.g. (001) or (111)) separated by atomic steps. Steps are unavoidably present in any real surface: for example, because the surface is always slightly miscut, but also because steps may be thermally activated or because a screw dislocation ends up in a step at the crystal surface; finally, steps may be created during the growth through nucleation. The first factor is the only one to produce steps all of the same sign (ascending or descending ones), and the second factor is completely negligible at small temperatures.

In the presence of an external flux, a step acts as a sink by capturing adatoms diffusing in the vicinity and therefore advancing. In average a straight step (as those which result from cutting the crystal) remains parallel to its original direction, while the steps due to screw dislocations give rise to a spiral growth. In this chapter, dislocations as well as thermally activated steps will be ignored.

A growing vicinal surface can only be stable if three conditions are fulfilled. i) Diffusing adatoms stick to preexisting steps rather than nucleate new islands on the terraces. ii) Terraces keep the same width. iii) Steps remain straight. When one of these conditions is not fulfilled, it gives rise to a well defined instability, called respectively i) three-dimensional growth, ii) step-bunching and iii) step-meandering.

Since the typical distance between nucleation centers on a high symmetry surface is the so called diffusion length ℓ_D (see App. B), we would be led to conclude that the condition for avoiding three-dimensional growth is simply $\ell < \ell_D$, where ℓ is the terrace width. Nonetheless nucleation is a stochastic process and therefore nucleation events take place, even if rarely, on a terrace smaller than ℓ_D . So, an important issue is the asymptotical stability of step-flow growth against nucleation: this question will be discussed at the end of the chapter, and till then nucleation will be ignored.

Let us start by showing what the ES effect has to do with step-bunching and meandering instabilities. To make a clear distinction between the two phenomena, we will consider the following limiting cases: i) a one dimensional vicinal surface (in order to avoid the possibility of meandering) and ii) a single step (in order to avoid step-bunching). i) Let us suppose that adatoms prefer to stick to the ascending step, as they do in the presence of an ES effect: this means that a terrace which is larger than its neighbours will reduce its width because the ascending step proceeds faster than the descending one. The opposite is true for a smaller terrace. The conclusion is that the ES effect

⁸We should also observe that in Ref. [97] fits are generally carried out at larger thicknesses than in Ref. [96].

stabilizes the width of the terraces *during growth*.⁹ Conversely, if the crystal surface evaporates, an ES effect means that an adatom will detach preferentially on the lower terrace and therefore a larger terrace will become even larger: a step-bunching instability takes place *during evaporation*. This scenario was predicted thirty years ago by Schwoebel and Shipsey [38].

ii) Now let us consider a single step. This makes sense only if evaporation is present, otherwise an infinite current of adatoms would stick to the step and it would move with infinite velocity. In the presence of desorption an adatom has a lifetime τ , which means that it travels through a linear distance $x_s = \sqrt{D\tau}$ before evaporating: so, only adatoms landing within a distance x_s from the step will contribute to the step advancement. If a train of steps is correctly considered (as in case i), the limit of vanishing desorption is still physical, because sinks at distance ℓ do exist.

The meandering instability is conceptually similar to the diffusion instabilities treated in chapter II: the growth front develops some protrusions which capture more atoms and therefore grow even more. The main difference is that also atoms coming from the ‘inner side’ of the front contribute to step motion, and the meandering instability can arise only if the inner contribution is too weak to compensate the outer contribution, in other words if an ES effect is present. However, Saito and Uwaha [99] have shown that a meandering instability can take place even in the absence of an ES effect, if the step velocity exceeds a critical value. In fact, during the growth, in the reference system of the step the adatoms of the lower terrace have a higher component of the velocity in the direction perpendicular to the step and therefore the ‘flux’ of the incoming adatoms from below is greater than from above.¹⁰ However, the required flux is so high that the diffusion length ℓ_D is very small and nucleation can no more be neglected. Finally, the drift of adatoms may be even increased and controlled *via* application of an external electric field, which produces the electromigration phenomenon [100].

We want to stress that the conditions for the meandering instability and those for step bunching are opposite: the former takes place if the surface grows, while the latter if the surface sublimates. Therefore, the consequence of points i) and ii) is that a two dimensional train of steps is generally expected to be unstable.

The study of the dynamics of a vicinal surface will proceed as follows: linear stability analysis of a single step [54] and of a train of steps [101]; study of the weakly nonlinear regime, close to the threshold of instability, for a single step [102] and for a train of steps [103,104]; Monte Carlo simulations [99,105]; continuum description of the vicinal surface [104–107]. We will conclude with some remarks on three-dimensional growth and step-flow [105,108].

B. Single step: linear stability analysis

Before starting we would like to point out the qualitatively different approach which is required by a vicinal surface, with respect to a high symmetry one. On a singular surface, steps are continuously created (through nucleation) and destroyed (through coalescence): at least in the case of stable growth, the lifetime of a step is given by the typical time necessary to fill one layer: $t_{ML} = 1/(F_0 a^2)$. Since the continuum description is valid on time scales larger than t_{ML} , steps do not enter ‘directly’ in such description. Conversely, steps have an infinite lifetime on a vicinal surface (if nucleation is neglected) because they all have the same sign (descending or ascending one). This means that a step motion picture is better than a ‘surface current’ picture to describe the dynamics of the surface.

A second remark concerns the microscopic dynamics: the density ρ of adatoms on a terrace is governed by the diffusion equation in the quasi static approximation:

$$D\nabla^2 \rho - \frac{\rho}{\tau} + F_0 = 0 \quad (75)$$

which is a *linear* equation. The nonlinear character of the step evolution derives from boundary conditions at steps.

In the following, x will be the average direction of the step and y the in-plane perpendicular direction, so that the step may be described by a single-valued function $\zeta(x, t)$ with the lower terrace corresponding to $y > \zeta$. The normal component to the step of the gradient of concentration ($\partial\rho/\partial n$) is proportional to the difference between the nonequilibrium (ρ) and equilibrium (ρ_{eq}) concentrations at the step itself:

$$D \left(\frac{\partial \rho}{\partial n} \right)_+ = k_+ (\rho - \rho_{eq})_+ \quad (76)$$

⁹It is important to recall that impurities can pin the steps and therefore play a major role in step-bunching during growth [98].

¹⁰In this case the instability may take place even during evaporation; however a finite ES effect stabilizes [99] the profile of the receding step.

$$-D \left(\frac{\partial \rho}{\partial n} \right)_- = k_- (\rho - \rho_{eq})_- \quad (77)$$

where the signs $+/-$ correspond to the lower/upper terrace (i.e. to $y = \zeta_{\pm}$) and the equilibrium concentration is given by:

$$\rho_{eq} = \rho_{eq}^0 (1 + \tilde{\Gamma} \kappa) \quad (78)$$

The second term depends on the curvature¹¹ κ of the step:

$$\kappa = - \frac{\partial_{xx}^2 \zeta}{[1 + (\partial_x \zeta)^2]^{3/2}} \quad (79)$$

and reflects the Gibbs-Thomson effect: close to a region of positive curvature the concentration is higher because of the higher rate of thermal detachment from the step. The coefficient $\tilde{\Gamma} = \Omega \beta \gamma$ depends on the surface area per atom Ω and the ratio between the step stiffness γ and the temperature $T = 1/(k_B \beta)$.

The existence of an ES barrier means that $k_+ > k_-$: if the barrier is perfectly reflecting (one-sided model), then $k_- = 0 = (\partial_n \rho)_-$; on the other side, if the step is in equilibrium with the lower terrace, then $(\rho - \rho_{eq})_+ = 0$ which corresponds to $k_+ = \infty$. In the case of a single step, the boundary condition to infinity ($y \rightarrow \pm\infty$) is that the concentration goes to a constant value, which corresponds to the balancing between deposition and evaporation:

$$\rho(x, y, t) \rightarrow \rho_{\infty} = \tau F_0 \quad \text{single step} \quad (80)$$

Once the concentration profile is known as a function of the step profile, the step velocity v_n may be determined via the relation:

$$(\Delta \rho_s) v_n = D[(\partial_n \rho)_- - (\partial_n \rho)_+] \quad (81)$$

where $\Delta \rho_s$ is the difference of surface concentration between the solid phase and the ‘adatom gas’ phase. Since the latter is negligible with respect to the former: $\Delta \rho_s = 1/\Omega$.

Finally, v_n and $\zeta(x, t)$ are linked by a kinematical relation:

$$v_n = \frac{v_0 + \partial_t \zeta}{\sqrt{1 + (\partial_x \zeta)^2}} \quad (82)$$

where v_0 is the ‘drift’ velocity, pertaining to a straight step. It is noteworthy that for the linear stability analysis, the formulas: $\kappa = -\partial_x^2 \zeta$ and $v_n = v_0 + \partial_t \zeta$ can be used.

Let us now consider the simplest case: a single step in the one-sided model (i.e. an infinite ES barrier). We will follow the treatment given by Bena, Misbah and Valance [102].

The concentration profile and the ‘drift’ velocity v_0 are given by:

$$\rho_0(y) = \rho_{\infty} - (\rho_{\infty} - \rho_{eq}^0) \exp(-y/x_s) \quad v_0 = \Omega x_s (F_0 - F_{eq}) \equiv \Omega x_s \Delta F \quad (83)$$

where $F_{eq} = \rho_{eq}^0/\tau$. Their interpretation is simple: only adatoms arriving within a distance x_s from the step are able to stick to it before evaporating and therefore contribute to the step velocity. If thermal detachment is forbidden, v_0 is simply given by the number of atoms sticking to the step per unit time and unit length, i.e. by the term proportional to F_0 in (83). The term proportional to F_{eq} takes into account the rate of detachment from the step. Finally, $\rho_0(y)$ is the one-dimensional solution of Eq. (75) ‘interpolating’ between ρ_{eq}^0 in $y = 0$ and ρ_{∞} at infinity.

The linear stability analysis proceeds by considering a small deviation from the stationary concentration:

$$\rho(x, y, t) = \rho_0(y) + \rho_1(y) \exp(iqx + \omega t) \quad (84)$$

and from the straight step profile:

$$\zeta(x, t) = \zeta_1 \exp(iqx + \omega t) \quad (85)$$

¹¹In the following the curvature is understood to be positive if $\partial_x^2 \zeta < 0$.

and by solving the differential equation at the first order in ρ_1, ζ_1 . The existence of a nontrivial solution ($\rho_1 \equiv \zeta_1 \equiv 0$) requires a dispersion relation between ω and q :

$$\frac{\omega(q)}{\Omega D} = -\tilde{\Gamma}\rho_{eq}^0\Lambda_q \cdot q^2 + \frac{\tau\Delta F}{x_s} \left(\Lambda_q - \frac{1}{x_s} \right) \quad (86)$$

with $\Lambda_q = \sqrt{q^2 + 1/x_s^2}$. It is indeed sufficient to expand the previous expression to order q^4 :

$$\frac{\omega(q)}{\Omega D} = \left[-\frac{\tilde{\Gamma}\rho_{eq}^0}{x_s} + \frac{\tau\Delta F}{2} \right] q^2 - \left[\frac{\tilde{\Gamma}\rho_{eq}^0 x_s}{2} + \frac{\tau\Delta F x_s^2}{8} \right] q^4 \quad (87)$$

The straight step is dynamically unstable if $\omega(q)$ is positive in some range of q -values. Since the q^4 term is always negative, there will be an instability only if the coefficient of q^2 is positive, and this requires that ΔF is larger than a threshold value given by:

$$(\Delta F)_{cr} = \frac{2\tilde{\Gamma}\rho_{eq}^0}{x_s\tau} \quad (88)$$

However, this threshold is physically unimportant, because it is much smaller than the value F_{eq} the flux must overcome in order to allow the crystal to grow instead to evaporate. In fact $(\Delta F)_{cr}/F_{eq} = 2(a/x_s)(a\beta\gamma)$, where (a/x_s) is much smaller than one and $(a\beta\gamma)$ is of order unity.

If $\Delta F > (\Delta F)_{cr}$ there is a band of unstable modes, ranging from $q = 0$ to $q = q^*$. The general expression for q^* is fairly complicated, because it is derived from a cubic equation. Nonetheless, if we are very close to the threshold instability the approximation (87) can be used and we find:

$$q^* = \frac{1}{x_s} \sqrt{\frac{8\epsilon}{3}} \quad \text{with} \quad \epsilon \equiv \frac{1}{2} - \frac{\tilde{\Gamma}\rho_{eq}^0}{\tau x_s \Delta F} \equiv \frac{1}{2} - \xi \quad (89)$$

The dimensionless parameter ϵ measures the distance from the threshold. For $\epsilon \ll 1$ we are in the so called weakly nonlinear regime, and its analysis will be done in the next paragraph.

Formula (86) clearly shows that stabilizing effects are entirely due to thermal detachment: In fact $\omega(q) \geq 0 \forall q$ if $\rho_{eq}^0 = 0$. Such effects derive from the fact that thermal detachment is encouraged in a region of positive curvature and discouraged if the curvature is negative: this process partly corresponds to an effective step-edge diffusion which resembles the Mullins-like term introduced in chapter IV D 2. As we will see in the next paragraph, it is possible to give a more solid basis to this interpretation.

However, thermal detachment is also at the origin of the negative term in the coefficient of the q^2 term (see Eq. (87)): in the absence of ρ_{eq}^0 we would simply have: $(\omega/\Omega D) \simeq (\tau F_0/2)q^2$. This means that step detachment ‘renormalizes’ and lowers the coefficient $(\tau F_0/2)$, but with the basic contribution of evaporation: in fact the threshold value vanishes in the limit $\tau \rightarrow \infty$. In other words, step detachment is only effective at short scales if it must ‘use’ surface diffusion, but becomes effective also at longer scales if it can use evaporation.

Now let us discuss the more general case of finite ES barriers and interacting steps. In their pioneering work, Bales and Zangwill [54] considered finite ES barriers for a train of in-phase steps; afterwards, Pimpinelli et al. [101] extended their study to arbitrary phases, showing the importance of this extension in the case of an evaporating surface.

The main result of the treatment of finite ES barriers is that the qualitative picture given in the previous chapter is confirmed: a nonvanishing k_- implies a larger threshold value for the flux. The condition $\Delta F > (\Delta F)_{cr}$ reads $\xi < \xi_c = 1/2$ for an infinite ES barrier (see Eq. (89)), while in the opposite limit of very weak asymmetry ($k_+ \simeq k_-$) we have [101]:

$$\xi_c = \frac{d_- - d_+}{2(d_+/x_s + 1)^2} \quad \text{with} \quad d_{\pm} = \frac{D}{k_{\pm}} \quad (90)$$

Here and in the following we will suppose that $d_+ = 0$ (fast attachment from the lower terrace) and therefore d_- is nothing but the ES length ℓ_{ES} . In the case of a single step it should be compared with x_s ($\ell_{ES} \gg x_s$ meaning a strong ES effect). With these notations, the previous value of ξ_c (valid for a weak ES effect) simply reads: $\xi_c = \ell_{ES}/2$.

C. Linear analysis for a train of steps

Now let us consider the stability of a train of steps. If ℓ is the step-step distance, the case of a single step is recovered in the limit $\ell \gg x_s$. In fact, in this case there is a region between each pair of neighbouring steps where the concentration ρ of adatoms has the constant value ρ_∞ and therefore the concentration profile is the one given in Eq. (83). Since the case $\ell \gg x_s$ has been studied in the previous paragraph, we consider the opposite limit: $\ell \ll x_s$.

Using the results of Ref. [101], the amplification rate can be written as:

$$\omega(q, \phi) = \Omega \Delta F [(\cos \phi - 1) + \ell^2 q^2 / 2] \left(\frac{\ell_{ES}}{\ell_{ES} + \ell} \right)^2 - \Omega D \tilde{\Gamma} \rho_{eq}^0 q^2 \left[\frac{2(1 - \cos \phi) + (q^2 + x_s^{-2}) \ell (\ell + \ell_{ES})}{\ell + \ell_{ES}} \right] \quad (91)$$

where ϕ , the phase shift between neighbouring steps, plays the role of the wavevector q_y in the direction perpendicular to the steps.

Separating terms of different order in q , the previous formula reads:

$$\omega(q, \phi) = \Omega \Delta F (\cos \phi - 1) \left(\frac{\ell_{ES}}{\ell_{ES} + \ell} \right)^2 + \left\{ \frac{\Omega \Delta F}{2} \left(\frac{\ell \ell_{ES}}{\ell_{ES} + \ell} \right)^2 - \Omega D \tilde{\Gamma} \rho_{eq}^0 \left[\frac{2(1 - \cos \phi)}{\ell + \ell_{ES}} + \frac{\ell}{x_s^2} \right] \right\} q^2 - \Omega D \tilde{\Gamma} \rho_{eq}^0 \ell \cdot q^4 \quad (92)$$

The quantity $\omega(0, \phi)$ corresponds to a rigid translation of each step and therefore it allows to study the step-bunching instability:

$$\omega(0, \phi) = \Omega \Delta F (\cos \phi - 1) \left(\frac{\ell_{ES}}{\ell_{ES} + \ell} \right)^2 \quad (93)$$

This quantity is always negative (and therefore the train of rigid steps is stable) if $\Delta F > 0$, i.e. if the surface is growing. The opposite is true (and therefore the train of rigid steps is unstable) during evaporation. Furthermore $\omega(0, \phi)$ is maximized by $\phi = 0$ (in-phase motion) if $\Delta F > 0$ and by $\phi = \pi$ if $\Delta F < 0$. This means that the single step approximation is acceptable in the former case, but it is not in the latter one.

In the case of evaporation, the coefficient of the q^2 -term in (92) is always negative and therefore the q^4 -term can be neglected:

$$\omega(q, \pi) = 2\Omega |\Delta F| \left(\frac{\ell_{ES}}{\ell_{ES} + \ell} \right)^2 - \frac{\Omega \rho_{eq}^0}{\tau} \left[\frac{1}{2} \left(\frac{\ell \ell_{ES}}{\ell_{ES} + \ell} \right)^2 + \tilde{\Gamma} \left(\frac{4x_s^2}{\ell + \ell_{ES}} + \ell \right) \right] q^2 \quad \text{evaporation} \quad (94)$$

The sum in square brackets reduces to $[\ell^2/2 + \tilde{\Gamma}\ell]$ for a strong ES effect ($\ell_{ES} \gg \ell$) and to $[\ell_{ES}^2/2 + 4\tilde{\Gamma}x_s^2/\ell]$ for a weak one ($\ell_{ES} \ll \ell$). It may also be interesting to evaluate the width of the band of unstable modes, i.e. the value q^* for which $\omega(q^*, \pi) = 0$. It is easily found that $q^* = 2/\sqrt{\ell^2 + 2\tilde{\Gamma}\ell}$ for $\ell_{ES} \gg \ell$ and $q^* = (\ell_{ES}/\ell x_s) \sqrt{\ell/2\tilde{\Gamma}}$ for $\ell_{ES} \ll \ell$.

In the case of growth the most destabilizing mode corresponds to $\phi = 0$ and the rate of increase

$$\omega(q, 0) = \left[\frac{\Omega \Delta F}{2} \left(\frac{\ell \ell_{ES}}{\ell_{ES} + \ell} \right)^2 - \Omega \tilde{\Gamma} \frac{\rho_{eq}^0}{\tau} \ell \right] q^2 - \Omega \tilde{\Gamma} \frac{\rho_{eq}^0}{\tau} \ell x_s^2 \cdot q^4 \quad \text{growth} \quad (95)$$

is positive when the flux exceeds a threshold, just as in the single-step case. The value of the threshold is now

$$(\Delta F)_{cr} = \frac{2\tilde{\Gamma} \rho_{eq}^0 \ell}{\tau} \left(\frac{\ell_{ES} + \ell}{\ell \ell_{ES}} \right)^2 \quad (96)$$

which reads $(\Delta F)_{cr} = 2\tilde{\Gamma} \rho_{eq}^0 / \tau \ell$ for a strong ES effect, and $(\Delta F)_{cr} = 2\tilde{\Gamma} \rho_{eq}^0 \ell / \tau \ell_{ES}^2$ for a weak one. The former expression is nothing but Eq. (88), where x_s has been replaced by ℓ : this is reasonable, because the adatoms contributing to the motion of a given steps are the ones landing within a distance x_s for a single step, and within a distance ℓ for a train of steps. A similar comparison is not possible for a weak ES effect because in this case there is a more subtle interplay between ℓ , ℓ_{ES} and x_s . Finally, in the absence of evaporation ($\tau \rightarrow \infty$) and for a strong ES effect ($\ell_{ES} \gg \ell$), Eq. (95) reads:

$$\omega(q, 0) = \frac{\Omega F \ell^2}{2} q^2 - \Omega D \tilde{\Gamma} \rho_{eq}^0 \ell \cdot q^4 \quad (97)$$

which is the same as Eq. (4) of Ref. [104].

D. Single step: weakly nonlinear analysis

The linear stability analysis is useful in two respects: because it allows to determine for which values of the different parameters step-flow growth is stable and because it allows to extract the time and space scales which are relevant for the subsequent nonlinear evolution. In this paragraph we will consider the dynamics of a single step, just above the threshold of the instability, i.e. for $\Delta F/(\Delta F)_c = 1 + 2\epsilon$, with $\epsilon \ll 1$, where ϵ was defined in (89). This analysis was carried out by Bena, Misbah and Valance in Ref. [102]. The calculations are a bit lengthy but instructive and therefore they will be given in App. D. Here we will just explain the main lines of reasoning.

The first step corresponds to make $x, y, \zeta(x, t)$ and t dimensionless, by rescaling lengths with x_s and time with τ , and to consider the concentration u with respect to its constant value $\rho_\infty = F_0\tau$ at infinity, rather than the ‘absolute’ concentration: $u = \rho - F_0\tau$. This way, the diffusion equation simply reads: $\nabla^2 u - u = 0$. In the same units, close to the threshold the dispersion relation is

$$\omega = \Omega\Gamma(2\epsilon q^2 - 3q^4/4) \quad (98)$$

where $\Gamma = \tilde{\Gamma}\rho_{eq}^0/x_s$.

The previous relation clearly shows that the ‘active’ modes (i.e. the unstable ones) are of the order of $q \simeq \sqrt{\epsilon}$ and ω is of the order of ϵ^2 . In other words, the unstable structure has an initial wavelength of the order of $\lambda^* = 1/\sqrt{\epsilon}$ and it takes a time $t^* = 1/\epsilon^2$ to develop: so λ^* and t^* are the good space and time units for the nonlinear analysis, and from x, t we will pass to $X = \sqrt{\epsilon}x$, $T = \epsilon^2 t$. (Note that y is not rescaled, because the step profile is only a function of x and t .)

The next step is to expand both the concentration field $u(X, y, T)$ and the step profile $\zeta(X, T)$ in powers of ϵ with the idea to solve the problem (differential equation + boundary conditions) recursively. Since ζ must vanish in the limit $\epsilon = 0$, the term in ϵ^0 in its expansion is not present and it is therefore useful to put $\zeta(X, T) = \epsilon H(X, T)$. At this point, the functions u and H can be written as: $u = \sum_{n=0}^{\infty} u_n \epsilon^n$ and $H = \sum_{n=0}^{\infty} H_n \epsilon^n$. At each order of the integration of the differential equation $\nabla^2 u - u = 0$ a new ‘integration function’ $A_n(X, T)$ appears, which should be determined *via* boundary conditions. What is found [102] is that A_1 and A_2 keep undetermined till the third order. At this order, the boundary conditions imply that $H_0(X, T)$ fulfills the differential equation

$$(\Omega\Gamma)^{-1}\partial_T H_0 = -2\partial_X^2 H_0 - \frac{3}{4}\partial_x^4 H_0 + (\partial_x H_0)^2 \quad (99)$$

This equation is called Kuramoto-Sivashinsky [109] (KS) equation and exhibits spatiotemporal chaos. Saito and Uwaha [99] have performed Monte Carlo simulations on a simple cubic (SC) lattice for different values of the parameters. In particular they have pointed out the importance of the crystalline anisotropy in the step stiffness γ : an effect which is not taken into account in the previous nonlinear analysis and whose study needs to get to the fifth order in the ϵ -expansion [110].

If the step is oriented along a direction of maximal stiffness (for example the [10] orientation for the SC lattice) the anisotropy does not play an important role and above the threshold $(\Delta F)_{cr}$ the step displays spatiotemporal chaos (Fig. 1c of Ref. [99]): grooves at average distance given by λ_u are constantly created (when locally the distance is larger than $2\lambda_u$) and destroyed (through collisions and annihilation). Conversely, if the step is oriented along a direction of minimal stiffness (the [11] for a SC lattice) this ‘stabilizes’ such orientation and a more regular pattern appears (Fig. 4c of Ref. [99]). In the limit of strong anisotropy a periodic structure emerges.

The previous scenario has been explained by the same authors in a subsequent paper [110]. In the presence of an anisotropic step stiffness, γ reads

$$\gamma = \gamma_0[1 + \nu(1 - \cos 4\theta)], \quad (100)$$

where θ is the angle between the step normal and the average growth direction y . Accordingly, the coefficient of the lower-order linear term $(\partial_X^2 H_0)$ in Eq. (99) is modified by the factor $[1 - 8\nu\epsilon^2(\partial_X H_0)^2]$. This implies that the effect of the anisotropy is vanishing at the threshold instability. Secondly, a marked difference exists between $\nu < 0$ (the stiffness is maximal) and $\nu > 0$ (the stiffness is minimal). In the former case the above factor is always positive and anisotropy effects are not relevant. In contrast, in the latter case ($\nu > 0$) the coefficient of $(\partial_X^2 H_0)$ may even change sign in regions of high slope and therefore stabilize the minimal stiffness orientation.

Let us now come back to Eq. (99). Its linear analysis gives the dispersion relation:

$$\omega(q) = \Omega\Gamma(2q^2 - 3q^4/4) \quad (101)$$

After having reintroduced the old variables ($q \rightarrow q/\sqrt{\epsilon}$ and $\omega \rightarrow \omega/\epsilon^2$) it takes exactly the form given in Eq. (98). So, the linear terms of Eq. (99) could be ‘inferred’ by the dispersion relation (98). With regard to the nonlinear

term in the KS equation, it is the simplest and lowest order nonlinear term which does not depend explicitly on H_0 (because of translational invariance, the dynamics cannot depend on the absolute position of the step). The sign of the nonlinear term is irrelevant for the subsequent analysis, because it may be changed passing from H_0 to $-H_0$.

It may be useful to display explicitly ϵ in the evolution equation for the interface. In order to avoid confusion let us come back to the initial variables (x, t, ζ) and—in terms of these— let us define: $x' = \sqrt{8/3}(x/x_s)$, $h = \zeta/x_s$ and $t' = (16\Omega\Gamma/3)t/\tau$. The evolution equation for $h(x', t')$ then reads:

$$\partial_{t'} h = (1/2)(\partial_{x'} h)^2 - \epsilon \partial_{x'}^2 h - \partial_{x'}^4 h \quad (102)$$

where ϵ (defined in Eq. (89)) has the form $\epsilon = \frac{1}{2}(\frac{\Delta F}{(\Delta F)_{cr}} - 1)$. When $\Delta F < (\Delta F)_{cr}$, ϵ is negative and the step is linearly stable. The quartic term is negligible and Eq. (102) takes the form of the deterministic Kardar-Parisi-Zhang equation: nonetheless, since no deterministic instability is present it is necessary to add a noise term $\theta(x', t')$ to its right hand side. Karma and Misbah [103] have therefore modified Eq. (102) to take into account stochastic fluctuations; Furthermore, to make it valid beyond the small range $\epsilon \ll 1$, the coefficients of the nonlinear $(\partial_{x'} h)^2$ and quartic $(\partial_{x'}^4 h)$ terms become dependent on the incoming flux. Finally, Eq. (102) is generalized in the following way:

$$\partial_{t'} h = \frac{\lambda}{2}(\partial_{x'} h)^2 - \epsilon \partial_{x'}^2 h - \mu \partial_{x'}^4 h + \theta(x', t') \quad (103)$$

where $\lambda = \Delta F/(\Delta F)_c$, $\mu = (2 + \lambda)/3$ and:

$$\langle \theta(x'_1, t'_1) \theta(x'_2, t'_2) \rangle = R \delta(x'_1 - x'_2) \delta(t'_1 - t'_2) \quad \text{with} \quad R = \sqrt{3/8}(T/\gamma x_s) \quad (104)$$

This equation has been solved numerically by Karma and Misbah [103] and discussed in details in a recent paper by Pierre-Louis and Misbah [107]. Stochastic fluctuations are important below the instability threshold (when the straight step is linearly stable) while deterministic ones are important above the threshold. In a small range around $\epsilon = 0$ both are relevant. This may be seen [107] by rescaling x' and t' in order to have the coefficients of the two linear terms of order unity. Afterwards, the rescaling of the amplitude h will fix the relative importance of the nonlinear term and the noise. If we put:

$$x' = \tilde{x}/\alpha_x \quad t' = \tilde{t}/\alpha_t \quad h(x, t) = \alpha_h \tilde{h}(\tilde{x}, \tilde{t}) \quad (105)$$

we obtain:

$$\partial_{\tilde{t}} \tilde{h} = -\alpha_x^2 \alpha_t^{-1} \epsilon \partial_{\tilde{x}}^2 \tilde{h} - \alpha_x^4 \alpha_t^{-1} \mu \partial_{\tilde{x}}^4 \tilde{h} + \alpha_h \alpha_x^2 \alpha_t^{-1} \frac{\lambda}{2} (\partial_{\tilde{x}} \tilde{h})^2 + \Theta \quad (106)$$

where $\Theta = (\alpha_h \alpha_t)^{-1} \theta$ and therefore:

$$\langle \Theta(\tilde{x}_1, \tilde{t}_1) \Theta(\tilde{x}_2, \tilde{t}_2) \rangle = R \alpha_h^{-2} \alpha_x \alpha_t^{-1} \delta(\tilde{x}_1 - \tilde{x}_2) \delta(\tilde{t}_1 - \tilde{t}_2) \quad (107)$$

The condition on the linear terms requires that $\alpha_x = \sqrt{|\epsilon|/\mu}$ and $\alpha_t = \epsilon^2/\mu$. On the other hand α_h may be determined by fixing the coefficient of the nonlinear term $((\alpha_h)_{NL} \alpha_x^2 \alpha_t^{-1} \lambda = 1)$ or the amplitude of the noise $(R(\alpha_h)_n^{-2} \alpha_x \alpha_t^{-1} = 1)$. The range of values of ϵ where both noise and instability are relevant is determined by the condition that $(\alpha_h)_{NL} \sim (\alpha_h)_n$, i.e. $|\epsilon| \sim R^{2/7}$.

E. Nonlinear analysis for a train of steps

The first study on the dynamics of a train of steps in the nonlinear regime is due to Pierre-Louis and Misbah [106,107,111], who also take into account the elastic repulsion between steps. They perform a coarse-graining procedure to pass from the discrete evolution equations for the steps (variables $\zeta_m(x, t)$) to its continuum version. Here, we will limit ourselves to observe that the resulting equation has the form of an anisotropic Kuramoto-Sivashinsky equation [112] which includes a propagative term. The relevant feature is that a numerical study [107] shows a morphology resembling the late-time evolution of a vicinal surface [105] in the absence of evaporation, but in the presence of nucleation (see section V G).

In the treatment of the linear dynamics of a train of steps, evaporation is not negligible in the sense that $x_s = \sqrt{D\tau}$ may be large (larger than the step-step distance), but it is smaller than the wavelength of the emerging pattern. This implies that the limit $x_s \rightarrow \infty$ requires a different study, which has been performed by O. Pierre-Louis et al. [104,106].

The analysis of the most unstable mode (the in-phase movement of the steps) close to the threshold of the instability (which now corresponds to a vanishing flux) gives the following evolution equation for the step $\zeta(x, t)$:

$$\partial_t \zeta = -\partial_x \left\{ \frac{\tilde{\alpha} \partial_x \zeta}{1 + (\partial_x \zeta)^2} + \frac{\tilde{\beta}}{1 + (\partial_x \zeta)^2} \partial_x \left[\frac{\partial_{xx} \zeta}{(1 + (\partial_x \zeta)^2)^{3/2}} \right] \right\} \quad (108)$$

where $\tilde{\alpha} = \epsilon D/2$ and $\tilde{\beta} = D\Gamma\ell$. As usual, $\epsilon = \Omega F_0 \ell^2 / D$ measures the distance from the threshold: since desorption is absent, it is equal to the Péclet number [113] and represents the ratio of the ‘step velocity’ ($\simeq F_0 \ell \Omega$) to the diffusion velocity of the adatoms ($\simeq D/\ell$).¹²

Eq. (108) –which is valid for the one-sided model (infinite ES barriers)– has the form of a conservation law: $\partial_t \zeta = -\partial_x J$. In fact the evolution of each step is determined by the adatoms falling and diffusing on the front terrace and by rearrangement of the step profile through detachment/reattachment of adatoms from the step itself. The effect of these processes is that Eq. (108) looks like the evolution of a one dimensional high-symmetry surface. Nevertheless, major differences must be stressed: the dynamics of a high-symmetry surface are only determined (in the absence of desorption) by surface diffusion, which would correspond in the present context to step-edge diffusion, a process which is indeed forbidden in the above model! Secondly, the form of Eq. (108) would be completely different if only one step was considered (see chapter VD) and the limit $x_s \rightarrow \infty$ would not be allowed.

It is now interesting to comment on the expression for the current J :

$$J = \frac{\tilde{\alpha} m}{1 + m^2} + \frac{\tilde{\beta}}{1 + m^2} \partial_x \left[\frac{m'}{(1 + m^2)^{3/2}} \right] \quad (109)$$

where we have introduced the local slope of the step $m = \partial_x \zeta$ in order to make the analogy with a one dimensional surface clearer.

The term proportional to $\tilde{\alpha}$ plays the role of the unstable current due to the ES effect, while the second term should represent a current *à la* Mullins, but not in its ‘standard’ linear form ($\sim m''$): the nonlinearity inside square brackets is nothing but the nonlinear chemical potential, if the surface tension σ does not depend on the orientation (see Eq. (23)). Conversely the prefactor $\tilde{\beta}/(1 + m^2)$ represents a sort of slope-dependent conductivity which is due –in the present context– to ‘kinetic’ interaction between steps.¹³

The latter nonlinearity plays a fundamental role, as easily seen by the study of the stationary configurations $J \equiv 0$. In fact, the reduction of the mobility exactly cancels the same factor in the $\tilde{\alpha}$ -term so that the unstable current never decreases. Introducing the variable $M = m/\sqrt{1 + m^2}$, the equation determining stationary configurations takes the form $\tilde{\beta} M''(x) = F(M) \equiv -\tilde{\alpha} M/\sqrt{1 - M^2}$. Since $|F(M)|/M$ is an increasing function of the slope, the wavelength λ of the profile is expected to *decrease* with the maximal slope (and therefore with the amplitude A). This analysis is confirmed by the exact evaluation of λ and A [104]. As a consequence of this, the system does not coarsen and the step develops an unstable pattern whose wavelength keeps constant and equal to the most unstable mode $\lambda_u = 2\pi\sqrt{2\tilde{\beta}/\tilde{\alpha}}$. The step width increases as $\sqrt{\ell}$ without bound, as can be easily checked by replacing the ansatz $\zeta(x, t) = A(t)g(x)$ in (108) [104,114]. A numerical solution of Eq. (108) and full lattice gas simulations confirm the previous picture [104]. Finally, an in-phase meandering of (1,1,17) Cu surfaces has been recently observed by Schwenger et al. [115] at a sufficiently low temperature.

Different and more phenomenological approaches [105] do not provide the nonlinear prefactor $\tilde{\beta}/(1 + m^2)$ in Eq. (109) and therefore coarsening along the step should be allowed. However, the direct integration of the continuum equation does not seem to display coarsening, which is indeed found in Monte Carlo simulations [105].

F. Continuum description and step flow

In this chapter we address the following question: is it possible to link the step-motion picture for a vicinal surface, with a continuum description based on the surface current? In the step-motion picture we have a train of steps

¹²It can also be read as the adatom density per lattice site, due to the incoming flux.

¹³If ℓ is the step-step distance in the direction perpendicular to straight steps, the shortest path between steps with slope m is $\ell/(1 + m^2)$. In a certain sense the adatom mobility must be reduced by the same factor in order to keep the travel time between neighbouring steps constant.

whose profiles are given by $\zeta_n(x, t)$, where x is the average direction of the steps. Let y be the in-plane direction perpendicular to x and ℓ the average distance between steps. If the steps are straight and equally spaced, then $\zeta_n \equiv 0$ and the height z of the surface is simply given by: $z(x, y, t) = -y/\ell$.

In the general case of a step profile depending both on x and n we should pass to a continuum function $\zeta(x, y, t)$. This is allowed only if $\zeta_n(x, t)$ changes by a small amount from one step to the next one: this is clearly true for an in-phase step-motion, but for an out-of-phase step-flow –as the one which takes place during evaporation because of step-bunching– it is surely not true.

For in-phase motion, it is easily found that:

$$z(x, y, t) = [\zeta(x, t) - y]/\ell \quad (110)$$

and

$$\partial_t z = \partial_t \zeta / \ell, \quad \vec{m} = \nabla z = (1/\ell)(\partial_x \zeta, -1) \quad (111)$$

Let us now suppose that evaporation is negligible so that the conservation equation $\partial_t z = -\nabla \cdot \vec{j}$ holds. Since \vec{j} depends on \vec{m} and higher order derivatives, $\nabla \cdot \vec{j} = \partial_x j_x$, and according to Eq. (111) we obtain:

$$\partial_t \zeta(x, t) = \ell \partial_t z = -\partial_x(\ell j_x) \equiv -\partial_x J \quad (112)$$

Therefore, the in-phase train of steps moves according to one-dimensional conserved dynamics via the current $J = \ell j_x$. To make this relation more explicit we can write:

$$J(\partial_x \zeta) = \ell j_x(m_x, m_y) = \ell j_x(\partial_x \zeta / \ell, -1/\ell) \quad (113)$$

As an example, we will consider the current:

$$\vec{j} = K \nabla(\nabla^2 z) + f(m) \vec{m} \quad (114)$$

which gives rise to the current J :

$$J = \ell [K \partial_x(\nabla^2 z) + m_x f(m)] = K \partial_x^3 \zeta(x, t) + f(m_0 [1 + (\partial_x \zeta)^2]^{1/2}) \partial_x \zeta(x, t) \quad (115)$$

where $m_0 = 1/\ell$.

Since $f(m_0) > 0$ the solution $\zeta = 0$ is unstable and the critical wavelength is given by $\lambda_c = 2\pi\sqrt{K/f(m_0)}$. It may be interesting to compare the expression of J with what is found from a step-motion approach in the linear limit $\zeta \rightarrow 0$. It is clear that the dispersion relation relevant for the current J is $\omega(q) = \alpha^* q^2 - \beta^* q^4$, with $\alpha^* = f(m_0)$ and $\beta^* = K$. The function f can be derived from the BCF theory in the limit $m_0 \ell_D \gg 1$ (corresponding to the absence of nucleation on the terraces, see Eq. (14)). We find $\alpha_1^* = F_0 \ell_{ES} \ell^2 / [2(\ell + \ell_{ES})]$. Conversely, the step-motion approach (Eq. (95)), in the absence of desorption gives $\alpha_2^* = F_0 \ell_{ES}^2 \ell^2 / [2(\ell + \ell_{ES})^2]$ and $\beta^* = \tilde{\Gamma} \rho_{eq}^0 \ell D$, which –for an infinite ES effect– reduce to the quantities $\tilde{\alpha}, \tilde{\beta}$ introduced in Eq. (108). Only in the same limit α_1^* and α_2^* are equal, while they differ for a weak ES effect. We have not been able to clarify the reason of this disagreement.

G. Step flow and nucleation

In this chapter we have seen that the steps of a growing vicinal surface are subject to a meandering instability, but do not undergo a step-bunching instability: the terrace width keeps constant and steps move in phase. In the introduction to the part on vicinal surfaces we raised the question of step-flow stability against ‘three-dimensional growth’. The transition may be induced by nucleation: between two steps a new terrace comes up and –because of the ES effect– a mound structure tends to develop; on the other side, the upper advancing step tends to capture and embed the new island, therefore restoring step-flow. In a certain sense, the faster of the two processes will establish if step-flow is stable or not. Competition between step-flow and two-dimensional nucleation has been seen –for example– by Tung and Schrey [116] during Silicon epitaxy.

The destabilizing phenomenon is not the nucleation event by itself, but the mound which can form on the new island. For a weak ES effect on a one dimensional surface, the probability to nucleate a second island on it before the incoming step captures the first one is of the order of $(\ell/\ell_D)^4$, a vanishing probability for $\ell_D \rightarrow \infty$. In the opposite limit of an infinite ES effect, this probability is of order unity and therefore the instability eventually develops. This is clearly shown in simulations by Krug and Schimschak [108], who also evaluate the time t_{ins} necessary for

the instability to take place. They calculate t_{ins} from the condition that a mound is formed whenever an atom is deposited on top of a mobile adatom and find [108] $t_{ins} \approx t_{ML} \ell^{-2} (D/F_0)^{3/4}$. We propose a different criterion: a mound is formed whenever a nucleation event takes place and therefore an island is formed. Since the nucleation probability per unit time on a terrace of size ℓ (see App. B) is [56,66] $P(\ell) \approx (1/t_{ML})(\ell/\ell_D)^4$, t_{ins} is nothing but $1/P(\ell)$: $t_{ins} \approx t_{ML}(\ell_D/\ell)^4 \approx t_{ML} \ell^{-4} (D/F_0)$.

The previous estimates are not applicable to a two-dimensional vicinal surface because they neglect step meandering. Indeed this phenomenon has been shown [105] to be relevant for the late time behaviour of the stepped surface in the absence of desorption, whose morphology looks very similar to that obtained on singular surfaces.

This is clearly seen in Fig. 15 which shows the evolution of a vicinal surface: points of the same step touch and join, and defects are therefore formed. These ones give rise –because of the ES effect– to the formation of three-dimensional structures and eventually to the destabilization of the surface.

VI. SHADOWING INSTABILITIES

When a crystal is grown from a beam, the beam is generally not normal to the surface, but has an oblique incidence. Then, if a bump is formed, it may have a ‘shadow’ which influences the growth and contributes to making the growing surface unstable (Fig. 2d). The resulting profile is obviously asymmetric. In certain cases of technological interest, the deposit takes a *columnar* structure (Fig. 16). The initial phase of column formation may be viewed as an instability, and has been treated by the same analytical methods as other instabilities [118,119], namely non-linear equations of the KPZ type.

Columnar growth is usually observed when an intense atomic beam is deposited on a fairly cold surface moving at a high velocity. This process is used in technological devices [120–122], for instance for the manufacture of magnetic tapes. This technology is quite different from MBE, since neither the substrate nor the deposit are single crystals, and columns are separated by voids. However, in both cases ballistic deposition takes place from a beam of incoming particles. In MBE, one tries to avoid bump formation, so that shadowing effects are negligible. This result is obtained by a slow deposition rate at high enough temperature on a rotating sample. If these conditions are not realized, bumps or crevasses can appear as described in chapter IV, and then oblique incidence produces shadowing.

The columns have a well defined direction which makes an angle β with the normal to the surface. This angle is an increasing function of the incidence angle α (Fig. 16). Experimentally, a simple relation

$$\tan \beta = \frac{1}{2} \tan \alpha \quad (116)$$

is sometimes observed [123]. Its validity is limited to low temperatures [124]. Theoretical attempts to relate β to α have been made, using either the continuous (linearized) equations valid in the incipient stage [124], or geometric considerations applicable to fully developed columnar growth [125,126]. The theoretical results are more complicated than formula (116) and suggest that β does not depend only on α , but also on the ratio of the beam intensity to the diffusion constant [124] or on the density of the deposited film [126]. It is noteworthy that the theories do not take the crystal structure into account, although the formation of columnar structures which can arise at normal incidence as a consequence of the Ehrlich-Schwoebel effect [56,58] is related to the crystal structure.

As mentioned above, the deposited film is porous and polycrystalline. However, the direction of the column is a symmetry axis of the crystals [121,126]. This property, which is of importance for technological use, does not seem to have received a theoretical explanation.

VII. WETTING AND NON-WETTING

In previous chapters it was assumed that the growing crystal is semi-infinite in the growth direction. However, for many applications, the growing crystal (‘adsorbate’) is deposited on a substrate which is a chemically different material. One generally wishes that the adsorbate forms a homogeneous layer with a planar surface. If it is so, it is said that the adsorbate *wets* the substrate, and layer by layer growth is possible. It is not always possible. The conditions of stability of a homogeneous adsorbate with a planar surface will be investigated in this chapter and in the following ones.

In contrast with the previous chapters, where the instability was of kinetic nature, we shall now mainly discuss thermodynamics.

A planar surface is stable at equilibrium if it minimizes the free energy. Alternatively, one can minimize the difference between the free energies of a state with a deformed surface (with bumps and valleys) and of the state with

a planar surface, and the same mass of adsorbate and substrate. This difference will be called ‘free energy increment’ and must be positive for all deformations if the plane surface is to be stable. The forthcoming search for instabilities will be a search for negative free energy increments.

A part of the free energy density excess is localized at the interfaces and surfaces. An obvious reason is the fact that chemical bonds should be broken to make a surface. This localized part is called *capillary* free energy, because it is responsible for the familiar phenomena which arise in thin (‘capillary’) pipes. It is present in liquids as well as solids.

Another part of the free energy density excess which results from the creation of interfaces and surfaces is due to elasticity. It is delocalized, in the sense that it decays but slowly when the distance to the interface increases. It may be interpreted as resulting from a distortion of the chemical bonds in the whole system. It exists only in solids, and is especially important when the adsorbate takes the lattice constant imposed by the substrate. In this case, called *coherent* epitaxy, the topology of the crystal is preserved.¹⁴ Since the misfit $\delta a/a$ defined in paragraph I A is never completely equal to 0, the adsorbate is strained with respect to its natural size, and this generates elastic effects which will be studied in the next chapters. In the present chapter, this elastic contribution will be neglected, as it is correct in the case of liquids. Elasticity is presumably not very important in the growth of a solid, even on another solid, if this growth is incoherent (i.e. the crystal topology is broken).¹⁵

If elasticity is ignored, the stability condition of a plane interface, established by Young at the beginning of the nineteenth century, is that the free energy per unit area $\tilde{\sigma}_{sg}$ of the substrate-gas interface is larger than the sum of the free energy per unit area $\tilde{\sigma}_{sa}$ of the substrate-adsorbate interface, plus the free energy per unit area $\tilde{\sigma}_{ag}$ of the adsorbate-gas interface, namely

$$\tilde{\sigma}_{sg} > \tilde{\sigma}_{sa} + \tilde{\sigma}_{ag} \quad (117)$$

If (117) is not satisfied, droplets form during growth. Their contact angle θ is given by Young’s formula

$$\cos \theta = (\tilde{\sigma}_{sg} - \tilde{\sigma}_{sa}) / \tilde{\sigma}_{ag} \quad (118)$$

In certain cases (Volmer-Weber growth) droplets form directly on the substrate. This occurs for Pb on graphite(0001). In other cases (Stranski-Krastanov growth) a few complete layers are deposited before droplets form (Fig. 17). This occurs for Pb on Ge(111) [4,127].

The droplet size is determined by kinetic mechanisms [128–130]. In MBE growth, it is mainly limited by diffusion of the atoms deposited on the surface, which try to go to the nearest forming droplet. Since diffusion is slow, Volmer-Weber and Stranski-Krastanov droplets are small, much smaller than water droplets which are familiar in our everyday life. The size of liquid droplets is close to the equilibrium size, determined by gravity. They form through collective, hydrodynamic motions, not through atom diffusion. In the small solid droplets which arise from Volmer-Weber and Stranski-Krastanov growth, gravity is negligible and the droplet shape is fully determined by surface tension. In the case of a liquid, droplets would actually be parts of spheres, whose angle with the plane is determined by (118). In the case of a crystal, the shape can be determined from the Wulff construction [3,4]. It is often rather spherical at high enough temperature, but it is faceted at low temperature, as mentioned in paragraph I B.

Droplet formation caused by the interface energy can be regarded as a growth instability, but there is not much to say about it. If one wishes to grow a smooth adsorbate, non-wetting materials are just excluded. On the other hand, there are, to our knowledge, no technological applications of *incoherent* Volmer-Weber and Stranski-Krastanov droplets. However similar droplets can arise from a cause which is not the surface tension, as will be seen in the next chapters. From now on, (117) will be assumed to be satisfied, but elastic effects will be taken into account.

VIII. COHERENT AND INCOHERENT EPITAXY: MISFIT DISLOCATIONS AND CRITICAL THICKNESS

¹⁴This statement applies to most of the cases considered in this review, but is an oversimplified generalization. For instance, coherent epitaxy of bcc Fe on fcc Ag is possible although the topology of the two lattices is different. Another example is MgO on Fe. The extension to these cases of the concept of coherence is straightforward.

¹⁵Elasticity can be important for the mechanics of two solids glued together, since temperature variations can produce bending or crack formation, independently of epitaxy and coherence.

A. Misfit dislocations

From now on, the attention will be focussed on the epitaxial deposit of an adsorbate on a substrate which has a fairly small misfit, say $\delta a/a < 0.1$. As seen in the previous chapter, the adsorbate can be coherent or incoherent. For a sufficiently small misfit (to be precised below) the ground state of an epitaxial adsorbate of given thickness h is coherent if h is small enough. In this state, the crystal topology is that of a perfect crystal, in particular each atom has the same number of nearest and next-nearest neighbours which form the same geometrical figure with only slightly modified distances.

The coherent state can become unstable if h is increased or for another reason. In the new, incoherent ground state, the crystal topology is perturbed at the interface. Far from the interface, a perturbation of the crystal topology involves a large energy (at least if h is large). Therefore, the crystal topology far from the interface will first be assumed to be the same as in the coherent state, although this assumption will be seen not to be always correct.¹⁶

At the interface, it can be shown [131] that, if $|\delta a/a| \ll 1$, the crystal topology is but weakly perturbed in large domains separated by lines. These lines, along which the perturbation is large and linear elasticity is not applicable, are called ‘misfit dislocations’.

These line defects are indeed dislocations of the coherent state. This can be understood if one measures the atomic displacements \vec{u} and the strain $\{\epsilon_{\alpha\gamma}\}$ with respect to this coherent state. Let us consider the variation $\delta\vec{u}$ of \vec{u} along a path joining the centers A and B of two neighbouring domains on the interface. If the path is through the substrate, $\delta\vec{u} = 0$. However, along a path through the adsorbate, the variation of this displacement is the integral of the strain from the coherent state, and the components ϵ_{xx} and ϵ_{yy} of this strain parallel to the surface have a well-defined sign, that of $\delta a/a$. The integral can therefore not vanish. Along a closed circuit going from A to B through the adsorbate and then from B to A through the substrate, the variation $\vec{b} = \delta\vec{u}$ does not vanish. This is the typical property of a dislocation and \vec{b} is the so-called ‘Burgers vector’ of this dislocation.

An example of a misfit dislocation imaged by high resolution electron microscopy is shown in Fig. 18.

If the crystal topology is perturbed only near the dislocation line (in the so-called dislocation ‘core’) the Burgers vector has to be a lattice vector and the dislocation is called a perfect dislocation. It turns out that, if h is not very large, the state of lowest energy often involves ‘partial dislocations’, characterized by a Burgers vector which is a rational fraction of a lattice vector. Partial dislocations are the edges of two-dimensional defects, e.g. stacking faults. For many crystal structures, e.g. the face-centered cubic lattice, stacking faults have a rather low energy, while the energy of a dislocation of large Burgers vector is high. Thus, it can be preferable to create partial dislocations. The low energy of stacking faults often results from the fact that the environment of each atom is weakly perturbed up to nearest neighbours, and the crystal topology is only modified if next-nearest neighbours are taken into account.

An example is provided by intrinsic stacking faults generated by Shockley partial dislocations with $\vec{b} = (1/6)[112]$ in FCC lattice (Fig. 19).

In an ordered alloy, the two-dimensional defect related to a partial dislocation can be an antiphase boundary rather than a stacking fault.

Misfit dislocations have the topological properties of ordinary dislocations. An essential difference is that they can be present in the ground state because their energy can become negative. Actually, the free energy associated with a dislocation can be written as a sum of 4 terms,

$$\mathcal{F}_{tot} = \mathcal{F}_{disloc} + \mathcal{F}_{step} + \mathcal{F}_{fault} + \mathcal{F}_{disloc/film} \quad (119)$$

The first 3 terms are also present in a pure system and are usually positive. The first term \mathcal{F}_{disloc} is the volume integral of the elastic energy associated, for $\delta a/a = 0$, to the strain produced by the dislocation. The second term \mathcal{F}_{step} is the free energy of the step which is necessarily created (or, exceptionally, destroyed) if the Burgers vector has a vertical component (i.e. normal to the interface). The third term \mathcal{F}_{fault} , only present in the case of a partial dislocation, is the free energy of the stacking fault or antiphase boundary created by the dislocation.

The last term $\mathcal{F}_{disloc/film}$ is negative. It is the elastic energy gain resulting from the strain relaxation in the adsorbate when the dislocation is created. It is responsible for the presence of misfit dislocation in the ground state. The free energy \mathcal{F}_{tot} depends on the thickness h of the adsorbate and becomes negative when h is greater than a threshold h_c called ‘critical thickness’, calculated in the next paragraph.

¹⁶In other words, the attention will first be focussed on perfect dislocations, while partial dislocations, to be defined below, are often created when h is not yet very large.

B. Critical thickness

Nucleated dislocations and threading dislocations

Misfit dislocations can originate from two different mechanisms, i) nucleation of dislocations on defects, surface etc. and ii) propagation of preexisting dislocations of the substrate (threading dislocations). The density of threading dislocations may be very low if the substrate is of good crystalline and surface quality, and the nucleation of new dislocations is not easy since it may involve a high energy barrier. Thus, the thickness of the coherent adsorbate may be larger than the critical thickness calculated from thermodynamics. Moreover, the dislocations which are observed are not necessarily those which have the lowest energy, but those which correspond to the lowest activation energy, as will be seen later. Nucleation of dislocations at the surface is of particular importance in this review.

Climb and glide of dislocations

In the case of dislocations which are nucleated at the surface, they have to propagate down to the substrate-adsorbate interface, and they have *a priori* two possible ways to do that, which are called ‘climb’ and ‘glide’. Climb implies mass transport by diffusion in the bulk and is generally possible only at high temperature. In Fig. 20, an edge dislocation with a Burgers vector parallel to the interface (the best way to relax the elastic energy) has been introduced by climb from the free surface.

In usual growth conditions, only glide of dislocations is possible. On the other hand, in the case of layer by layer growth, the epilayer is continuous and the glide plane cannot be parallel to the interface. A consequence, which might be seen from geometry, and also results from the formulae given below, is that \vec{b} is in the glide plane. On the other hand, in the case of layer by layer growth, the epilayer is continuous and the glide plane cannot be parallel to the interface. This implies that the Burgers vector has a vertical component (Figs. 21 and 19). As will be seen, this component does not contribute to the relaxation, but has a cost in energy.

Critical thickness for the equilibrium state.

One can imagine two extreme definitions of the critical thickness. i) In a strictly thermodynamic sense, one might state that the critical thickness is reached as soon as one can find a dislocation of any kind which has a negative energy per unit length. This approach would lead to a strongly underestimated value of h_c . ii) A complete study would evaluate all energy barriers which correspond to all possible dislocations. This would be rather tedious.

Our approach in this paragraph is intermediate. The critical thickness h_c will be defined as the thickness beyond which the energy per unit length $U_{tot}(h)$ of a dislocation lying at the interface is negative, *provided this dislocation can be created by glide*. This definition discards dislocations with a Burgers vector parallel to the surface plane, which, as will be seen, have a lower energy but can only be created by climb, an extremely slow process. As will be seen in chapter X, it may happen that, on a planar, high symmetry surface, dislocations do not appear, presumably because their nucleation energy is too high. Instead, the adsorbate forms bumps or clusters, and only then, dislocations appear, probably because surface irregularities allow the formation of dislocations of lower energy.

The critical thickness h_c is given by

$$U_{tot}(h_c) = U_{disloc}(h_c) + s\gamma + U_{fault} + U_{disloc/film}(h_c) = 0 \quad (120)$$

where the 4 terms correspond to the 4 terms of (119), γ is the step energy per unit length, which has to be respectively added ($s=1$) or subtracted ($s=-1$) if creating a dislocation emerging at the surface creates or destroys an atomic step. The case $s=-1$, where the dislocation has nucleated on a preexisting step, lowers the critical thickness. However this process seems unlikely because the step would have to be a straight line whose direction is imposed by the intersection of the glide plane and the surface. A schematic representation of a dislocation propagating in the glide plane is shown on Fig. 22. The glide system is defined by the angle β between the Burgers vector and the dislocation line lying on the interface between the substrate and the epilayer, and the angle ϕ between the glide plane and the surface of the epilayer. The procedure is i) to evaluate the dislocation energy and the nucleation barrier for all possible¹⁷ values of β and ϕ , and ii) to look for the values of these parameters which yield the lowest energy for a reasonable barrier height. The step (ii) will not be carried out in detail here.

¹⁷Here, ‘possible’ means that these parameters correspond to an actual glide system.

In this paper, we will present only the case where the substrate and the epilayer are isotropic elastic media with identical Poisson ratio ν and Young modulus E . The self-energy per unit length of a dislocation lying at the interface may be written [132] as

$$U_{disloc}(h) = Eb^2 \frac{1 - \nu \cos^2 \beta}{8\pi(1 - \nu^2)} \ln\left(\frac{\alpha h}{b}\right) \quad (121)$$

where α depends on β and ϕ , and on the core of the dislocation, a region where linear, continuous elasticity does not hold, since it would predict infinite strains and stresses. The value of α is controversial. The estimates for $\beta = 60^\circ$ and $\bar{b} = (1/2) < 110 >$ lie between 0.6 [133] and 2.0 [134]. In works related to Si-Ge strained layer structures, α is often taken [132] equal to 4. The expression of the dislocation energy in Matthews' paper [135] corresponds to $\ln \alpha = 1$. A precise expression of the energy of a dislocation near a free surface has been obtained by Freund [136]. It relates $U_{disloc}(h)$ to ϕ , the core radius r_c and the core energy U_{core} which can be evaluated in semiconductors, using atomistic simulations based on empirical interatomic potentials [137,138].

The third term of (120), present in the case of a partial dislocation only (Fig. 19) is

$$U_{fault} = \tilde{\sigma}_{fault} \frac{h}{\sin \phi} \quad (122)$$

where $\tilde{\sigma}_{fault}$ is the energy per unit area of the stacking fault or antiphase boundary associated with the dislocation.

The fourth term of (120) is negative and proportional to the misfit,

$$U_{disloc/film}(h) = \frac{-E}{1 - \nu} \left| \frac{\delta a}{a} \right| hb \sin \beta \cos \phi \quad (123)$$

The factor $b \sin \beta \cos \phi$ can be justified as follows. Let the y axis be chosen parallel to the dislocation, z normal to the interface, and x perpendicular to z and y . With respect to the free material, the coherent adsorbate is compressed (if $\delta a/a > 0$) or stretched (if $\delta a/a < 0$) in the directions parallel to the plane. The effect of a misfit dislocation is to relax a part of this constraint. The amplitude of the relaxation is measured by $b_x = b \sin \beta \cos \phi$. The components b_z and b_y measure respectively a strain perpendicular to the interface, and a shear, which both do not contribute to the relaxation.¹⁸

Using formulae (121) to (123), the equation for the critical thickness (120) can be rewritten as¹⁹

$$h_c = \frac{b(1 - \nu \cos^2 \beta) \ln\left(\frac{\alpha h_c}{b}\right) + \frac{8\pi(1 - \nu^2)s\gamma}{bE}}{8\pi(1 + \nu) \sin \beta \cos \phi \left(\left| \frac{\delta a}{a} \right| - 2 \frac{1 - \nu}{E} \frac{\tilde{\sigma}_{fault}}{b \cos(2\phi) \sin \beta} \right)} \quad (124)$$

In Fig. 23, the dependence of the critical thickness on the misfit is displayed in the case of a perfect dislocation $(1/2)[101]$ with the glide plane (111) in a FCC lattice (case of Fig. 21). For this glide system, $\beta = 60^\circ$ and $\phi = 54.7^\circ$. The step energy has been neglected. The two values of α used in Fig. 23 correspond to two typical values of the core energy, which depends on the material. The critical thickness is seen to decrease rapidly with increasing misfit. For a misfit of about 4% the critical thickness reaches the lattice parameter and continuous elasticity theory must be replaced by calculations taking into account the discrete nature of atomic layers.

In metals the predicted and experimental values of h_c agree fairly well and are not very large in most of the cases which have been studied. However the critical thickness may be much larger than the prediction in some materials. For example, under certain growth conditions, Ge/GaAs remains coherent up to 2 μm , while the theory gives 300 nm [139]. This discrepancy is presumably related to the large value of h_c .

¹⁸A detailed calculation would make use of formula (149) of chapter IX.

¹⁹If the denominator in (124) is negative, the critical thickness for the particular type of defect of interest is infinite, and that type of defect is discarded because the energy cost of the fault is larger than the gain due to relaxation.

C. Nucleation of a dislocation at the growing surface

If the density of preexisting dislocations in the substrate is not sufficient to relax the stresses during growth by the extension of threading dislocations, dislocations must be nucleated, and this involves an activation barrier. Possible sources for dislocations are:

- Homogeneous nucleation of half-loops (whole or partial) at the free surface of the epilayer.
- Homogeneous nucleation of half-loops at the substrate/epilayer interface.
- Heterogeneous nucleation of complete loops at a growth defect in the bulk of the epilayer.
- Nucleation of half-loops at the edges of islands in 3d growth or at the free surface defects.
- Multiplication of dislocations, for instance by cross-slip.

The homogeneous nucleation of a dislocation half-loop at the free surface (Fig. 24) is energetically more favourable than the homogeneous nucleation of a complete loop at the substrate/epilayer interface [140]. The formation energy \mathcal{F}_{tot} of a half-loop of radius r on a plane inclined at an angle ϕ with respect to the surface has the form (119), where [141]

- The self-energy is approximately equal²⁰ to

$$\mathcal{F}_{disloc} = \frac{E (1 - \nu/2) r b^2}{8 (1 - \nu^2)} \ln\left(\frac{\alpha r}{b}\right) \quad (125)$$

- The step energy is

$$\mathcal{F}_{step} = 2 r s \gamma \quad (126)$$

where $s = 1$ if a step is created, $s = -1$ if a step is annihilated.

- The stacking fault free energy (in the case of a partial dislocation) is

$$\mathcal{F}_{fault} = \frac{\pi r^2}{2} \tilde{\sigma}_{fault} \quad (127)$$

- The elastic energy relieved by the loop is the work done by the biaxial stress $\{\sigma_{\alpha\gamma}\}$ applied to the area of the loop for a displacement equal to the Burgers vector \vec{b} :

$$\mathcal{F}_{disloc/film} = -\text{Area} \times \sum_{\alpha\gamma} n_{\alpha,\gamma} \sigma_{\alpha\gamma} b_\gamma = -\frac{\pi r^2}{2} b \sigma \sin \beta \sin \phi \cos \phi \quad (128)$$

where \vec{n} is the unit vector perpendicular to the area of the half loop. Near the surface, the non-vanishing stress components are only $\sigma_{xx} = \sigma_{yy} = \sigma$, proportional to $\delta a/a$ as seen below from formula (131).

In addition to the factor $\sin \beta \cos \phi$, already present in (123), formula (128) contains the factor $\sin \phi$. Thus, only inclined glide planes ($\phi \neq 0$ or $\pi/2$) can be involved in the nucleation process.

As r increases from 0, the total energy (119) of the half-loop increases, reaches a maximum for $r = r_c$ and then decreases. The critical radius r_c is then given by $d\mathcal{F}_{tot}/dr = 0$ or

$$r_c = \frac{E (1 - \nu/2) b^2 [1 + \ln(\alpha r_c/b)] + 16 (1 - \nu^2) s \gamma}{8 \pi (1 - \nu^2) (\sigma b \sin \beta \sin \phi \cos \phi - \tilde{\sigma}_{fault})} \quad (129)$$

This gives the energy barrier for dislocation nucleation,

$$\mathcal{F}_c = r_c s \gamma + \frac{E r_c b^2 (1 - \nu/2) [\ln(\alpha r_c/b) - 1]}{16 (1 - \nu^2)} \quad (130)$$

²⁰There is a close parallelism between the formulae of this paragraph and those of paragraph VIII B. For instance, formula (125) can be obtained from (121) by multiplying by the half-loop length πr and replacing $\cos^2 \beta$ by $1/2$ and h by r .

At the beginning of the relaxation, the biaxial stress for an isotropic material is :

$$\sigma = \frac{-E}{1-\nu} \frac{\delta a}{a} \quad (131)$$

If γ and $\tilde{\sigma}_{fault}$ are neglected as well as logarithmic factors, insertion of (129) into (130) shows that \mathcal{F}_c varies as b^3 . This favours nucleation of *partial* dislocations, which have smaller Burgers vectors. For instance, Dynna et al. [142] calculated the loop energy as a function of the loop radius for the epitaxial system $\text{Au}_{80}\text{Ni}_{20}/\text{Au}(001)$ for Shockley partial 90° dislocations $(1/6)[112]$ and perfect 60° dislocation $(1/2)[101]$ (see Fig. 25). At this composition, the misfit is 2.3%. The energy barrier for the nucleation of partial dislocations is clearly lower than that of perfect ones. This result may explain why stacking faults and twins have been observed in this system and similar ones.

D. Relaxation by an array of dislocations

Above the critical thickness, it is energetically favorable to introduce dislocations. The number of dislocations is limited by their interaction and depends on the substrate thickness. The epitaxial strains are progressively relaxed by the formation of a lattice of dislocations located at or near the interface between the epilayer and the substrate. The equilibrium density of dislocations is reached when the total elastic energy \mathcal{F}_{tot} is minimum. If, for the sake of simplicity, the step and fault energies are neglected, \mathcal{F}_{tot} can be written as the sum of the elastic energy \mathcal{F}_{film} of the homogeneously strained film, the self-energy of the dislocation lattice \mathcal{F}_{disloc} , the interaction $\mathcal{F}_{disloc/film}$ between the dislocations and the film, and the interaction $\mathcal{F}_{disloc/disloc}$ between dislocations. Thus

$$\mathcal{F}_{tot} = \mathcal{F}_{film} + \mathcal{F}_{disloc} + \mathcal{F}_{disloc/film} + \mathcal{F}_{disloc/disloc} \quad (132)$$

In homogeneous and isotropic materials, the first three terms are rather simple, and can be written readily. Indeed, \mathcal{F}_{film} is the elastic energy of a film strained biaxially by the substrate :

$$\mathcal{F}_{film} = \frac{E}{1-\nu} \left(\frac{\delta a}{a} \right)^2 hA \quad (133)$$

The self-energy and the dislocation/film interaction energy are proportional to the quantities U_{disloc} and $U_{disloc/film}$ given by (121) and (123).

In the case of an epilayer relaxed by two orthogonal periodic arrays of dislocations, one has

$$\mathcal{F}_{disloc} + \mathcal{F}_{disloc/film} = \frac{2\mathcal{A}}{\bar{d}} (U_{disloc} + U_{disloc/film}) \quad (134)$$

where \bar{d} is the average distance between dislocations and the factor 2 appears because of the 2 dislocation arrays. The most complicated term in (132) is the interaction between dislocations, $\mathcal{F}_{disloc/disloc}$. It depends on the distribution of the dislocations at the interface, which can be periodic or not. Furthermore, due to oblique glide plane, the Burgers vector has a component perpendicular to the surface. This component does not contribute to the relaxation. Two possible arrays of misfit dislocation may be considered:

1. An array of dislocations characterized by the two angles β and ϕ defined in paragraph VIII B, all dislocations having the same orientation.
2. An array of dislocations characterized by β and ϕ in which those components of the Burgers vector not relieving misfit strain alternate in sign. This case is represented in Fig. 26.

Exact expressions have been derived for the energy of an infinite array of identical periodic dislocations taking into account the interactions between them [143]. Using this theory, Jain et al. [144] calculated the strain relaxation. More recently, Dynna et al. [145] gave a closed form of the total energy for an alternating dislocation array. Their evaluation was based on Head's analytical calculation [146] of the stress field for a dislocation in a semi-infinite, isotropic body. Their results will be presented below, but let us begin with the earlier theories [139,147,148] which do not take into account the inhomogeneous part of the stress and strain fields associated with dislocations interactions. The total energy is written as the sum of the elastic energy of the epilayer homogeneously strained to ϵ_{res} (residual elastic strain) and the energy of the set of dislocations.

$$\mathcal{F}_{tot} = \mathcal{F}_{homo}(\epsilon_{res}) + \rho_{disloc} U_{disloc} \mathcal{A} \quad (135)$$

where \mathcal{F}_{homo} is the energy of the homogeneously strained epilayer and

$$\rho_{disloc} = \frac{2 \left| \frac{\delta a}{a} + \epsilon_{res} \right|}{b \sin \beta \cos \phi} \quad (136)$$

is the dislocation density. \mathcal{F}_{homo} is similar to \mathcal{F}_{film} in (133), but the misfit $\delta a/a$ must be replaced by the residual strain ϵ_{res} . The difference between \mathcal{F}_{homo} and \mathcal{F}_{film} takes into account both interaction energies $\mathcal{F}_{disloc/film}$ and $\mathcal{F}_{disloc/disloc}$ in a mean field way i.e. only the homogeneous part of the strain and stress due the dislocation array is considered. Then using (135, 136) and (123) the total energy can be written as :

$$\mathcal{F}_{tot} = \frac{E}{1-\nu} h \mathcal{A} \epsilon_{res}^2 + \left| \frac{\delta a}{a} + \epsilon_{res} \right| \mathcal{A} \frac{E b (1-\nu \cos^2 \beta)}{4 \pi (1-\nu^2) \sin \beta \cos \phi} \log \frac{\alpha R_{cut}}{b} \quad (137)$$

where the cut-off radius, R_{cut} is the minimum value of the thickness h and the interdislocation average distance \bar{d} . Fig. 27 displays the energy versus the residual strain (lower axis) and dislocation density (upper axis) for several adsorbate thicknesses. Below the critical thickness, the energy exhibits a singular minimum for a residual strain equal to the misfit and zero dislocation density. Above the critical thickness, the equilibrium occurs at ϵ_{eq} for a finite dislocation density. The critical thickness corresponds to the curve with a horizontal tangent when the residual strain is equal to the misfit.

When the inhomogeneous part of the stress and strain fields generated by the dislocation array is taken into account to calculate the interaction energy, the expression of the total energy is much more complicated. We present here an example of such an expression for the case of an epilayer relaxed by two orthogonal periodic arrays of alternating dislocations [142,149] (Fig. 26). The interaction energy is :

$$\mathcal{F}_{disloc/disloc} = \frac{2\mathcal{A}}{d} (U_{disloc,array}^{para} + U_{disloc,array}^{perp}) \quad (138)$$

where the factor 2 arises from the two sets of orthogonal dislocations, $U_{disloc,array}^{para}$ is the interaction per unit length of one dislocation with all other parallel dislocations and $U_{disloc,array}^{perp}$ is the interaction of one dislocation with all perpendicular dislocations. Their expressions are

$$\begin{aligned} U_{disloc,array}^{para} = & \frac{E b^2 \sin^2 \beta \cos^2 \phi}{8 \pi (1-\nu^2)} \times \\ & \left[\ln\left(\frac{d}{2\pi h} \sinh\left(\frac{2\pi h}{d}\right)\right) + \frac{2\pi h}{d} \coth\left(\frac{2\pi h}{d}\right) - \frac{2\pi^2 h^2}{d^2} \operatorname{csch}^2\left(\frac{2\pi h}{d}\right) - \frac{1}{2} \right] \\ & + \frac{E b^2 \sin^2 \beta \sin^2 \phi}{8 \pi (1-\nu^2)} \times \\ & \left[\ln\left(\frac{d}{\pi h} \tanh\left(\frac{\pi h}{d}\right)\right) + \frac{\pi h}{d} \left(\tanh\left(\frac{\pi h}{d}\right) - \coth\left(\frac{\pi h}{d}\right) \right) \right. \\ & \quad \left. - \frac{\pi^2 h^2}{2d^2} \left(\operatorname{sech}^2\left(\frac{\pi h}{d}\right) + \operatorname{csch}^2\left(\frac{\pi h}{d}\right) \right) + \frac{3}{2} \right] \\ & + \frac{E b^2 \cos^2 \beta}{8 \pi (1-\nu^2)} \left[\ln\left(\frac{d}{\pi h} \tanh\left(\frac{\pi h}{d}\right)\right) \right] \end{aligned} \quad (139)$$

and

$$U_{disloc,array}^{perp} = \frac{E \nu h b^2 \sin^2 \beta \cos^2 \phi}{2 (1-\nu^2) d} \quad (140)$$

Such an expression has been used to calculate the relaxation of MgO grown on the (001) surface of bcc iron at room temperature [149]. In this system the misfit is about 3.8%. The results of the measurements and the calculations are presented on Fig. 28. The open circles correspond to the experimental values of the relaxation as measured by electron diffraction (RHEED) during the growth. The glide system consists of perfect edge dislocations of Burgers vector $(1/2) < 011 >$ gliding on (101) planes. The curve called ‘equilibrium calculation’ corresponds to the minimization of the total energy \mathcal{F}_{tot} (eq. 132) with respect to the distance d between dislocations.

It is clear that the calculated relaxation within the equilibrium model is overestimated. The nonperiodic nature of the real dislocations arrays may explain this discrepancy. Indeed, even if the nucleation is homogeneous and the initial dislocation distribution is periodic, it is difficult to maintain the periodicity as the thickness and the number of dislocations increase. The periodicity can be maintained only if all existing dislocations move continuously to smaller spacings to make room for new dislocations. It has been shown [150] that this process requires more energy than the introduction of new dislocations in a nonperiodic way. Numerical calculations have been performed by Jain et al. [144] involving a uniform-random or a Gaussian dislocation distribution showing that the energy of the dislocation arrays is increased with respect total energy of periodic arrays having the same average dislocation density (i.e. the same relaxation ratio). This leads to a lower or slower relaxation rate. However, the real distribution of dislocations depends on the mechanism of nucleation and propagation. The nucleation may be the limiting process, when no threading dislocations are expected from the substrate of high quality. Nucleation plays also an important role in selecting a particular glide system of dislocations. The propagation of dislocations may also be the limiting process due to inhomogeneities of the stress field present in the layer where the dislocations are moving. The inhomogeneities of the stress field may result in a retaining force which may block the dislocation propagation. Such a phenomenon, when the source of inhomogeneous stresses are the other misfit dislocations, is called 'blocking mechanism'. It is the subject of the following paragraph.

E. Blocking mechanism

Just above the critical thickness, dislocations propagate to form two arrays of orthogonal dislocations. Freund [136] has shown that the interaction between a moving dislocation \mathcal{D}_1 and an orthogonal dislocation \mathcal{D}_2 impedes the motion of the segment \mathcal{D}_1 . Then this results in a lower relaxation rate than predicted by previous equilibrium calculations. This is shown schematically on Fig. 29. A moving dislocation \mathcal{D}_1 encounters a misfit dislocation \mathcal{D}_2 . The stress field generated by the blocking dislocation can completely suppress the traction force due to the residual stress in the epilayer. To bypass the blocking dislocation, \mathcal{D}_1 may alter its path by moving in the same glide plane but closer to the surface i.e. in a channel of width $h^* < h$. This reduction of the thickness reduces the driving force acting on \mathcal{D}_1 . Furthermore, the retaining line tension increases due to interaction with the surface (image forces). When \mathcal{D}_1 passes above \mathcal{D}_2 , three forces are acting on it :

- the driving force due to the residual homogeneous strain ϵ_{res}
- the retaining force due to the line tension of \mathcal{D}_1
- the interaction force associated with the stress field resulting from \mathcal{D}_2 .

Let us express the retaining forces acting on the element of \mathcal{D}_1 in terms of the residual strain needed to just compensate these forces.

i) The residual strain ϵ_{line} which exactly compensates the dislocation line tension can be found readily within the homogeneous strain approximation of the relaxation by minimizing \mathcal{F}_{tot} in (137) with respect to ϵ_{res} , and replacing h and R_{cut} by h^* (which corresponds to neglecting interactions between dislocations) :

$$\epsilon_{line} = \frac{(1 - \nu \cos^2 \beta) b \log(\frac{\alpha h^*}{b})}{8 \pi (1 + \nu) h^* \sin \beta \cos \phi} \quad (141)$$

ii) The residual strain, ϵ_{res} compensating the stress field $\sigma_D(x, z)$ of \mathcal{D}_2 can be expressed in terms of the forces resolved in the glide plane acting on an elementary segment of the dislocation:

$$\sum_{\alpha\gamma} \sigma_{D,\alpha\gamma} n_\gamma b_\alpha + \sum_{\alpha\gamma} \sigma_{res,\alpha\gamma} n_\gamma b_\alpha = 0 \quad (142)$$

where $\vec{n} = (1/\sqrt{2}) < 1\bar{1}0 >$ is the glide plane normal unit vector and $\vec{n} = (1/2) < 110 >$ the Burgers vector. The homogeneous biaxial stress tensor is related to the residual strain by :

$$\sigma_{res} = -\frac{E}{1 - \nu} \begin{pmatrix} \epsilon_{res} & 0 & 0 \\ 0 & \epsilon_{res} & 0 \\ 0 & 0 & 0 \end{pmatrix} \quad (143)$$

Now, the residual strain compensating the stress due to the blocking dislocation \mathcal{D}_2 for an elementary segment of \mathcal{D}_1 passing at the position (x, h^*) may be written for this glide system as :

$$\epsilon_{res}(x, h^*) = \frac{(1 - \nu)}{E} [(\nu - 1) \sigma_{D,xx}(x, h^*) + \nu \sigma_{D,zz}(x, h^*)] \quad (144)$$

To bypass the orthogonal dislocation stress field in the channel of width h^* , the residual strain $\epsilon_D(h^*)$ has to be greater than $\epsilon_{res}(x, h^*)$ for every position x . Then $\epsilon_D(h^*)$ is the maximum value of $\epsilon_{res}(x, h^*)$ when x is varying, this condition may be written :

$$\epsilon_D(h^*) = \epsilon_{res}(x_{max}, h^*) \quad (145)$$

$$\frac{\partial \epsilon_{res}(x_{max}, h^*)}{\partial x} = 0 \quad (146)$$

Since linear elasticity theory has been used, the two residual strains required to balance both retaining forces should be added to obtain the total residual strain as a function of the channel width h^* . Since the channel width is a free variable, the actual residual strain below which the moving dislocations are stopped is :

$$\epsilon_{min} = \text{Min}_{h^*} [\epsilon_D(h^*) + \epsilon_{line}(h^*)] \quad (147)$$

Relations (145), (146) and (147) constitute Freund's blocking criterion. They mean that the residual strain corresponds to a saddle point of the function $\epsilon_{res}(x, h^*) + \epsilon_{line}(h^*)$ in the two-dimensional space (x, h^*) . It has been found [151] that Freund's blocking criterion predicts a residual strain which is in good agreement with the strains found experimentally in $\text{Si}_{1-x}\text{Ge}_x$ film on Si(001). We have applied this blocking criterion to the relaxation of MgO grown on Fe(001) presented above [149]. The expressions of the stresses due to the blocking dislocation may be derived [150] from the Airy stress function as done by Freund [136] or more directly obtained from Dynna et al. [145]. Fig. 30 displays the residual strains $\epsilon_D(h^*)$, $\epsilon_{line}(h^*)$ and the sum of these, $\epsilon_{tot}(h^*)$ for a 100 Å layer of MgO deposited on Fe(001). Both residual strains behave as expected. The residual strain compensating the line tension is maximum near the surface and then decreases when the channel width, h^* increases. On the contrary, the residual strain compensating the orthogonal dislocation stress field increases as the channel width approaches the layer thickness h . The minimum of the total residual strain occurs at about $h^* = 70$ Å and $\epsilon_{tot} = 1.5\%$. Then at this layer thickness, the expected relaxation is estimated to 2.1% (the misfit between MgO and Fe is 3.6%). This value is in good agreement with the experimental one. On the Fig. 28, the relaxation calculated from the blocking criterion is represented. It is in better agreement than the equilibrium one presented above at least for high thicknesses. Although Freund's criterion predicts no relaxation when $h < 27$ to 30 Å, relaxation is clearly observed experimentally when $h > 20$ Å. This relaxation is possible because the density of blocking misfit dislocations is insufficient to block all of the threading segments present in the MgO film. Above 50 Å the agreement between theory and experiment improves continuously and the agreement is excellent at about 100 Å. The experimental results presented in Fig. 28 correspond to room temperature growth. For layers grown at higher temperature, the relaxation is faster [149,150]. This can indicate that nucleation is enhanced or that the blocking barrier is overcome by thermal activation. This example shows that other aspects of relaxation must be taken into account, e.g. the frictional stresses [152], the non-periodic nature of the dislocation array [144] or the multiplication mechanism [153]. The prediction of the relaxation rate depends on the growth conditions and is currently an active field of research.

IX. THE ASARO-TILLER-GRINFELD INSTABILITY AND RELATED PHENOMENA

A. Three-dimensional clusters as an alternative to misfit dislocations

1. Experimental facts

If a crystalline material is coherently adsorbed on a substrate which has a different atomic distance, it does not like it and tries to escape from this unpleasant situation which costs energy. There are several ways to escape. The most usual way is to make misfit dislocations (Fig. 31a) as seen in the previous chapter. However, mismatched epitaxial films can relax their strain through a different mechanism, namely a deformation of the surface or '2d-3d transition'. In III-V semiconductors, for example, this frequently occurs for a lattice mismatch above typically 2% in layers under compressive stress and for lower mismatch in layers under tensile stress. If the misfit is moderate, this deformation leads to alternating hills and valleys (Fig. 31b and 32) while for a stronger misfit, the adsorbed film splits into clusters (Fig. 33). These clusters will be studied in the next chapter.

The base of each hill is still highly constrained by the substrate, and the elastic energy density is high. However, at the top and on the sides of the hills, the adsorbate lattice constant is closer to that of the free adsorbate: the adsorbate is said to be 'relaxed'. The adsorbate is still coherent although dislocations always form in the later stages of the growth. The gain in elastic energy at the top of the clusters is the reason of the deformation, as will be seen more quantitatively in this chapter and in the following one.

For a given substrate and a given adsorbate, stress relaxation can occur through misfit dislocations or, without loss of coherence, through surface deformation according to the growth conditions. For instance, in InAs/GaAs or InAs/InP systems, cluster formation precedes dislocation formation on the (100) substrate, and on several high index surfaces [155–157]. On the contrary it is not observed on the other low index surfaces, e.g. [158] (110), (111)A and (111)B. A Ge deposit forms coherent clusters on Si(100), while it directly forms large incoherent clusters on Si(111) [159]. The substrate orientation obviously determines the surface energetics and kinetics. This hesitation of nature between the two kinds of instability has been analyzed for instance by Joyce et al. [158] and is not very well understood.

Nevertheless, we will try to understand a part of these phenomena.

2. Energetics

It is of interest to wonder about the ground state of a coherent, epitaxial film, even though it is never reached. Let us first ignore the interface energy and assume that there is only a surface energy and an elastic energy. For a large thickness, the elastic energy is proportional to the volume and dominates the surface contribution, so that the adsorbate tends to separate from the substrate and to form a single big cluster almost detached from the substrate (Fig. 34, last picture). This state obviously minimizes the elastic energy, and therefore the total free energy.

In reality, the ideal ground state can of course not be reached since the atoms would have to diffuse on very long distances, but, if the deposit is thick enough, big clusters can form and lower the energy.

The waves of figure 31b and 32 are presumably the incipient stage of the instability which leads to isolated clusters.

However, it turns out that big, coherent clusters (Fig. 34, last two pictures) are never observed. Dislocations appear in the cluster when it reaches a critical size [160–163] (Fig. 33) but the above argument helps us to understand why there is an instability, and also to predict the evolution of a population of clusters—a problem which will be addressed in chapter X. Moreover, even though shapes corresponding to the last two pictures of Fig. 34 are never observed, the shape of coherent clusters does depend on the size, in contrast with incoherent clusters of chapter VII. In particular, it will be seen in the next chapter that small clusters, dominated by the surface energy, are ‘platelets’ (Fig. 34, first picture).

To close these qualitative remarks on energetics, it is appropriate to consider the interface energy. When one wishes to make good epitaxial layers, one needs to have a strongly negative interface energy σ_{sa} , so that (117) is satisfied. This highly negative value is obtained by the choice of the materials, of the temperature, the fluxes, the growth rate, etc. If the interface energy is sufficiently negative, the first adsorbed monolayer(s) is/are stable even if the misfit is fairly strong. This stable layer is called a ‘wetting layer’ [164]. It is sometimes related to complex chemical reactions, e.g. in InAs on GaAs, where a (In,Ga)As alloy forms [158].

In the simplest cases, the existence of the wetting layer implies only a small modification of the above discussion. Cluster formation and wavy deformations do lower the free energy, but only after the wetting layer has formed. This picture applies to Ge/Si. In more complicated cases, there is experimental evidence that a considerable transfer of matter takes place from the wetting layer to the clusters. This seems to be the case in InAs/GaAs(001). This feature can be taken into account by simple theories [165] but, for the sake of simplicity, it will be ignored in the remainder of this review.

3. Kinetics

The thermodynamical analysis is probably not sufficient to determine the structure of an epitaxial deposit. Kinetic factors are presumably often essential, for instance for the choice between misfit dislocations and a three-dimensional modulation. The crystal chooses the fastest relaxation path in the phase space. The formation of misfit dislocations requires, as seen in the previous chapter, a purely microscopic atom motion inside the material, on a distance of the order of the atomic distance. In contrast, the formation of a three-dimensional structure involves atomic diffusion on the surface (which is much easier than in the bulk) but on much larger distances, typically hundreds of atomic distances. It is difficult to say which mechanism will be preferred.

A way to make the discussion more quantitative is to calculate the activation energy. That of misfit dislocations has been calculated in the previous chapter. The activation energy for the formation of a coherent cluster will be evaluated in the next one in the case of a singular surface.

4. Singular and non-singular orientations

In this chapter, the onset of the 2d-3d instability will be studied in the only case where a quantitative theory exists, [166,167] namely the case of a non-singular surface ($T > T_R$, see chapter I).

Unfortunately, most of the experiments and most of the technological applications, are concerned with (001) surfaces which are believed to be singular at the growth temperature. Nevertheless, experiments on non-singular surfaces would be feasible, and this justifies the forthcoming study. Moreover, the wavy deformations observed in weak misfits are in qualitative agreement with the theories of this chapter, as will be seen.

It will be shown in the present chapter that a plane surface of non-singular orientation is unstable with respect to spontaneous deformations of wavelength larger than some value λ_c . This value will be evaluated. This instability of a non-singular surface will be found to involve no activation energy, although the time of establishment of the instability will be seen to be very long for small misfits. The case of singular surfaces, e.g. the (001) surface of body centered cubic crystals, will be investigated in the next chapter and their instability will be seen to be subject to an activation energy.

B. The Asaro-Tiller-Grinfeld instability: thermodynamics

The stability of an initially planar system was investigated first by Asaro and Tiller [166] and later in great detail by Grinfeld [167] and other authors [3,168,169].

The simplest possible approach is the following: one calculates the energy of the system (substrate + adsorbate) when its surface has a weak sinusoidal plastic modulation of amplitude δh (Fig. 35a) and compares this energy to that of the planar surface ($\delta h = 0$). Here, the word ‘plastic’ means that the height modulation results from an irreversible modulation of the number of atoms, in contrast with an elastic strain.²¹ If the modulation produces an energy decrease, the planar surface is unstable. The method is in fact applicable to any *weak modulation*, because such a modulation can be Fourier transformed, and the strains produced by the various Fourier components below the modulated region can be calculated by linear elasticity theory and can just be added as in any linear problem. This additivity rule is not applicable in the modulated region but it does not matter since this region is very thin. This approach, in which the problem becomes linear, is called *linear stability analysis*. This method has already been used in chapters IV and V.

In this approach, the height of the surface can be assumed sinusoidal, namely

$$z(x, y) = \langle z \rangle + \delta h \cos(qx) \quad (148)$$

where q is a real, positive number.

Before going further, one should mention that the assumption of a sinusoidal, and therefore *continuous* modulation is acceptable only above T_R . Below T_R , continuous height changes are not possible as noticed in chapter I. In the remainder of the present chapter, the temperature T will be assumed higher than T_R . The case $T < T_R$, which presumably corresponds to a defect-free, high symmetry crystal surface, will be addressed in the next chapter X. The applicability of the various theories to real surfaces will be addressed in paragraph IX D.

It will be seen that (if gravity is neglected) the modulation (148) lowers the energy if q is small enough, so that the planar surface is *always* unstable.

This energy gain comes from the fact that, in the modulated part of the adsorbate, one can strain the material, so that its lattice constant becomes closer to the one it would like to have (i.e. that of the free adsorbate).

The free energy can be most conveniently written if the strain is measured with respect to the completely strained state, in which the lattice constant in the x and y directions is that of the substrate.²² If it were measured from the free adsorbate, it would be discontinuous at the interface. The free energy change resulting from the strain can be written as

$$\delta \mathcal{F}_1 = -\text{Const} \times \frac{\delta a}{a} \int_A d^3 r [\epsilon_{xx}(\vec{r}) + \epsilon_{yy}(\vec{r})] \quad (149)$$

²¹The word ‘plastic’ is often understood as implying dislocation formation. It is not the case here.

²² If it were measured from the free adsorbate, it would be discontinuous at the interface. Thus, the quantity denoted ϵ in this chapter and the following ones was called $\delta a/a + \epsilon_{res}$ in chapter VIII.

where \int_A denotes the integral over the adsorbate. The strain $\epsilon_{\alpha\gamma}(\vec{r})$ is measured with respect to the completely strained, coherent state, in which the lattice constant in the x and y directions is that of the substrate. A positive misfit corresponds to an adsorbate bigger than the substrate, so that the coherent adsorbate is compressed by the substrate (in the directions parallel to the surface). Relaxing this compression corresponds to a positive strain (from the completely strained state) and to a negative $\delta\mathcal{F}_1$. The constant depends on the elastic constants of the adsorbate. The integral on x and y vanishes for complete layers, so that (149) is proportional to the thickness δh of the modulated region. It is also proportional to the strain modulation amplitude ϵ , the misfit and of course to the area \mathcal{A} . Therefore

$$\delta\mathcal{F}_1 = -C_1 E_a \delta h \frac{\delta a}{a} \epsilon \mathcal{A} \quad (150)$$

where E_a is a typical elastic constant (e.g. the Young modulus) of the adsorbate and C_1 is a positive constant of order unity. The detailed calculation for an isotropic elastic medium²³ is available in original articles and textbooks [3,166–169]. The result is

$$C_1 = 1/(1 - \nu_a) \quad (151)$$

where ν_a is the Poisson ratio of the adsorbate.

The energy gain (150) is partially compensated by the quadratic part of the elastic energy, which can be written as

$$\delta\mathcal{F}_2 = \frac{1}{4} \sum_{\alpha,\gamma,\xi,\zeta} \int d^3r \Omega_{\alpha,\gamma}^{\xi,\zeta}(\vec{r}) \epsilon_{\alpha,\gamma}(\vec{r}) \epsilon_{\xi,\zeta}(\vec{r}) \quad (152)$$

where $\alpha, \gamma, \xi, \zeta = x, y, z$ and $\Omega_{\alpha,\gamma}^{\xi,\zeta}$ are the elastic constants, which are (known) functions of \vec{r} because they are not identical in the substrate and in the adsorbate.

The exact minimization of the total elastic energy $\delta\mathcal{F}_1 + \delta\mathcal{F}_2$ would be a hard task, on which mathematicians of the nineteenth century, e.g. Green and Dirichlet, have concentrated their efforts. For a small modulation δh , the problem is easy [3,166–169]. The strain which minimizes $\delta\mathcal{F}_1 + \delta\mathcal{F}_2$ when the surface is given by (148) is expected to be the real part of an expression of the form

$$\epsilon_{\alpha\gamma}(x, y, z) = \epsilon_{\alpha\gamma}^0 \exp(iqx) f(z) \quad (153)$$

where $\epsilon_{\alpha\gamma}^0$ and $f(z)$ can be determined from the equations of elasticity which have the form [171]

$$\sum_{\gamma\xi\zeta} \Omega_{\alpha\gamma}^{\xi\zeta} \partial_\gamma \partial_\xi u_\zeta = 0 \quad (154)$$

According to (153), the operator ∂_x should be replaced by iq and ∂_y by 0. Therefore, (153) can be solved by replacing ∂_z by $\alpha_0 q$, where the constant α_0 depends on the elastic constants, and should have a positive real part since the perturbation has to vanish for $z = -\infty$. In the case of an isotropic elastic medium, $\alpha_0 = 1$ [3,4]. In all cases, the penetration depth of the perturbation is proportional to the wavelength $2\pi/q$.

The quadratic part of the elastic energy in the bulk is thus proportional to $1/q$. In addition it is proportional to ϵ^2 and to the area \mathcal{A} . Finally,

$$\delta\mathcal{F}_2 = C_2 E \epsilon^2 \mathcal{A} / q \quad (155)$$

where E can be chosen as the Young modulus of the substrate, and the constant C_2 is of order unity. If the wavelength is much longer than the adsorbate thickness h , C_2 does not depend on the elastic constants of the adsorbate.

In the case of an isotropic solids [3,4],

$$EC_2 = \frac{E}{1 - \nu^2} \quad (156)$$

where ν and E are the Poisson ratio of the adsorbate (if $qh \gg 1$) or of the substrate (if $qh \ll 1$). If both materials have identical elastic constants E and ν , (156) applies without restriction.

²³The calculation might be done for a cubic crystal bounded by a (001) surface, using the corresponding elastic Green's functions [170].

Minimization of the total elastic energy $\delta\mathcal{F}_{el} = \delta\mathcal{F}_1 + \delta\mathcal{F}_2$ with respect to ϵ yields (assuming $E_a = E$, which is sufficient for our qualitative analysis)

$$\epsilon = \frac{qC_1}{2C_2} \frac{\delta a}{a} \delta h \quad (157)$$

and the total elastic energy $\delta\mathcal{F}_{el} = \delta\mathcal{F}_1 + \delta\mathcal{F}_2$ is

$$\delta\mathcal{F}_{el} = -\frac{q\delta h^2 C_1^2}{4C_2} \left(\frac{\delta a}{a}\right)^2 E\mathcal{A} \quad (158)$$

Thus, the elastic free energy change resulting from the sinusoidal deformation is negative.

However, there is another contribution to the free energy, which opposes the sinusoidal modulation. Indeed, this modulation increases the surface area, and therefore the surface energy or ‘capillary’ energy. The area increase is easily seen to be $\mathcal{A}\delta h^2 q^2/4$, and the capillary energy increment $\delta\mathcal{F}_{cap}$ is obtained by multiplying by a coefficient $\tilde{\sigma}$, called *surface stiffness*. Hence,

$$\delta\mathcal{F}_{cap} = \mathcal{A}\tilde{\sigma}\delta h^2 q^2/4 \quad (159)$$

If the strain is small, its effect on $\tilde{\sigma}$ can be neglected and the total energy is the sum

$$\mathcal{F}_{tot} = \mathcal{F}_{cap} + \mathcal{F}_{el} \quad (160)$$

Thus, the total energy increment per unit area is obtained by adding (158) and (159), and equal to

$$\delta\mathcal{F}_{tot}/\mathcal{A} = -\frac{q\delta h^2 C_1^2}{4C_2} \left(\frac{\delta a}{a}\right)^2 E + \tilde{\sigma}\delta h^2 q^2/4 \quad (161)$$

We conclude that, if a material is adsorbed on a substrate which has a different lattice parameter, its surface cannot be planar. The planar shape is unstable with respect to modulations of wavelength larger than

$$\lambda^* = \frac{2\pi C_2}{C_1^2} \frac{\tilde{\sigma}}{E} \left(\frac{a}{\delta a}\right)^2 \quad (162)$$

since (161) is negative is that case.

It follows from (161) and (162) that the free energy gain per unit area is proportional to $(\delta a/a)^4$ for a given amplitude δh .

In the instability discussed in this paragraph, the effect of the substrate is merely to produce an anisotropic, external stress. Such a stress can also be produced mechanically. This is the situation addressed for instance by Nozières [172], Grillé [173] and Kassner & Misbah [174] in their theoretical, nonlinear analysis, and by Thiel et al [175] in their experiments on He. An instability arises in both cases, but the long time evolution is quite different. In a mechanically stressed homogeneous material, the amplitude of the surface modulation can be very large. In contrast, when the stress is due to a substrate, the modulation is not expected to penetrate into the substrate. The former situation will not be addressed in the following, while the consequence of the presence of the substrate-adsorbate interface below the free surface will be discussed in paragraph IX E.

If, as we have just seen in this paragraph, the initially planar surface is unstable with respect to modulations of all wavelengths longer than (162), the actual structure which will appear is not yet clear. For short times, one can expect that the wavelength which will dominate the actual structure will be the one which develops more rapidly than the other ones. Thus, the preceding thermodynamic study is not sufficient and a kinetic treatment is necessary.

C. The Asaro-Tiller-Grinfeld instability: kinetics

1. Classical theory near equilibrium

Without calculation, we expect that fluctuations of longer wavelength require a longer time to form, since the atoms should come from longer distances to form the modulation. A more precise study of the evolution in time of the modulation (148) was initially done by Spencer et al. [176,177] and is reproduced below.

The translational invariance of the problem implies that, at short time, a small initial sinusoidal deformation remains sinusoidal, namely

$$z(x, y, t) = \langle z \rangle + \delta h(t) \cos(qx) \quad (163)$$

Insertion of (7) into (163) yields, neglecting the noise,

$$\frac{d\delta h}{dt} \cos(qx) = -\partial j(x, t)/\partial x \quad (164)$$

where the surface current density $j(x, t)$ is usually assumed [176] to be related to the chemical potential μ by a linear relation as explained in paragraph IV D 2,

$$j(x, t) = -\Upsilon \partial \mu(x, t)/\partial x \quad (165)$$

Relations (164) and (165) imply that the chemical potential μ has the form

$$\mu(x, t) = \mu_1(t) \cos(qx) \quad (166)$$

where the function $\mu_1(t)$ is related to $\delta h(t)$ by the following relation which follows from formulae (164) to (166).

$$\frac{d\delta h}{dt} = -\Upsilon q^2 \mu_1(t) \quad (167)$$

On the other hand, $\mu(x, t)$ is the free energy per atom, so that the free energy variation per unit time is, if $a^2 c$ is the volume per atom

$$\frac{d\mathcal{F}}{dt} = (a^2 c)^{-1} \int dx dy \mu(x, t) \frac{\partial z(x, t)}{\partial t} = (a^2 c)^{-1} \frac{dh(t)}{dt} \mu_1(t) \int dx dy \cos^2(qx) = \frac{1}{2} (a^2 c)^{-1} \mathcal{A} \frac{dh(t)}{dt} \mu_1(t) \quad (168)$$

Now, $d\mathcal{F}/dt$ can be related to the free energy calculated in paragraph IX B for a non-singular surface. In order to extend the theory to singular surfaces, we shall assume, following textbooks [178] that, as in any system, the free energy of weak fluctuations is quadratic with respect to the variables which describe the system, which are here the height variations. Because of translational invariance, it is appropriate to use the Fourier components z_k , which diagonalize the free energy increment

$$\delta\mathcal{F} = \sum_k B(k) |z_k|^2 \quad (169)$$

If (163) holds, only the components z_q and z_{-q} are appreciable and

$$\delta\mathcal{F}(t) = B(q) \mathcal{A} \delta h^2(t) \quad (170)$$

Taking the time derivative of (170) and comparing with (168), one finds

$$\mu_1(t) = 4a^2 c B(q) \delta h(t) \quad (171)$$

For a rough (i.e. non-singular) surface, $B(q)$ is obtained if one identifies (170) with (161). This yields $B(q) = -B_1|q| + B_2q^2$, where

$$B_1 = \frac{C_1^2}{4C_2} \left(\frac{\delta a}{a} \right)^2 E \quad \text{and} \quad B_2 = \tilde{\sigma}/4 \quad (172)$$

We have written $|q|$ instead of q in order to include the case $\vec{q} = (q_x, q_y)$ with $|q| = q_x^2 + q_y^2$.

An appropriate treatment of a singular surface requires renormalization group methods [3,6]. If one wishes to preserve simplicity at the expense of rigor, one can introduce into (169) a positive coefficient B_0 of order 0.

$$B(q) = B_0 - B_1|q| + B_2q^2 \quad (173)$$

This heuristic form does not satisfy invariance under the translation $z \rightarrow z + c$, but correctly describes the stability with respect to deformations of any wavelength if T is sufficiently lower than T_R . Moreover, the form (173)

is justified in the presence of a substrate since translational invariance is suppressed. We shall come back to this point in paragraph IX E. For an infinite adsorbate thickness, the coefficient B_0 vanishes at and above T_R .²⁴

Insertion of (171) into (167) yields

$$\frac{d\delta h(t)}{dt} = -4\Upsilon a^2 c B(q) q^2 \delta h(t) \quad (174)$$

the solution of which is

$$\delta h(t) = \delta h(0) \exp(\omega_q t) \quad (175)$$

with

$$\omega_q = -4a^2 c \Upsilon B(q) q^2 = -4\Upsilon a^2 c (B_0 - B_1 |q| + B_2 q^2) q^2 \quad (176)$$

The condition of stability of a plane surface is $\omega_q < 0$ for any q . For a non-singular surface, $B_0 = 0$, ω_q is always positive for small $q < 2\pi/\lambda^*$, given by (162), and the plane surface is unstable in agreement with paragraph IX B.

Moreover, as expected, the absolute value of expression (176) decreases rapidly with q for $q < 2\pi/\lambda^*$, so that long wavelength components $z_q(t)$ develop very slowly. The components which will actually appear are those of wavelength slightly larger than λ^* . Those which are shorter are stable, those which are much larger are too slow.

Even in the case of a singular surface, there may be a window $\lambda^* < \lambda < \lambda^{**}$, in which (176) is positive and the surface linearly unstable (i.e. without an activation barrier). In the absence of growth, this can probably occur only very near T_R . It will be argued in the next chapter that MBE growth conditions can alter this conclusion.

Before doing that, it is of interest to give more details on the instability. The above formulae tell us how an initial perturbation evolves, but say nothing about the initial perturbation. In a somewhat heuristic approach *à la* Langevin, one can assume that it is produced randomly by some ‘noise’ and write an equation analogous to (7). Eliminating the current as above and performing a Fourier transformation, one obtains

$$\frac{\partial z_q}{\partial t} = \omega_q z_q + \varphi_q(t) \quad (177)$$

where the ‘noise’ $\varphi_q(t)$ satisfies the following relations analogous to (12)

$$\langle \varphi_q(t) \rangle = 0 \quad , \quad \langle \varphi_q(t) \varphi_{q'}^*(t') \rangle = \varphi_0^2 \delta(t - t') \delta_{qq'} \quad (178)$$

In the absence of noise, $\varphi_0 = 0$, (177) yields (175). In the presence of noise, integration of (177) yields

$$z_q(t) = \int_0^t e^{\omega_q(t-t')} \varphi_q(t') dt' \quad (179)$$

and use of (178) gives

$$\langle z_q(t) z_{q'}^*(t) \rangle = \delta_{qq'} \frac{\varphi_0^2}{2\omega_q} [e^{2\omega_q t} - 1] \quad (180)$$

which describes the surface morphology at time t .

2. High symmetry surfaces and MBE growth

The previous calculation applies near equilibrium. It is therefore not clear that it can be applied to a growing crystal.

The theory of the previous paragraphs applies to non-singular surfaces near equilibrium. Instabilities are generally observed during growth, e.g. MBE, and the surfaces are often believed to be singular. In this paragraph, attention will be focussed on high symmetry orientations, (001) or (111).

²⁴Formula (173) is only acceptable for fluctuations near equilibrium. The energy of a bump of thickness equal or larger than the atomic distance on a singular surface is given by a quite different formula as will be seen in the next chapter.

Such surfaces are quite different in the equilibrium state and during growth. The most obvious difference is the existence of long, closed steps which bound large terraces or valleys which appear and die at the frequency $F_0 a^2$ of the RHEED oscillations. Another difference is that the average adatom density can be much larger than at equilibrium, and this can increase the absolute value of the average current, and even change its sign, as will be seen.

The effect of short-lived terraces is difficult to analyze but can presumably favour an instability since these terraces create a kind of roughness, which actually increases with time [4] and evolves toward true roughness, with diverging height fluctuations.

The remainder of this paragraph is devoted to the effect of the current due to freshly deposited adatoms from the beam, which have not yet been incorporated by a step. The surface density $\rho_{inc}(x, y, t)$ of these adatoms can be much larger than the equilibrium adatom density $\rho_0(T)$, in particular in the growth of an element (e.g. Si or Ge or a metal) when $\rho_0(T)$ is given by (3). In the case of metals, values of the adatom energy W_0 are given by Stoltze [40]. The density $\rho_{inc}(x, y, t)$ in MBE is discussed in App. B. At low temperature, it depends only on the ratio F_0/D of the flux rate to the diffusion constant [4,179,180] and is much larger than $\rho_0(T)$. This inequality is not so clear at the temperatures used in MBE growth. In the case of III-V semiconductors, it has been argued [35] that the equilibrium adatom density, given by (4), can be large, of the same order as the adatom density during growth.

In this paragraph, ρ_0 will be assumed to be much smaller than ρ_{inc} , and the consequences of this situation will be investigated. The current $j_{inc}(x, y, t)$ of freshly deposited adatoms on the surface contains a part $j_{inc}^{el}(x, y, t)$ which results from elasticity, and a part $j_{inc}^{(2)}(x, y, t)$ which results from other factors, in particular terrace nucleation. The latter has been discussed in chapter IV, where its main effect was found to be a modification of the coefficient B_2 in (173). In the absence of Ehrlich-Schwoebel effect, B_2 is increased with respect to its equilibrium value. The Ehrlich-Schwoebel effect is generally weak at usual growth temperatures, at least in the case of semiconductors, and will be neglected in this chapter and in the following ones. The part which results from elasticity can be roughly written as proportional to the average $\bar{\rho}_{inc}$ of the incoming adatom density.²⁵

$$j_{inc}^{el}(x, t) = -\beta D \bar{\rho}_{inc} \partial \mathcal{V}_{el}(x, t) / \partial x \quad (181)$$

where \mathcal{V}_{el} is the elastic potential energy of an adatom. It has to be proportional to the strain,

$$\mathcal{V}_{el}(x, t) = -K_1 \epsilon(x, t) \quad (182)$$

and the strain associated to the modulation (163) has the form

$$\epsilon(x, t) = \epsilon(t) \cos(qx) \quad (183)$$

where $\epsilon(t)$ is related to the amplitude $\delta h(t)$ by (157).

Now, there is a surprise [181]. The coefficient K_1 can be positive or negative, independently of the sign of $\delta a/a$! The reason is the following. The coupling of adatoms to the strain, expressed by (181), is partly due to the size of the atom, but also has chemical reasons which, a priori, are hard to predict. Only the part of K_1 which results from size effects has necessarily the sign of $\delta a/a$.

Formulae (181), (182) and (183) yield

$$j_{inc}^{el}(x, t) = -\beta D K_1 \bar{\rho}_{inc} q \epsilon(t) \sin(qx) \quad (184)$$

or, replacing $\epsilon(t)$ by its expression (157),

$$j_{inc}^{el}(x, t) = -\beta D K_1 \bar{\rho}_{inc} q^2 \frac{C_1}{2C_2} \frac{\delta a}{a} \delta h(t) \sin(qx) \quad (185)$$

When inserted into (164), this expression yields a contribution to (176) proportional to q^3 , and therefore replaces B_1 by B'_1 given by

²⁵In reality, $\rho_{inc}(x, y, t)$ is strongly modulated and vanishes in the neighbourhood of a step. The elastic potential is also modulated. In a correct treatment, the current should be proportional to the average value of $\rho_{inc}(x, t) \mathcal{V}_{el}(x, t)$ on a distance large with respect to the distance between steps. Here, we approximate the average value of this product by the product of the average values. A more accurate treatment [181] has been done in the case of a vicinal surface and leads to the prediction of step bunching if the coefficient K_1 of formula (182) has the sign of $\delta a/a$. In the case of a high symmetry surface, step bunching is likely to appear too, thus leading to higher harmonics to be added to (163). This effect does not show up in the linear stability analysis.

$$B'_1/B_1 = 1 + \frac{\bar{\rho}_{inc}}{\rho_0} \frac{K_1}{2a^2 c E C_1} \frac{a}{\delta a} \quad (186)$$

If $K_1 \delta a/a < 0$, the instability can disappear if ρ_{inc}/ρ_0 is large enough. If $K_1 \delta a/a > 0$, the instability should develop more rapidly during growth than in the absence of flux. Formula (162) which gives λ^* should be multiplied by (186), so that the wavelength of the surface modulation can be smaller than in the absence of growth.

Another possible effect of MBE growth is a high concentration of surface vacancies instead of surface atoms. The extension of the previous argument to this case would be straightforward.

D. Experiments

As will be seen, instabilities are observed in heteroepitaxial growth, and can be explained by the mechanism of paragraphs IX A to IX C. However, a precise comparison is not possible, in particular because thermodynamical surface properties (T_R , $\tilde{\sigma}$...) are generally not well known.

The instability of coherent, epitaxial films has been observed for instance in the growth of Ge on Si(111) [182], and of $\text{Ge}_{1-x}\text{Si}_x$ on Si(001) [183–185]. The observed features depend on the Germanium concentration, presumably because the misfit does. The misfit of pure Ge on Si is 0.0417. The non-stoichiometric composition allows to obtain a tunable misfit, but makes comparison with theory difficult since the concentration can become inhomogeneous for kinetic [186] or thermodynamic [187] reasons.

For small misfits (low Ge concentration), it is possible to grow rather thick layers, and at a ‘critical’ thickness²⁶ a three-dimensional modulation appears, which is ‘quasi-periodical’ [184] and reminiscent of formula (148).

For large misfits, the adsorbate splits into clusters and this happens at a much lower critical thickness. For instance, this thickness is about 100 nm for $\text{Ge}_{0.83}\text{Si}_{0.17}$ on Si(001) [184], and only 3 monolayers [188] for pure Ge on Si(001) and 2 bilayers [182] for Ge on Si(111), where the misfit is about 0.04. In the case of InAs on GaAs(001), the misfit is even larger (0.07) and the adsorbate splits into clusters at an even lower thickness, about 1.6 monolayers [189].

Berb  zier et al. [185] have found that the amplitude of the modulation increases proportionally to $(\delta a/a)^2$. According to previous paragraphs, this amplitude, at a given time, should be given by (180), where ω_q is given by (176). From these formulae, the amplitude would be expected to increase more rapidly than $(\delta a/a)^2$ for long times.

The case $\text{Ge}_{1-x}\text{Si}_x$ on Si corresponds to $\delta a/a > 0$, i.e. the adsorbate is compressed by the substrate. A modulation has also been observed (Fig. 32) for $\delta a/a < 0$ [154].

The case of large misfits will be addressed in the next chapter, but the splitting into clusters is in agreement with the argument of paragraph IX A. The cluster size is just limited by diffusion.

In the case of small misfits, the roughly sinusoidal modulation which has been observed is presumably a transient state, which *apparently* does not evolve because the dynamics is too slow. Separation into clusters would still lower the free energy. The qualitative agreement between the theory of paragraph IX B, which predicts an instability, and the experiments, which provide an observation of this instability, does not imply that everything is well understood. In particular, the theory was made for a non-singular surface, i.e. a rough surface in the sense of chapter I. However, a (001) surface is generally believed to be singular at the temperature at which the crystal is grown. The complete solution of this puzzle would require a quantitative theory which is not yet available, but the following elements may contribute to the explanation.

- i) The surface may contain steps or other defects to be thermodynamically rough.
- ii) Even if the surface of the ‘free’ material is smooth, the surface of the constrained material may be rough or closer to roughness. It is especially interesting that waves appear in tensile films ($\delta a/a < 0$) at a lower misfit than in compressive films. An increase of the atomic distance clearly favours surface melting (as it favours ordinary, bulk melting) and therefore surface roughness (since a liquid surface is rough).
- iii) As seen in paragraph IX C 2, a growing surface can be linearly unstable even if a surface which has a similar morphology, but is at equilibrium, is stable.

In any case, it is not surprising that separated clusters have not been observed for a moderate misfit. Indeed, theories based on an activated process predict a huge activation energy proportional to $(\delta a/a)^{-4}$, as seen from formula 198) below. On the other hand, if the plane surface is linearly unstable, the instability is established at a rate proportional to λ^{*-3} if the stabilizing terms of (176) are ignored, and λ^* is very large in weak misfit as seen from (162).

²⁶This critical thickness for the 2d-3d transition is generally different from the critical thickness for misfit dislocation formation, introduced in chapter VIII.

One can wonder whether the existence of a ‘critical’ thickness below which the plane surface is apparently stable is a thermodynamic or kinetic property. In other words, is a three monolayer thick deposit of Ge on Si thermodynamically stable or does it only lack time to deform? This point is not yet clarified. The fact that the ‘critical’ thickness can be considerably increased by surfactants, as will be seen in chapter XIII, suggests that kinetic effects are important. The same conclusion is suggested by the argument of paragraph IX A, according to which cluster formation always lowers the energy. However, it will be argued in the next paragraph that the stability of thin layers can also have thermodynamical grounds.

E. Effect of the adsorbate thickness

If the stress is produced by a substrate, the previous treatment is only reliable if the adsorbate is sufficiently thick, as noticed by Grinfeld [190,191]. A finite thickness of the adsorbate has in particular the following effects.

i) The elastic constants are usually not the same in the adsorbate and in the substrate. This introduces computational complications [177,192], apart from simple particular cases, e.g. if the adsorbate is very thin. This case is treated in paragraph X D below in the case $T < T_R$, and the case $T > T_R$ might be treated as well. This effect modifies the instability threshold λ^* [177,192] but does not introduce a critical thickness,²⁷ except in the unphysical case of an infinitely hard, undeformable substrate.

ii) A greater thickness implies a longer growth time, and the instability is enhanced by growth as argued in paragraph IX C.

iii) Another effect of a finite adsorbate thickness $\langle z \rangle$ is the limitation of height fluctuations in the direction $\delta z < 0$, where $\delta z = z - \langle z \rangle$. Indeed a local fluctuation always costs capillary energy, but if $\delta z < -\langle z \rangle$, it does not bring any elastic energy. It is thus tempting to assume that such a fluctuation is completely forbidden, i.e. the condition

$$z \geq 0 \quad (187)$$

is satisfied on the whole surface. This is a reasonable approximation if the substrate (but not necessarily the adsorbate) is below its roughening temperature. For instance, if the adsorbate becomes thinner than 1 monolayer, the height is in most places equal to 0 or 1, as the spins of an Ising model. Now, the free energy of an Ising paramagnet has the form (169) (where z would be replaced by the magnetization M in a magnet) with a *non-vanishing* coefficient B_0 . More generally, a finite adsorbate thickness introduces a non-vanishing coefficient B_0 , which is now allowed by symmetry, even above T_R . Thus, a small adsorbate thickness makes the instability more difficult. Moreover, if δz is equal to 0 or 1, a continuous variation of the form (148) is hardly acceptable and the instability should have different features.

These special features are well illustrated by recent experiments by Ponchet et al. [194,195]. Layers of InAs of different thickness were deposited on InP(001) by MBE during a short time at about 500°C, then maintained in an As flux (but without In flux) at the same temperature during 30 seconds, then buried under InP. The result is the following. Deposits thicker than 2 monolayers²⁸ give rise to a fairly regular array of small clusters. Deposits of thickness comprised between 1.5 and 2 monolayers give rise to an irregular array of clusters whose volume is about 5 times as large as when resulting from a thick deposit.

A possible interpretation of the experiment is the following. For thick deposits, the calculation of paragraph IX B will be assumed to be valid. Then a modulation of well-defined wavelength λ appears –more precisely, two modulations in two orthogonal directions. The amplitude δh increases with time, and when it becomes of the order of the adsorbate thickness, the substrate has to be taken into account and the adsorbed film splits into clusters. The shape of these clusters is the subject of the next chapter. The wavelength λ , as seen above, is of the order of magnitude of λ^* .

For thin deposits, the substrate cannot be ignored even at the beginning of the instability. Since there is a wetting layer, its effect is summarized by a condition stronger than (187), namely $z \geq c$, where c is the thickness of a monolayer.

For thin deposits, but thicker than 1 monolayer, the theory of paragraph IX B has to be modified. The instability does not appear in the linearized treatment. The system is not ‘linearly unstable’. However, it is not stable either since, as argued in paragraph IX A 2, the formation of *big* clusters does lower the energy. Thus, thin adsorbates are not stable, but metastable. They can only reach their equilibrium state if they overcome an activation barrier. This

²⁷However, a thickness threshold, below which the instability is not observable in practice, has been introduced by various authors [177,193].

²⁸In the case of a binary semiconductor, a (001) monolayer designates a set of an atomic layer of metal and an atomic layer of metalloid.

activated process may be expected to give rise to a rather disordered array of clusters, as observed experimentally. Indeed, it is a localized effect rather than a cooperative one. The nucleation barrier can be overcome at some place and not elsewhere, while the linear instability described in paragraph IX B corresponds to the increase of a density wave in the whole surface.

Another point which has to be understood is that clusters which arise from thin deposits are bigger than those which result from thick deposits. This may seem paradoxical since, for the same cluster size, the atoms have to diffuse on a longer distance in the case of a thinner film. The following arguments can explain the experimental facts.

i) A theoretical value of the typical linear size $V_c^{1/3}$ of clusters arising from activated processes will be evaluated in the next chapter (see formula (197) below). It is the product of $(\delta a/a)^{-2}$ by the ratio of a surface tension divided by an elastic constant, just as wavelength λ^* given by (162). This suggests that both lengths $V_c^{1/3}$ and λ^* have the same order of magnitude. However, the volume of the clusters should be, in the activated case, essentially the cube of the linear size, i.e. proportional to $(\delta a/a)^{-6}$, while in the linearly unstable case, it should be proportional to $\langle z \rangle$ times the square of the linear size, i.e. proportional to $\langle z \rangle (\delta a/a)^{-4}$ as seen above. In other words, in the case of nucleation, the volume is that of the critical cluster. If there is a smooth modulation of the surface, the wavelength is the critical wavelength.

ii) The following argument is slightly different, but related. In the Asaro-Tiller-Grinfeld scenario, assumed to be valid for thick films, the instability is collective, all mounds appear at the same time and cannot go fishing atoms outside their own domain which has a well-defined radius λ^* . In contrast, if clusters are randomly nucleated, the nucleation of new clusters in their vicinity does not occur at once, and the first created clusters have some time to sweep remote atoms.

iii) In the case of thick deposits, the instability can begin during the growth, and the wavelength can be smaller as seen in paragraph IX C 2.

The above interpretation of the experiments of Ponchet et al. is only tentative and can be subject to controversy. Indeed, the average cluster size has been supposed to be selected at the onset of the instability in a two-dimensional layer, which then splits into ‘islands’ or clusters which have this size. In reality, the evolution after cluster separation is not negligible [158,164,196–198] as will be seen in chapter XI. A support of our view may be seen in the observation that deposits of InGaAs on GaAs or AlGaAs give more regular structures for (311)B surfaces²⁹ than for the (100) orientation, in the case of MOVPE [155,156] as well as MBE [157]. Indeed, the roughening transition temperature is expected to be lower for a (311) face than for (100), so that the argument of paragraph IX B is more likely to be applicable.

F. Solid-solid interfaces and other generalizations

A case of interest is that of coherent, epitaxial solid-solid interfaces. Such interfaces are commonly encountered in semiconductor technology (quantum wells, multilayers). One can for instance consider [199,200] a quantum well constituted by a thin slab of a material A in a infinite crystal of a material S . The elastic properties are simpler in this case than a multilayer or a single interface between two solids because the lattice constant is that imposed by the material S .

Using the same arguments as for a free surface, one can show that a coherent interface is not planar at equilibrium above its roughening transition, which can be defined as that of a free surface. The planar shape is linearly unstable with respect to small deformations, just as the surface of a coherent adsorbate [199,200].

If one goes beyond the linear stability analysis, the two cases are different. Large modulations of a solid-solid interface are not so favourable as those of a free surface.

On the other hand, volume dynamics is very slow and solid-solid interfaces can remain planar during a long time. We do not need to worry about our TV, its transistors will not be damaged by interdiffusion.

We conclude this chapter by a hint on possible generalizations of the Asaro-Tiller-Grinfeld instability. In (158), δh is the amplitude of a height modulation. As a matter of fact, it might be the amplitude of the modulation of any continuous ‘field’, for instance the surface impurity density. If this field is linearly coupled to the elastic strain, then a modulation of this field lowers the *elastic* energy as shown in paragraph IX B. However, this does not give rise to an instability if the coefficient B_0 of formula (173) is strongly positive.

²⁹In the (311)B GaAs surface, the steps are As, while they are Ga in the (311)A surface. The (311)A surface is quite different and will not be considered here.

X. THERMODYNAMICS OF AN EPITAXIAL, COHERENT CLUSTER

A. Energy of a cluster

In the previous chapter we have seen that a plane adsorbate surface is unstable if adsorption is coherent. The final stage of this instability is an array of clusters. If the cluster size has a narrow distribution, these can be used as ‘quantum dots’ in microelectronics after being ‘buried’ into the material which constitutes the substrate. These clusters are the subject of the present chapter. In contrast with the previous chapter, we now study the final or nearly final result of the instability, rather than its onset. In the first few paragraphs of this chapter, simple theoretical considerations will be made, which then will be compared with experimental observations.

In contrast with the three-dimensional clusters addressed in chapter VII, those which result from coherent, epitaxial growth often form a fairly regular array and have a narrow distribution of sizes [155,156,189,194,195,197,201,202], so that they can be used as quantum dots. This phenomenon is called *self-organization*. Its mechanism is not well understood, but a few conjectures will be presented in the next chapter. We shall first consider a single cluster and determine its equilibrium shape. The standard way to do this is to minimize its energy.

In the linear stability analysis of chapter IX, the energy was supposed to be the sum of an elastic part resulting from the elastic strain in the whole sample, and a surface (or ‘capillary’) term independent of the strain. This assumption is in principle not correct for strongly deformed surfaces, and the surface energy does depend on the strain through the ‘surface stress’. The surface stress can be viewed either as a strain-dependent part of the surface energy, or as an elastic stress which is concentrated on the surface and should be added to the part which varies continuously in the solid and has only discontinuities at interfaces. In other words, the surface stress is a delta-function singularity of the elastic stress at the surface. As will be seen in paragraph XIF, certain experimental properties might be explained by taking the surface stress into account, as was done for instance by Shchukin et al. [203] and Müller & Kern [204]. For the sake of simplicity, the surface stress will generally be ignored in the present chapter. This is correct in certain limiting cases, e.g. i) for weak strains, which do not affect very much the surface energy. ii) For big clusters, where the elastic energy is not much affected by the surface.

While in chapter IX the temperature was assumed to be higher than the transition temperature T_R which corresponds to the average surface orientation, in the present chapter the condition $T < T_R$ will be assumed to hold.

B. Capillary energy of a cluster

If a smooth film splits into clusters, this modifies the free energy density. As in the previous chapter, one can distinguish a ‘capillary’ energy, localized near the interfaces, and an elastic energy, which is not. The elastic energy is simpler because its variation in space obeys linear equations which only depend on the known elastic constants of the materials. The capillary energy is difficult to evaluate from first principles, and even from empirical potentials since it depends, for instance, on surface reconstruction, which is an essential feature of all semiconductors. We shall present here a qualitative view.

The capillary energy of a cluster contains in principle two parts. One corresponds to the free surface, and the other to the adsorbate-substrate interface. The main effect of the latter is to produce, in many cases, as seen above, a wetting layer. The energy of the cluster-wetting layer interface will be ignored.

The property $T < T_R$ implies that the capillary energy increment $\delta\mathcal{F}_{cap}$ resulting from a modulation is no longer proportional to δh^2 as it was in (159). Instead, it is proportional to δh for small values of δh . Indeed, the perturbed surface may be viewed as formed by flat parts separated by steps. The step free energy per unit length γ is positive below T_R and the number of steps is proportional to δh .

Similarly, a cluster of height h whose basis has a linear size R has a capillary free energy equal to

$$\mathcal{F}_{cap} = \text{Const} \times \gamma h R / c$$

where the constant is positive since a negative value would imply that the plane surface is unstable even in the absence of misfit. The constant depends on the details of the shape of the cluster. We shall assume that it is a truncated pyramid (Fig. 36) with a square basis of side R , and that the sides make an angle θ with the substrate surface. Then the detailed expression for small θ is

$$\mathcal{F}_{cap} = 4\gamma(h^2/c)\frac{1+x}{1-x}\cot\theta \quad (188)$$

where

$$x = R'/R = 1 - \frac{2h}{R} \cot \theta \quad (189)$$

is the ratio of the sides R and R' of the two square faces.

Expression, (188) is correct for $|\tan \theta| \ll 1$ and qualitatively valid for $|\tan \theta| < 1$. For larger values, the interaction between steps are not taken into account, but (188) still gives the right order of magnitude.

In the following, it will be assumed that the cluster is a truncated pyramid. The ambition of a theoretical treatment is thus restricted to find the three parameters R , h , x which minimize the free energy. In the absence of elastic effects, it is possible to do much better and to find the equilibrium shape without any restriction by the *Wulff construction* [3,4]. The existence of an elastic energy makes things more difficult. The experimentally observed shape is not always a truncated pyramid. Fig. 37 shows a more complicated shape which results from the fact that the surface of a semiconductor has a rectangular rather than square symmetry. The cluster shape will be addressed in greater detail in paragraph X G.

C. Scaling laws for the elastic free energy of a cluster

The explicit form of the elastic Green's functions for a semi-infinite isotropic medium [171] or cubic crystal [170] bounded by a planar, stress-free (001) surface is known. However, these Green's functions are not directly applicable in the presence of adsorbed clusters except if these clusters are very thin. This special case will be addressed in paragraph X D for an isotropic medium.

In the general case, the only simple statements which can be made about the elastic free energy are scaling laws, which hold for any cluster shape.

As in the previous chapter, the energy will be counted from a state where the substrate has its 'natural' lattice constant and where the adsorbate has the lattice constant of the free substrate. The energy of that state (set equal to 0 by our choice of origin) is higher than that of the equilibrium state, since the elastic strain precisely tries to lower the elastic energy. Therefore, with our convention, the elastic energy at equilibrium is *negative*. The strain will also be counted, as in the previous chapter, from the above defined state where the substrate will be said to be 'totally unconstrained' and the adsorbate 'totally constrained'.

A list of scaling laws, *which hold within linear elasticity theory and ignoring surface stress*, will first be given.

A. The elastic free energy of a coherent, epitaxial cluster of a given shape and size is proportional to the square $(\delta a/a)^2$ of the misfit.

B. The elastic free energy of a coherent, epitaxial cluster of a given shape with a given misfit is proportional to the cluster volume.

In other words, if all linear dimensions are multiplied by λ the elastic free energy is multiplied by λ^3 . The shape may be a pyramid, a truncated pyramid, a half-sphere, etc.

C. The strain created by a coherent, epitaxial cluster of a given shape at a long, given distance \vec{r} is proportional to the cluster volume V .

D. The strain created by a coherent, epitaxial cluster of given shape and size at a long distance \vec{r} is proportional to $1/r^3$ for any given direction \vec{r}/r .

The same law holds for an isolated adatom.

E. The elastic interaction free energy between two coherent, epitaxial clusters of given shapes at distance \vec{r} is repulsive and proportional to $1/r^3$ for large r .

$$V_{el}(r) = B/r^3 \quad (190)$$

The same law holds for two isolated adatoms.

These scaling laws are derived in App. E. Property (A) is a straightforward consequence of the linear and continuous nature of elasticity theory, which as a matter of fact is an approximation. The other scaling laws, especially (D) and (E), are well-known for an isotropic elastic medium. The quantitative formulae which give the response of an isotropic solid to superficial forces have been obtained by J.V. Boussinesq [205] at the end of the nineteenth century and can be found in textbooks [4,171].

It is of interest to compare the elastic interaction between adatoms and the phonon-mediated interaction between electrons in the BCS theory of superconductivity. Although electrons are quantum particles, there is a strong analogy between their interaction and the elastic interaction between two point impurities in a *bulk* solid. However, the interaction between electrons is generally assumed to be short ranged, in strong contrast with (190). As a matter of fact, the elastic *strain* created by a point impurity in a *bulk* solid is proportional to $1/r^3$ as in the surface problem ... but the term in $1/r^3$ of the interaction *energy* between two point impurities turns out to vanish [4].

D. Case of a thin cluster: Tersoff approximation

We can say a little more if the adsorbed cluster is sufficiently thin. For the pyramid of Fig. 36, this means that $h \ll R$ or/and $\tan \theta \ll 1$. In this case, an approximate calculation of the elastic energy, often used by Tersoff and his coworkers [206,207] and hereafter called ‘Tersoff approximation’ is possible. It relies on two simplifications.

i) In (149), the strain is assumed independent on z , so that

$$\delta \mathcal{F}_1 = -\text{Const} \times \frac{\delta a}{a} \int dx dy [\epsilon_{xx}(x, y) + \epsilon_{yy}(x, y)] z(x, y) \quad (191)$$

where the integral is on the substrate-adsorbate interface and z is the height of the adsorbate surface with respect to this interface. Thus, the integral is over the substrate-adsorbate interface, which is assumed to be a plane. If the adsorbate is an isotropic solid of Young modulus E_a and Poisson ratio ν_a , the constant is equal to $(\delta a/a)E_a/(1-\nu_a)$.

ii) Since the adsorbate is thin, its contribution to the term \mathcal{F}_2 defined by (152) is negligible.

With these approximations, the problem is reduced to finding the response of a semi-infinite crystal limited by a plane (the substrate) to known forces acting on the surface, which are fully defined by (191).

In the case of a truncated pyramid with $h \ll R$, the strain is proportional to h for fixed R and θ , so that \mathcal{F}_2 is proportional to h^2 . The linear part \mathcal{F}_1 is also proportional to h^2 since z is proportional to h in (191). Thus, the total elastic energy is proportional to h^2 . On the other hand, according to paragraph X C, the energy is proportional to R^3 for fixed h/R and θ . We conclude that the elastic energy of a low pyramid is proportional to $h^2 R$, in agreement with the quantitative formula (192) below, valid for a coherent epitaxial cluster of a pyramidal form in the limit $\tan \theta \ll 1$ in the isotropic limit ($c_{11} - c_{12} = 2c_{44}$). The (tedious) derivation of this formula essentially relies on the fact that, in the limit $\tan \theta \ll 1$, one can use the elastic Green’s function (i.e. the elastic response to a localized stress) of a solid bounded by a plane surface, which is known. The Green’s function method yields the energy as a multiple integral which can be calculated for an isotropic solid. If both R and h are much larger than the atomic distance, one obtains [208,209]

$$\mathcal{F}_{el} = -12 \frac{1 - \nu_s^2}{(1 - \nu_a)^2} \frac{E_a^2}{2\pi E_s} \left(\frac{\delta a}{a} \right)^2 V G(x) \tan \theta \quad (192)$$

where E_s and E_a , ν_s and ν_a are the Young modulus and the Poisson ratio of the substrate and the adsorbate respectively, V is the volume of the cluster, x is defined by (189) and $G(x)$ is a function which decreases smoothly from a value close to 0.5 (for $x = 0$, i.e. a full pyramid) to reach the value 0 with a finite slope for $x = 1$, i.e. a slab (Fig. 38). For a given shape, x is fixed and \mathcal{F}_{el} is proportional to $\tan \theta$ which is itself proportional to $h^2 R$ as stated above.

The analytic form of $G(x)$ is impressive, namely

$$G(x) = \frac{1}{1-x^3} \left\{ \frac{1}{3} \left[\sqrt{2} - \ln(\sqrt{2} + 1) \right] (2+x)(1-x)^2 + \frac{2}{3} \left[\sqrt{2} \ln(1 + \sqrt{2}) - 1 \right] (1+x^3) - \Xi(x) \right\} \quad (193)$$

with

$$\begin{aligned} \Xi(x) = & -\frac{2x}{3} \sqrt{2+2x^2} + \frac{2x^3\sqrt{2}}{3} \ln \frac{1+\sqrt{1+x^2}}{x} + \frac{2\sqrt{2}}{3} \ln(x + \sqrt{1+x^2}) \\ & - \frac{1-x-x^2+x^3}{2} \ln \frac{1+x+\sqrt{2(1+x^2)}}{1-x} + \frac{1+x-x^2-x^3}{2} \ln \frac{1-x+\sqrt{2(1+x^2)}}{1+x} \end{aligned} \quad (194)$$

Numerical calculations [210] are in qualitative agreement with (192) in the case of interest, i.e. $h \ll R$ and $\tan \theta \ll 1$.

The Tersoff approximation makes calculations much easier, but reveals consistency problems. Consider a coherent, epitaxial cluster which is infinitely long in the y direction, and whose section by any plane parallel to xOz is a triangle of thickness $2R$ and height h , so that the height $h(x, y) = h(x)$ is $h(x) = h - h|x|/R$ if $|x| < R$, otherwise $h(x) = 0$. The strain on the surface of the substrate, at a distance a of the cluster edge, has the form

$$\epsilon(a) = \text{Const} \times \int_{-R}^R \frac{h(x)}{(x+R+a)^2} dx \quad (195)$$

where the response function $1/(x+R+a)^2$ results from the scaling law (D) of paragraph X C, after integration on y . For large R , (195) diverges as $\ln(R/a)$. A similar divergence would arise in the case of a pyramidal cluster as

well. This divergence is unphysical, since a strain cannot diverge. It may be an artifact of the Tersoff approximation. However, a failure of linear elasticity theory is not excluded, although more elaborate versions of linear elasticity have apparently been applied successfully to this problem by Freund et al. [163,211] and by Shchukin et al. [203]. The Tersoff approximation is erroneous in at least two respects: i) The stress in the z direction is not correctly taken into account. ii) When replacing the cluster by a surface density of external stress, one has to take into account the fact that the resistance of the cluster to deformation is proportional to its thickness, so that surface elastic constants, proportional to the cluster thickness, should be introduced. Since the logarithmic divergence is weak, and the results are compatible with the scaling laws, the Tersoff approximation will be assumed to give the right order of magnitude.

E. Equilibrium shape of a coherent cluster: 2d-3d transition

When the energy (160) is known, it can be minimized at a fixed volume V with respect to θ and x , and this yields the equilibrium shape.

For small volumes V , the elastic energy (proportional to V) is small and the capillary energy is mainly due to the sides of the pyramid. The area of these sides should therefore be as small as possible. This area is proportional to \sqrt{Vh} multiplied by a coefficient of order unity which depends on the shape (see formula (188)). It follows that the cluster should be as thin as possible, i.e. it should reduce to a single monolayer.

For larger values, the elastic energy dominates the capillary energy. It is given by (192) with an acceptable approximation for $\tan \theta < 1$. For larger values, other approximations can be used, and it can be seen [208] that the elastic energy is minimized if the cluster is three-dimensional, with $h \approx R$ and $\tan \theta \approx 1$. As a matter of fact, experiments are consistent with a smaller value, $\tan \theta \approx 1/4$ to $1/2$.

We conclude that there is a ‘2d-3d’ (two-dimensional to three-dimensional) transition when the volume increases. An analysis based on the formulae of the previous chapter shows that this transition is discontinuous. Clusters initially have the shape of platelets, then abruptly change their shape and become pyramids with $\tan \theta \approx 1/4$. The transition takes place for a volume V_c which will be now roughly evaluated. A detailed calculation will be found elsewhere [206,208].

The energy of a cluster is the sum of (188) and (192) or, dropping constants which depend of the sample shape, but are generally of order unity,

$$\mathcal{F}_{clus} \approx \gamma V^{2/3}/c - E \left(\frac{\delta a}{a} \right)^2 V \quad (196)$$

This expression is positive for small volumes V , reaches a maximum when V increases, and is negative for a linear size larger than

$$V_c^{1/3} \approx \frac{\gamma}{cE} \left(\frac{\delta a}{a} \right)^{-2} \quad (197)$$

The maximum of the energy is obtained for a value of order $V_{ac} \approx 2V_c/3$ and the corresponding energy is the activation energy

$$\mathcal{F}_{ac} \approx \frac{\gamma^3}{c^3 E^2} \left(\frac{\delta a}{a} \right)^{-4} \quad (198)$$

Thus, the theory predicts a first order transition (‘2d-3d transition’) from flat, one monolayer thick clusters to three-dimensional clusters when the volume increases. The transition occurs for a volume close to V_c .

As a matter of fact, the 2d-3d transition had been observed experimentally before any theoretical prediction, as will be seen in paragraph X G.

In spite of its success in ‘predicting’ the 2d-3d transition, formula (196) is only qualitatively correct. The elastic part (192), in particular, must be modified in the case of clusters of thickness one monolayer. The correct formula contains a logarithmic correction, and the energy of such a platelet turns out to be [206,207]

$$\mathcal{F} = 4\gamma R - 8 \frac{1 - \nu_s^2}{(1 - \nu_a)^2} \frac{E_a^2}{2\pi E_s} c^2 \left(\frac{\delta a}{a} \right)^2 R \ln \frac{R\eta}{a} \quad (199)$$

where c is the monolayer thickness, a is such that $a^2 c$ is the volume of the unit cell, and

$$\ln \eta = 2 \ln 2 - 2 + \sqrt{2} - \ln(\sqrt{2} + 1) = -0.081 = \ln 0.922 \quad (200)$$

The logarithm in the elastic part (second term) of expression (199) violates the scaling law $\mathcal{F}_{el} \sim V$ of paragraph X C.³⁰

Relation (199) has been obtained by applying elasticity theory to an object of atomic thickness. This is obviously not quantitatively correct. An idea of the correction to be made is obtained by taking into account the surface stress [204].

It is of interest to use (199) to obtain an order of magnitude of the elastic energy per atom. Typical values of the Young modulus are $E_s c_s^3 = 12$ eV for GaAs and $E_a c_a^3 = 9.3$ eV for InAs. The energy per atom is proportional to $\ln(R/c)/(R/c)$, with a multiplying factor of the order of 0.01 eV for InAs/GaAs, proportional to the square of the misfit. Elastic forces are really weak at the atomic level because the misfit cannot be very large. But they are important for a big enough cluster because of their long range character.

F. More ambitious treatments

In this review we addressed an isotropic material and approximated the energy by formula (160), ignoring the effect of the strain on the surface energy, i.e., the surface stress [3,4].

Shchukin et al. [203] have given expressions which are far more ambitious in three respects. Firstly, they are valid in the physical case of a cubic crystal. Secondly they take into account the surface stress (which has also been considered by Moll et al. [212]). Thirdly, they are not restricted to thin adsorbates. However, the formulae of Shchukin et al. contain the elastic functions of a single material and therefore hold only if the adsorbate has the same elastic constants as the substrate.

The complications with respect to (192) in the work of Shchukin et al. are moderate. The surface stress just introduces two additional terms, which are negligible if the cluster size is large enough. Shchukin et al. [203] do not give explicit expressions of the various terms, but write useful scaling laws in terms of functions which can be calculated numerically by means of numerical integration of the equations of elasticity (the so-called finite element method).

Using this method, Freund et al. [211] and Johnson & Freund [163] demonstrated a spectacular deviation from the predictions of the Tersoff approximation for thick clusters. They find that the strain perpendicular to the substrate surface changes its sign beyond a height of about $0.22 \times 2R$, where $2R$ is the basis diameter. Usually, cluster formation or other instabilities of the Asaro-Tiller-Grinfeld type are observed when the substrate is bigger than the adsorbate (i.e. $\delta a > 0$), otherwise other types of instabilities generally occur, e.g. dislocations or twins. Then, near the interface, the adsorbate is obviously compressed by the substrate in the x and y directions. However, at a height larger than $0.22 a$, it is stretched! An intuitive explanation for this surprising behaviour may be as follows. The compression in the x and y directions is accompanied by an extension in the z direction, because the Poisson ratio is positive in all materials. Thus, the lower layers of a cluster push the upper layers upward. This can produce a stretching in the perpendicular direction, as happens if you press the center of a rubber leaf. Freund et al. were able to find an analytic version of their numerical results in a much older article by Ling [213] who himself used previous analytic theories [214,215] made during the second world war. Elasticity is indeed a very old science, and an accurate bibliography requires a very good library!

A quantitative treatment of the capillary energy is even more difficult than for the elastic energy. One can represent the interaction between atoms by an empirical potential [216] or make a first principle calculation [217]. In both cases many reconstructed structures are *a priori* possible, and are a source of serious difficulties, since it is in principle necessary to compare the energies of all of them, to take into account the possibility of transitions from a structure to another, etc. Moreover, the reconstructed structures are experimentally known only for simple surfaces, and not for all the orientations which appear, for instance on the cluster sides.

³⁰In short, the logarithm arises from the following fact. Any two atoms of the adsorbate at points \vec{r} and \vec{r}' produce a strain in the substrate, which in turn produces an effective, elastic interaction proportional to $1/|\vec{r} - \vec{r}'|^3$ between the two atoms according to (190). The calculation of the energy of a platelet requires 4 integrations, namely on the two components of \vec{r} and \vec{r}' . Three of these 4 integrations yield the logarithm of (199), while the last integration yields the factor R before this logarithm. It is noteworthy that, in (192), the logarithm has been cancelled by further integration on the vertical coordinate.

G. Experiments

An essential prediction of the simple theory presented in this chapter is the discontinuous 2d-3d transition. This is consistent with the experimental fact that, for a large enough misfit, three-dimensional clusters appear rather suddenly after the deposition of an appreciable mass of material, which, as expected, decreases with increasing misfit. For InAs/GaAs(001), it is about half a monolayer [196,197] above the wetting layer.

Another prediction of the simple theory is that big clusters are somewhat sharper than smaller ones. This is also in agreement with observations. As a matter of fact, the first clusters which appear in the growth of Ge on Si(001) are ‘huts’ [218] (Fig. 37). These elongated islands are favoured by the symmetry of the (001) faces of the diamond lattice, but seem to be metastable [219]. The stable shapes, according to Medeiros-Ribeiro et al. [219] are pyramids (square-based islands bounded, as huts, by {105} facets) and ‘domes’ (“structures with a large number of facets that look rounded at lower resolution” [219]). Domes seem to be the stable shape of bigger clusters [219], and the fact that they are also steeper [219] is in qualitative agreement with theory.³¹

However, this agreement is only qualitative and the experimental situation seems more complicated than the simple theoretical description given above. First of all, the size distribution is ‘bimodal’, i.e. it has two maxima which respectively correspond to pyramids and domes. Second, the sides of the pyramids have a low slope which would be expected to be unstable.

Intermediate stages between platelets and three-dimensional clusters are difficult to observe, in agreement with the fact that they should be excluded in a discontinuous transition. An indirect investigation is however possible using luminescence study. This method is essentially a measurement of the energy of the electronic wave functions localized in the adsorbate, and is more sensitive to the thickness h of the adsorbate than to its lateral size R . As it is applied to buried layers, the 2d-3d transition process is stopped, and a comparison of different steps of the adsorbate evolution is allowed.

Rudra et al. [221] have deposited a thin InAs layer on InP (2 ML for example) and covered it by InP. When the InAs layer is immediately covered, they observe a single luminescence line, corresponding to a thin, two-dimensional quantum well. When the coverage is performed after a certain time, they observe several luminescence lines, which can be attributed to different thicknesses of the layer. Calculation of the energy of transition showed that each line corresponds to an entire number of ML, between 4 and 8 MLs [222]. When a longer growth interruption is performed before coverage by InP, the luminescence exhibits a wide line, characteristic of an array of InAs islands [221]. Similar results were obtained by Lambert et al. [223].

An interesting study of the smallest possible three-dimensional clusters has been made for InAs/GaAs by Colocci et al. [224] using luminescence. When increasing the coverage, they obtained an increasing number (1, 2, 3...) of luminescence lines, which they attributed to an increasing number of layers of the clusters.

This seems to contradict the theoretical statement that the cluster shape should jump abruptly from a two-dimensional state (1 layer + the wetting layer) to a three-dimensional shape with many layers. The reason of the unexpected observation of two-monolayer-thick clusters may be attributed to a lack of thermal equilibrium. The quasi-critical clusters of Colocci et al. have a size of several thousands of atoms, in qualitative agreement with theoretical predictions [208].

XI. FORMATION AND EVOLUTION OF A POPULATION OF CLUSTERS

A. The three stages

In the present chapter, cluster formation will be addressed, as well as the evolution of the resulting population of clusters. In contrast with chapter IX, the misfit is assumed to be rather large, so that three-dimensional clusters form directly on the wetting layer, while a smaller misfit allows several adsorbate layers to be deposited before the onset of the instability. The case of large misfit corresponds, for instance, to InAs/GaAs(001), where $\delta a/a \approx 0.07$.

The evolution proceeds as follows. i) Formation of two-dimensional clusters on the wetting layer. Their number is determined by kinematic factors, mainly the diffusion constant D . At lower temperature, D is small, adatoms cannot diffuse very far, and there are many small islands. For a given coverage, the island size increases with temperature. ii) As more matter is deposited, clusters grow and become three-dimensional (the 2d-3d transition studied in the previous chapter). iii) As growth proceeds, the cluster size increases and the cluster distribution evolves.

³¹A transition from huts to domes has also been observed with a weaker misfit of 0.008, in SiGe/Si(100) [220].

For lower misfits, e.g. in the case of Ge on Si, the beginning of the growth will be different, but stage (iii) is fairly analogous.

During stage (i), addressed in paragraph XI B, the effect of elasticity is presumably not very strong, because the elastic interactions between adatoms and very small clusters are generally weak with respect to chemical, short range interactions responsible for capillary effects. In contrast, stage (ii) is an elastic effect. In phase (iii), the importance of elasticity is not so clear.

As will be seen in paragraph XI E, the size distribution of three-dimensional clusters is generally narrow. This fact, which is not observed for incoherent clusters [159,225] is often attributed to elasticity. Actually, as will be seen in paragraph XI B, a population of two-dimensional, coherent clusters at equilibrium, would have a narrow distribution, but the case of three-dimensional clusters is controversial.

The next three paragraphs XI B, XI C, XI D address simple, well understood and commonly accepted theoretical concepts which, unfortunately, do not give the complete solution of the essential problem, which is the evolution of a set of three-dimensional clusters. The experimental data about this problem are treated in paragraph XI E and compared with theoretical views in paragraph XI F.

B. When a monolayer starts growing

As summarized in App. B, the growth of an uncompleted monolayer (or ‘submonolayer’) is rather well understood [4,179,180,226–228] when elastic effects are absent, and indeed, as argued in paragraph XI A, elasticity is presumably not essential at low coverage.

The usual theory [4,179,180,226] deals with the growth of an element. Atoms of a single species are deposited at the rate of F_0 monolayers per unit time (Fig. 39) on an initially planar, high symmetry surface (e.g. (001)). As seen in chapter III, application to binary semiconductors is possible although some caution is necessary.

The best physical insight is provided by rate equations [179,180,226] which describe the evolution of the number of atoms and islands. In the simplest approximation (acceptable at low temperature) only the adatom density $\rho(t)$ and the cluster density $\rho_>(t)$ are considered, and very simplified forms of the rate equations are, omitting numerical factors:

$$\frac{d\rho}{dt} = F_0 - 2D\rho^2 - D\rho\rho_> \quad (201)$$

and

$$\frac{d\rho_>}{dt} = D\rho^2 \quad (202)$$

The various terms correspond to deposition from the beam, formation of a pair and sticking of an adatom on a cluster. Since local effects are ignored, numerical check by Monte-Carlo simulations is necessary [228].

The rate equations express the fact that freshly deposited atoms have two possibilities to form chemical bonds. They can either go to already formed terraces or nucleate new terraces. The former process requires a long diffusion on the surface, which is more likely to be possible (for a given coverage) if the diffusion constant D is high and if the growth rate F_0 is slow.³² Therefore, the number of terraces per unit area after deposition of, say, 10% of a monolayer, is an increasing function of F_0 and a *decreasing function* of D . More precise formulae are given in App. B. In practice, F_0 is rarely much larger or much smaller than 0.1 monolayer per second (within a factor 10) but D is very sensitive to temperature and can also be influenced by additives or ‘surfactants’ (see chapter XIII).

If elastic effects and other causes of instability are not too important, terraces begin to coalesce when the coverage becomes close to 1/2, and a complete layer forms when the coverage is equal to 1. This happens for the first (‘wetting’) layer in the case of InAs/InP and InAs/GaAs. The formation of the next layers, in coherent epitaxy, is only possible if the misfit is very weak.

³²Of course, nucleation dominates at the very beginning of the growth process, while it becomes very unlikely when the coverage is an appreciable fraction of a monolayer

C. Elasticity and the 2d-3d transition

While elasticity can be neglected at the very beginning of the growth, it should be taken into account when clusters are big enough to become three-dimensional, and the rate equations 201 and 202 must be generalized to incorporate the 2d-3d transition. This has been done by Dobbs et al. [165,229]. They write a set of three equations for 3 time-dependent (but space-independent) quantities which are the numbers of adatoms, of two-dimensional clusters and of three-dimensional clusters. Since these quantities are space-independent, the rate equations are global and cannot describe the effect of elastic forces on the current of matter. Elasticity is implicitly contained in the theory since it is the cause of the 2d-3d transition. Moreover, elasticity determines the detachment rate of atoms from steps.³³

This detachment rate is especially important for two-dimensional clusters, because “atoms detaching from the edge of a three-dimensional island are more likely to find the energetically favourable sites in the higher levels than to completely detach from the island” [229]. In the case of two-dimensional islands, the detachment rate depends on the island size and this effect favours a particular island size as will be seen below.

Even though we are mainly concerned with growth, it is of interest to investigate the equilibrium distribution of a cluster population. A good reason for this interest is that it is often convenient to anneal a deposit after it has been grown.

The equilibrium cluster size R_0 at a given coverage can be determined by minimizing the total free energy, or alternatively the free energy per unit adsorbate volume, which is obtained by dividing the free energy per cluster (199) by the cluster volume $V = cR^2$. Thus, one has to minimize

$$\mathcal{F}_{clus}/(R^2) = 4\gamma R^{-1} - 8 \frac{1 - \nu_s^2}{(1 - \nu_a)^2} \frac{E_a^2}{2\pi E_s} c^2 \left(\frac{\delta a}{a} \right)^2 R^{-1} \ln \frac{R\eta}{a} \quad (203)$$

with respect to R . The result is a finite value, namely

$$R_0 = \exp \left[\frac{\pi\gamma(1 - \nu_a)^2 E_s}{(1 - \nu_s^2) E_a^2 c^2} \left(\frac{\delta a}{a} \right)^{-2} - 1 \right] \quad (204)$$

We conclude that the equilibrium state of a population of platelets corresponds to nearly identical platelets with a finite size close to R_0 , with rather weak thermal fluctuations.

The above argument neglects interactions between platelets, but is probably qualitatively correct even if the coverage is not very low.

Thus, if a population of epitaxial, coherent platelets is annealed, their distribution should tend toward the equilibrium distribution and therefore, toward a narrow size distribution... provided they do not become three-dimensional, as they are expected to do. However, Priester and Lannoo [198] have pointed out that the existence of an optimal size R_0 for two-dimensional clusters can contribute to the mechanism responsible for the narrow size distribution of *three-dimensional* epitaxial, coherent clusters. The kinetics associated to this mechanism have been studied by Dobbs et al. [165,229]. The time evolution of the size and number of three-dimensional clusters is well reproduced by Dobbs et al. but they cannot say anything about the size distribution since it is not included in the theory.

D. Annealing of a population of incoherent clusters in the absence of growth: the Lifshitz-Slyozov mechanism

Before investigating more in detail the evolution of a population of clusters on a growing surface, it is of interest to examine this problem in the simpler case of a surface which does not grow (and does not evaporate either). In the absence of elastic effects, when only the surface energy has to be taken into account, the problem has been solved by Chakraverty & Avignon [128–130]. The evolution tends to reduce the surface energy, and therefore the total surface of the clusters. Since the adsorbate volume is constant, the ratio Surface/Volume decreases, and therefore the average cluster size increases. The microscopic mechanism is the following. Adatoms escape from smaller clusters and diffuse on the surface to bigger clusters where the free energy per atom (i.e. the chemical potential) is lower on smaller

³³ The concept of detachment rate, in the frame of global rate equations, is ambiguous. For instance, if an atom detaches from a cluster and attaches immediately after that to the same cluster, should this event be called ‘detachment’? Dobbs et al. [229] do not, since, in their formula (23), they introduce a barrier to detachment from 2-D clusters, defined as the elastic energy necessary to detach an atom and to bring it to an infinite distance.

clusters (Fig. 40). This mechanism, called ‘Ostwald ripening’ is rather universal and was first discovered in demixing solid alloys [230,231].

The theory predicts that the average cluster size $\bar{R}(t)$ is proportional to $\bar{R}(t) \simeq t^{1/4}$ for three-dimensional, incoherently adsorbed clusters [128–130] and $\bar{R}(t) \simeq t^{1/3}$ in three-dimensional alloys [230,231]. The effect is also present for two-dimensional adsorbed clusters [232] in the absence of elasticity, and then $\bar{R}(t) \simeq t^{1/3}$.

The expected size distribution is broad.

Experiments on incoherent clusters [159,225] are in qualitative agreement with theory, although the exponents do not always fit very well. The behaviour $\bar{R}(t) \simeq t^n$ is presumably only valid at very large times [88].

How are the above conclusions modified by elasticity? In particular, does the average size increase with time? A negative answer might reasonably be expected since the elastic interaction between adatoms is repulsive and long-ranged. These features explain the fact that two-dimensional, coherent, epitaxial clusters have an optimal size. In the case of three-dimensional clusters, the answer is not so clear, but qualitative considerations (App. E) suggest that the total elastic energy of a population of three-dimensional clusters is a decreasing function of the average size and therefore favours an increase of this size. In other words, atoms are still expected to detach preferably from small clusters and to diffuse toward small ones. As seen in the next paragraph, this seems to be in contradiction with experiment. This discrepancy suggests that new concepts should be introduced, as will be seen in paragraph XIF.

E. Experiments

In this paragraph are reported some experimental results on the evolution and size distribution of coherent clusters where elasticity has a role to play.

Many studies have been devoted to Ge/Si(001), and only a small part of them will be reported here.

According to Goldfarb et al. [159], qualitative agreement with the Lifshitz-Slyozov theory has been observed in this system at temperatures $T > 700$ K. However, the size distribution, as said in paragraph XG, has two maxima. The maximum which corresponds to small pyramids disappears at sufficiently high coverage. Then, the micrographs and histograms published by Ross et al. [233] show a remarkably narrow size distribution. Moreover, there is no hint of any increase of the average size of the coherent ‘domes’ which correspond to the higher maximum. This seems hardly compatible with the Lifshitz-Slyozov theory.

The tendency to ripening predicted in paragraph XID (decreasing number of clusters, increasing size) has been observed in III-V compounds under certain growth conditions. When the cluster size reaches a certain value (‘critical size’), dislocations appear in the cluster, and the situation described in paragraph XID becomes effective. However, a precise comparison with theory is often difficult because of the coexistence of coherent and incoherent clusters, where the latter are larger than the critical size and the former are smaller. This has been reported for example [162] in InAs/InP(001) [162] and InAs/GaAs(001) [160]. A general feature when misfit dislocations have formed is that the size distribution is wide, as expected from theory. However, it should be pointed out that this evolution is possible only under certain favourable growth conditions, for instance a long annealing after deposition [162]. Actually, very often, the whole population of clusters remains coherent, which probably implies that their size does not exceed the critical value. Gérard et al. [197] have observed in the InAs/GaAs system that after the initial nucleation of numerous small islands, the average cluster size tends to increase when an annealing is performed after the deposit. However, the size does no longer increase after a certain annealing time.

These results suggest that there is a competition between two effects and that there is a barrier which opposes usual Ostwald ripening. The different experimental results reported above show a strong dependence on the growth conditions and on the lattice mismatch. This implies that the evolution towards cluster ripening, although it is energetically favourable, can be kinetically delayed.

What happens when the clusters are still coherent (and strained) is rather complex. An interesting set of results concerns the evolution of the average size as a function of the quantity of strained material. When this quantity is large, the cluster density is large too, and the average size increases with the deposited quantity [189] as it is usually expected. This is contrast to what has been observed in the InAs/GaAs [164,197] and InAs/InP [194] systems when the deposited quantity is very small, i.e. just enough to induce the 2d-3d transition. When the deposited amount increases, the cluster density increases too, but the average size decreases.

A remarkable experimental feature is the relatively narrow size distribution of such population of coherent clusters. The size distribution is particularly narrow when the cluster density is high. This fact suggests a possible role of elastic interactions between islands [164,197]. According to Kobayashi et al. [164], a sufficiently dense population of adsorbed clusters evolves, through inter-cluster exchange of matter, towards a more uniform size distribution. This is exactly opposite to what is predicted for incoherent adsorption, as seen in paragraph XII-D.

F. Open questions

Various explanations have been proposed for the narrow cluster size distribution and for the absence of Ostwald ripening, at least in certain cases. Our feeling is that the situation is unclear, and we shall mainly formulate questions, which are subject to controversy at the moment, but will presumably be answered in the next future, since research in this field is particularly active.

Question 1. What is the potential energy of an adatom outside clusters? Is there an energy barrier near the cluster surface?

As seen in paragraph X C, the strain produced by a cluster increases with decreasing distance. The elastic potential felt by an adatom should also increase in absolute value. In principle, although the elastic interaction between two adatoms or between two large, coherent clusters is repulsive, the cluster-adatom interaction can be attractive [234]. Such an attraction would enhance Ostwald's ripening and therefore would not help to explain the experimental facts. Therefore, we will accept the general belief that an energy barrier [235] exists near a cluster. It opposes attachment of adatoms to clusters but, according to the detailed balance principle, it should also oppose adatom detachment from islands³⁴ and therefore slow down the evolution during annealing. This suggests a second question.

Question 2. Are there big differences between the evolution when the beam is on and when it is off?

As reported in paragraph IX E, this difference is clear when the 2d-3d transition takes place during annealing [194,221,236].

In the case of three-dimensional clusters, one could imagine that there is no evolution during annealing without beam, and a rapid change of the size distribution during growth. This would mean that atom detachment from islands is negligible and that the evolution is fully due to freshly deposited adatoms. Actually, the evolution during annealing can be slower than under irradiation [197], but is yet present.

Question 3. How high can be an energy barrier to adatom attachment, and how does it depend on the cluster size?

The barrier height is related to the local strain. In the limit of very large clusters, the strain should reach a finite limit. The barrier height is also expected to have a limit W_{bar} which is reached for some value R_{lim} of the cluster radius. According to Barabàsi [235], this limit can be comparable to the chemical bonding energy, and thus the cluster size cannot grow beyond R_{lim} . This saturation is a non-linear effect which suggests a breakdown of linear elasticity theory ...

Question 4. Is linear elasticity theory applicable in the presence of coherent, epitaxial clusters?

In paragraph X D, the strain in the vicinity of a cluster has been evaluated by the Tersoff approximation and found to diverge with the cluster size. This may be an artifact of the approximation, but, in the present state of our knowledge, a divergence of the strain calculated by linear, continuous elasticity theory is not excluded. This would mean that this theory breaks down for big enough clusters, and a plausible criterion is that it breaks down when the elastic energy per bond is comparable to the chemical energy, in agreement with Barabàsi's statement [235]. For reasonable cluster sizes, this breakdown takes place only for large misfits, since the logarithmic divergence of (195) is very weak.

Question 5. What is the effect of the 2d-3d transition?

The 2d-3d transition can favour a narrow distribution of clusters [198]. The following mechanisms are possible. First, platelets have a preferred size and therefore should have a rather uniform distribution before they transform. The distribution may remain rather uniform after transformation. Second, the barrier for incoming adatoms is somewhat higher for three-dimensional clusters than for platelets. Thus, platelets grow faster than three-dimensional clusters. Third, there is a purely geometric effect, when the biggest clusters are already three-dimensional while some smaller clusters are still flat, the incoming atoms can be expected to go preferably to the latter, just because they occupy more space on the surface. Thus, in the neighbourhood of the 2d-3d transition, small platelets grow faster than bigger, three-dimensional clusters. However, as seen in the previous paragraph, there is experimental evidence that equalization still operates a long time after the 2d-3d transition.

³⁴So far as we understand, we disagree on this point with Barabàsi [235].

Question 6. Can adatom detachment from big islands be made easier by elasticity, in comparison with smaller islands?

This has been suggested by Kobayashi [164] on experimental grounds, and by various theorists [235,237]. If it is so, this may produce a current of atoms from big to small islands and favour a finite cluster size. The difficulty is to explain this easy detachment. An energy barrier at the surface does not provide an explanation since it opposes both attachment of adatoms to clusters and detachment from clusters, as said above. The explanation can result from a failure of linear elasticity theory, since the elastic energy gain will be lower than predicted by linear elasticity, when the cluster size becomes larger than the threshold R_{lim} defined above.

Other possible solutions have been proposed, which suggests a last question.

Question 7. Is the picture given in chapter X correct?

The postulates of this description are the following.

- i) Microscopic details, e.g. the strain dependence of the diffusion constant, have been disregarded.
- ii) The only contributions to the energy are the elastic energy (the volume integral of a continuous energy density) and a strain-independent surface energy. The surface stress, which generates a strain-independent surface energy, is neglected.
- iii) There is no three-dimensional diffusion, no mixing of the substrate and adsorbate materials.
- iv) The clusters have their equilibrium shape and the equilibrium energy.

The modulation of the diffusion constant has been addressed in various papers reviewed by Schroeder & Wolf [238]. In our opinion, such effects should not be essential for a qualitative understanding of phenomena. For instance, they can modify the speed of Ostwald's ripening or the critical thickness, but cannot explain the narrow cluster size distribution. The effect of surface stress has been already addressed in paragraph X F. According to Shchukin et al. [203] it can stabilize an intermediate cluster size.³⁵ As in the case of two-dimensional clusters addressed in paragraph XI C, this can explain a narrow size distribution around this size. A more complete investigation seems necessary to check whether this interpretation is compatible with the relatively large cluster sizes which are observed.

Chemical mixing depends on the materials and on temperature. In the case of InAs/GaAs, Joyce et al. [158] have given good arguments in favour of a strong mixing, both in the wetting layer and within clusters. Indeed, they succeeded in measuring the total volume of clusters with a reasonable accuracy, and found that it is larger than the deposited volume. Mixing can strongly influence the evolution of the clusters [239]. In case of 3d cluster, the alloy segregation is probably enhanced by strain-driven atomic diffusion [240]. For instance, one might imagine that penetration of the substrate material into the weakly relaxed cluster core lowers the elastic energy, and that this penetration becomes more difficult as clusters grow, thus making the growth of big clusters more difficult, in agreement with experiments. As mentioned in chapter III, chemical inhomogeneities can also result from segregation or demixing within the adsorbate. An example is provided by the clusters resulting from the deposit of GaInAs alloy on GaAs(100). Indeed, an enrichment in Indium on the top of clusters was experimentally evidenced by different methods [241,242]

The fact that clusters need an appreciable time to reach equilibrium is testified by experiments [219,243] which demonstrate, for example, the occurrence of metastable states. Jesson et al. [244,245] have described mechanisms which slow down the establishment of equilibrium. They consider a pyramidal cluster with faceted sides, and argue that adding a new layer on a side requires to overcome an increasingly high activation barrier when the size increases. This implies that the sides of the clusters are faceted, with a roughening temperature higher than the growth temperature, a property which is not necessarily general, even though faceting at room temperature is rather well established (see Fig. 37).

XII. STACKING FAULTS AND TWINS

In this short chapter we come back to kinetic instabilities, those which are present at low temperature but not at high temperatures. A particular type of kinetic instabilities was studied in great detail in chapters IV and V, namely those which arise from the Ehrlich-Schwoebel effect. The emphasis given to Ehrlich-Schwoebel instabilities in the present review is justified by the large amount of theoretical work which has cast a good physical insight on these phenomena. There are, however, other types of instabilities, and it might be misleading to omit them completely in

³⁵This size is rather metastable than stable, since the most stable state is constituted by big bubbles (strictly speaking, a single bubble) according to the argument given at the beginning of chapter IX.

this review, since one might be tempted to attribute to the Ehrlich-Schwoebel effect instabilities which are due to other causes.

Another possible and perhaps more frequent source of growth instability is constituted by stacking faults. These defects can arise during the growth of a crystal of a material which has another crystal form with a comparable energy.

A well known example is provided by the face centered cubic Bravais lattice, which is the most common crystal among metallic elements. It is well known that a different stacking of the (111) planes leads to another Bravais lattice which is the hexagonal close packed lattice. Each atom has the same number of neighbours in both lattices, the atoms form triangles in both cases, and the energy difference can be expected to be small. Similarly, random stacking faults which destroy the periodicity are expected to have a low energy and to form rather easily during growth in the (111) direction. A growth model in which atoms are represented by hard spheres should reproduce this feature.

Stacking faults are also possible in semiconducting elements, such as Si or Ge, although the interactions are quite different. Indeed, atoms cannot be represented by hard spheres. The rigid unit is not the atom, but tetrahedra of 5 atoms (a central one and its 4 neighbours). Nevertheless, as in the case of metals, stacking faults in the (111) direction have a fairly low energy. Indeed they can be obtained by rotating the tetrahedra without distorting them.

Gallas et al. [246] have observed growth instabilities resulting from stacking faults during the growth of Si(111) in the (111) direction at low enough temperature (about 300°C) although a perfect crystal easily grows at higher temperature. These stacking faults observed in the growth of Si(111) are certainly of kinetic origin since they do not appear at higher temperature. We have seen in chapter VIII that stacking faults of thermodynamical origin can also appear in heteroepitaxy. The example of Si is interesting because the Ehrlich-Schwoebel effect has also been suggested [46] to explain instabilities observed at low temperature in the growth of Si in the (001) direction. The controversy about existence or non-existence of an Ehrlich-Schwoebel effect is reported in paragraph IV A.

Twins (Fig. 41) are more severe crystal defects than stacking faults, in the sense that they do not break only the periodicity, but also the orientational long range order. They are directly responsible for the formation of polycrystals, as seen from Fig. 42. As stacking faults, twins can be interpreted as resulting from dislocations, as seen from Fig. 43.

XIII. EFFECT OF ADDITIVES (SURFACTANTS)

In soft matter physics, ‘surfactants’ are materials which lower the surface free energy. A typical example is soap in soap bubbles.

Applied to crystal growth, the word ‘surfactant’ has taken a completely different meaning. It designates an additive which i) stays on the surface during growth, instead of being incorporated as impurities, and ii) modifies the kinetic and/or thermodynamic properties of the surface. Those surfactants which facilitate layer by layer growth with respect to three-dimensional growth in heteroepitaxy are of particular interest. Examples for Ge/Si are As, Sb, Bi, Te [247]. The coverage in these instances is of the order of 1/3 of a monolayer. Without any surfactant, as seen in paragraph IX D, it is possible to grow 3 Ge monolayers on Si(001) at 700 K before forming three-dimensional clusters. With As, one can grow 50 layers and probably more [248,249]. At such high thicknesses, the stress is relaxed, and this implies that the adsorbate is no longer coherent, although it is epitaxial [248,249].

Factors which may explain the effect of surfactants in crystal growth are the following.

- Reduction of the surface energy. It is the essential property of surfactants in soft matter physics. In the case of interest here, it may have the important effect of favouring the floating of surfactants during growth [247] but is not especially appropriate for growth of good crystals [246]. Most of the current theories of surfactant-favoured growth invoke modifications of the kinetic behaviour rather than thermodynamic effects.
- Modification of the surface diffusion coefficient [246–252].

Slow surface diffusion makes the equilibrium state harder to reach and therefore should help to avoid thermodynamical instabilities in heteroepitaxy. A way to reduce surface diffusion is to reduce temperature, but this can favour kinetic instabilities. Surfactants can therefore be a good alternative method. Of course, diffusion should not be *too* low. Another caveat is that a low diffusion coefficient increases the adatom density, and this effect tends to accelerate the evolution, so that the overall result is not easy to evaluate quantitatively, except by Monte Carlo simulations.

Voigtlaender et al. [247] have observed the effect of several surfactants during the growth in the (111) direction i) of pure Si(001) and ii) epitaxial Ge/Si(001). They argued that surfactants which favour layer by layer growth in heteroepitaxy are precisely those which reduce surface diffusion in the pure material. Conversely, ‘surfactants’ which accelerate diffusion (Ga, Sn, In, Pb) favour three-dimensional growth.

The paper of Voigtlaender et al. [247] has the merit to propose a simple picture. It also suggests an explanation of the different effect of different surfactants: those which accelerate diffusion are elements which just provide the number of electrons necessary to passivate dangling bonds, while those which provide more electrons can also retain adatoms and therefore slow down diffusion.

Even if not fully correct, a simple picture has always the merit to provide a starting point for further progress and discussion. A point which has been criticized [246,253] is the method used by Voigtlaender et al. to estimate the surface diffusion velocity. Their criterion was the distance between islands after deposit of a submonolayer (see App. B). In the simplest cases, a small surface diffusion favours a short distance between islands. However, the case of surfactant-covered Si(001) at high temperatures may be more complicated as suggested by first principle calculations and Monte Carlo simulations of Kandel & Kaxiras [253].

- Modification of the detachment rate from steps. This is the other way to slow down the evolution toward equilibrium. Kandel & Kaxiras [253] have performed Monte Carlo simulations where a barrier to detachment from steps was taken into account in a phenomenological way and obtained a good agreement with experiment. In spite of the controversy between Kandel & Kaxiras and Voigtlaender et al., both points of view are to some extent complementary. The remarkably synthetic picture given by Voigtlaender et al. provides much insight, but it involves oversimplifications which are not always confirmed by first-principle calculations [254].
- Modification of the Ehrlich-Schwoebel effect. For example, Markov [255] has suggested that a surfactant can induce an *inverse* Ehrlich-Schwoebel effect, which favours downward motion of the atoms. Roughly speaking, the reason would be that the atoms willing to stick to an upper terrace (k_- process of Fig. 10) are prevented to do so because the surfactant is already there, while an atom coming from above (k_+ process) can easily push the surfactant.
- Segregation of the surfactant on the lower terraces [256]. The result would be that the adatom mobility would be different on the lower and upper terraces.

This enumeration shows that the action of surfactants is complex and controversial.

Note that, when surfactants do not prevent cluster formation, they can affect their size and shape [257,258].

XIV. CONCLUSION

This review is the common work of theorists and experimentalists, and has been an opportunity for many discussions between them.

Such discussions are not always easy. Theorists tend to introduce oversimplified models, which help to understand some basic mechanisms, but may conceal other mechanisms which are not less basic. For instance, they have devoted more attention to phenomena which can be described by the simple S.O.S. model [4] than to twinning.

This review is, in this sense, rather theoretical. For instance, the distinction between kinetic and thermodynamic instabilities is an oversimplification because both kinetics and thermodynamics may contribute to the same process. Such mixed effects have been taken into account in the present review, but more attention should be paid to this point in the future.

Another source of misunderstanding between theorists and experimentalist, and technologists even more, is that when a difficulty appears, the theorist tries to understand it, while the technologist tries to avoid it, usually by using a more complicated method. For instance, instead of wondering how one can have a better self-organization of quantum dots, one can organize them artificially. Artificial organization of quantum dots is clearly outside the scope of the present review, but can be a better technology. Even then, it is of interest, both for fundamental and technological purposes, to understand the self-organization of quantum dots. This is still an open problem.

Another point which is not completely understood is why the Asaro-Tiller-Grinfeld theory seems to be applicable to surfaces which are believed to be singular.

In both cases, qualitative hints have been suggested in the present review, but a quantitative treatment is still to be done. It will presumably be numerical to a large extent, and we hope that the qualitative considerations presented here will help in the choice of the models to use in the simulations.

The comparison between theory and experiment is probably easier in heteroepitaxy because most of the basic mechanisms are well identified. But the growth of a simple material can also be difficult. A typical example is diamond, of which it is impossible to produce big, artificial crystals. We would have liked to include this problem in this review, but it looks difficult to isolate simple concepts in a complicated chemical game, in spite of interesting theoretical attempts [259]. The above considerations suggest directions for future research. We would recommend

- A deeper fundamental understanding of basic mechanisms in experimental facts.
- A more detailed theoretical description, to compare with a more systematic experimental study of the various factors which affect the various physical or chemical systems.

This difficult program, is now being carried out by many research groups throughout the world, and a rapid progress can be expected.

ACKNOWLEDGMENTS

It is a pleasure to acknowledge illuminating discussions with Isabelle Berb  zier, Jean Grilh  , Reinhold Koch, Max Lagally, Martin Rost, Vitali Shchukin, Martin Siegert, Pavel   milauer, Bert Voigtlaender, Ir  ne Xueref and many other colleagues. We also thank Joachim Krug for his critical reading of a part of the manuscript. We are grateful to our colleagues Erwan Adam and Alessandro Verciani for their friendly and efficient help in our conflicting relation with computing systems. P.P. gratefully acknowledges financial support from Alexander von Humboldt Stiftung.

APPENDIX A: LIST OF SYMBOLS

a	atomic distance, or a related length
d	distance, or space dimension
D	surface diffusion coefficient of adatoms
2d, 3d	jargon for two-dimensional and three-dimensional
c	monolayer thickness
E	Young modulus
ES	Ehrlich-Schwoebel (effect, length, ...)
F, F_0	Flux of atoms in MBE
h	typical linear size of bumps, mounds, clusters, etc. perpendicular to the terrace direction ('height')
j, \vec{j}	one and two-dimensional current density (in atoms per second and per length unit)
k_B	Boltzmann constant
m, \vec{m}	slope (has the dimension of a reciprocal length in chapter IV, but is dimensionless in chapter V)
n	coarsening exponent, see paragraph IV E
q	a wave vector
R	typical linear size of bumps, mounds, clusters, etc. in the terrace direction
T	temperature
T_R	roughening transition temperature (depends on the surface orientation)
v	velocity
V	volume
x	a coordinate parallel to the terraces In chapter X, quantity defined by (189) concentration of an alloy
y	a coordinate parallel to the terraces
z	the coordinate perpendicular to terraces in chapters IV and V, this coordinate divided by the monolayer thickness c)
α	kinetic coefficient, ratio of the current density to the surface slope (see paragraph IV D 1) coordinate x, y, z (e.g. in a summand)
β	$1/(k_B T)$
$\delta a/a$	lattice misfit (positive if the adsorbate is bigger than the substrate)
γ	step free energy per unit length, step stiffness (paragraph IV D 2) dimensionless exponent (paragraph IV F) coordinate x, y, z (e.g. in a summand)
$\tilde{\Gamma}$	$\tilde{\Gamma} = \Omega \beta \gamma$
ϵ	strain (chapters VIII and following) dimensionless distance from the instability threshold (chapters IV and V)
κ	reciprocal width of a domain wall (paragraph IV F) curvature of a step (paragraph V B)
μ	chemical potential
ν	Poisson ratio (chapters VIII IX and X)
ρ	number of adatoms per unit area
$\tilde{\sigma}$	surface stiffness, surface energy per unit area
σ	stress
Ω	area per surface atom (chapter V)
$\Omega_{\alpha, \gamma}^{\xi, \zeta}$	Elastic constants
\mathcal{A}	area of the growth front
\mathcal{F}	free energy
ℓ	distance between steps
ℓ_D	diffusion length

APPENDIX B: THE DIFFUSION LENGTH AND THE NUCLEATION LENGTHS

The diffusion length ℓ_D is the typical distance travelled by an adatom on a flat, high-symmetry surface before being trapped. The requirement on the surface orientation ensures that the adatom is not trapped by a preexisting step,

but by another adatom (nucleation process) or by the closed step of a growing island. The length ℓ_D can also be defined as the average distance between islands, in the stationary regime when the island density does not change (see Ref. [260]).

The simplest model (a nucleus of two adatoms is stable and it does not diffuse) requires solely the knowledge of the diffusion constant D and the flux intensity F_0 . Dimensional analysis suggests the expression (the lattice constant is put equal to one) $\ell_D = (D/F_0)^\delta$. A very simple argument allows to determine the exponent δ .

If $P(\ell)$ is the probability of nucleation per unit time in a region of size ℓ , in the stationary regime it is given by the number N of incoming adatoms times the probability p that an adatom encounters another one. N is simply given by $F_0 \ell^d$ ($d = 1, 2$ being the dimension of the substrate) and p is the product of the number of distinct sites visited by the adatom ($\approx \ell^d$) times the probability a site is occupied, i.e. the (average) density of adatoms. Finally, we have

$$P(\ell) = F_0 \ell^{2d} \langle \rho \rangle \quad (\text{B1})$$

The diffusion length is given by the condition that the probability of nucleation in a region of size ℓ_D during the deposition of one layer of material is of order unity:

$$P(\ell_D) \cdot 1/F_0 \approx 1 \quad \Rightarrow \quad \ell_D^{2d} \langle \rho \rangle \approx 1 \quad (\text{B2})$$

Since there are no preexisting steps, adatom density is not influenced by ES barriers: $\langle \rho \rangle$ may be simply evaluated as the solution of the diffusion equation $F_0 + D \nabla^2 \rho = 0$ in a region of size ℓ_D , with ρ vanishing on the boundary: $\langle \rho \rangle \approx (F_0/D) \ell_D^2$. The final result is:

$$\ell_D \approx \left(\frac{D}{F_0} \right)^{\frac{1}{2(d+1)}} \quad (\text{B3})$$

So $\delta = 1/4$ and $\delta = 1/6$, respectively in 1+1 and 2+1 dimensions. The hypothesis that a dimer is stable and does not diffuse is valid only at low temperatures: when the size of the largest cluster which is mobile and ‘unstable’ is larger than one, the exponent δ is modified [260,261].

In the main text the ‘region of size ℓ ’ must be meant as a terrace of size ℓ which therefore can be a top, a bottom, or a vicinal terrace (see Fig. 10). This distinction is necessary in the presence of step-edge barriers, because the average density $\langle \rho \rangle$ depends on the type of the terrace. In this context it is preferable to speak of ‘nucleation lengths’ for a top (ℓ_n^T), a bottom (ℓ_n^B), and a vicinal (ℓ_n^V) terrace, rather than of diffusion lengths. Since ES barriers are irrelevant for a bottom terrace, we simply have $\ell_n^B = \ell_D$. Conversely, for top and vicinal terraces $\langle \rho \rangle$ is obviously an increasing function of ℓ_{ES} . For a vicinal one it has a very weak dependence on ℓ_{ES} and goes to a finite value for $\ell_{ES} \rightarrow \infty$; in contrast, $\langle \rho \rangle$ diverges for a top terrace. In 1+1 dimensions the nucleation lengths are found via the implicit equations [56,66]:

$$(\ell_n^T)^4 + 6\ell_{ES}(\ell_n^T)^3 - \ell_D^4 = 0 \quad 1+1 \text{ dim} \quad (\text{B4})$$

$$(\ell_n^V)^5 + 4\ell_{ES}(\ell_n^V)^4 - \ell_D^4(\ell_n^V + \ell_{ES}) = 0 \quad (\text{B5})$$

whose solutions are plotted in Fig. 44.

In 2+1 dimensions we must assume that terraces have circular edges, in order to obtain an analytical expression for the adatom density. In fact, if ρ depends solely on the radius r the diffusion equation reads $\rho''(r) + (1/r)\rho'(r) = -F_0/D$, whose general solution is $\rho(r) = \rho_0 + \rho_1 \ln r - (F_0/4D)r^2$. For bottom and top terraces, analyticity in $r = 0$ requires $\rho_1 = 0$. The diffusion length is found to be $\ell_D = (8D/F_0)^{1/6}$, while the nucleation length for a top terrace is determined by the equation:

$$(\ell_n^T)^6 + 4\ell_{ES}(\ell_n^T)^5 - \ell_D^6 = 0 \quad 2+1 \text{ dim} \quad (\text{B6})$$

whose limiting solution for $\ell_{ES}/\ell_D \rightarrow \infty$ differs from the one dimensional case. In units of ℓ_D , $\ell_n^T \simeq (1/6\ell_{ES})^{1/3}$ in 1+1 dimensions and $\ell_n^T \simeq (1/4\ell_{ES})^{1/5}$ in 2+1 dimensions.

The case of a vicinal terrace is not so easy: in fact it is characterized by two different quantities, the inner (r_1) and outer (r_2) radii. If $\ell = r_2 - r_1$, it is no more true that the number N of incoming atoms per unit time is simply $N \approx F_0 \ell^2$. The average adatom density itself is a function of both r_1 and r_2 , but in the limit $r_1 \gg \ell$ it depends solely on ℓ : $\langle \rho \rangle \approx (F_0/2D)\ell^2$. In the opposite limit ($r_1 \ll \ell$) the attention must be paid to the logarithmic term, which diverges for $r_1 = 0$. This limit is relevant for the vicinal terrace neighbouring a top terrace, when $\ell_{ES} \rightarrow \infty$ (because in this limit $\ell_n^T \rightarrow 0$).

APPENDIX C: QUALITATIVE CONSIDERATIONS ON THE COARSENING EXPONENT

Let us develop here some qualitative or semiquantitative considerations on the coarsening exponent n . Krug [94] and Tang et al. [93] lay stress on noise, with the following argument: the ‘coarsening time’ is set by the condition that the fluctuations of the height of a mound of size L and average height \bar{h} , induced by shot noise, are of the same order of the height itself. In chapter IV B we wrote that, because of shot noise: $\Delta h \sim \sqrt{t/L^d}$. Now we use the extra condition that $\Delta h \sim \bar{h} \sim m^* L$, m^* being the largest slope in the profile. As a general rule: $m^* \sim L^\psi$, where $\psi = 0$ for a current with zeros at some finite m_0 and $\psi = 1$ by following the Burton-Cabrera-Frank model [it is sufficient to insert the current (43) with $\gamma = 1$ into Eq. (47)]. Therefore we will have:

$$L^{\psi+1} \sim \sqrt{t/L^d} \implies L(t) \sim t^n \quad \text{with} \quad n = \frac{1}{d+2(\psi+1)} \quad (\text{C1})$$

If the slope of the mounds is constant, $\psi = 0$ and we obtain $n = 1/(d+2)$, i.e. $n = 1/3$ in 1+1 dimensions and $n = 1/4$ in 2+1 dimensions. In one dimension, the value $n = 1/3$ agrees with exact theories [85,86]; in two dimensions, the value $n = 1/4$ seems to agree with the coarsening exponent found on (100) oriented substrates (quartic symmetry) or on isotropic substrates [67,68,91], but there is no agreement if the substrate has a triangular symmetry [81,91], in which case $n = 1/3$.

A different, nonrigorous approach to coarsening has also been developed by Golubović [262] and by Rost and Krug [263]. We report it here (in a slightly modified way) because it may clarify some differences between 1+1 and 2+1 dimensions, and –conversely to the previous argument– it neglects noise and stresses the deterministic character of coarsening. We will concentrate on the case of an asymptotic constant slope ($\psi = 0$ in the previous notation), with in-plane symmetry.

The evolution of the surface is governed by the current:

$$\vec{j} = \vec{j}_{ES} + \vec{j}_M = \alpha \vec{m}(1 - m^2/m_0^2) + K \nabla^2 \vec{m} \quad (\text{C2})$$

As coarsening proceeds the two terms vanish separately, because $|m| \rightarrow m_0$ almost everywhere. So a first question is: Do they remain of the same order, or does one of the two become negligible? The answer is: They *must* keep of the same order, otherwise the surface would not have the displayed ‘regular’ profile and coarsening (a deterministic process) would not be possible.

This condition implies a relation between the coarsening exponent n and the exponent ϑ which governs the asymptotic behaviour of m : $(m_0 - |m|)/m_0 \sim t^{-\vartheta}$. In fact a qualitative evaluation of the two terms give:

$$|\vec{j}_{ES}| \sim |\vec{j}_M| \implies t^{-\vartheta} \sim \frac{1}{L^2} \implies \vartheta = 2n \quad (\text{C3})$$

Once established that $|\vec{j}_{ES}| \sim |\vec{j}_M|$, two possibilities are left: $|\vec{j}_{ES} + \vec{j}_M| \sim |\vec{j}_{ES}| \sim |\vec{j}_M|$ or $|\vec{j}_{ES} + \vec{j}_M|$ is much smaller than each single term in the current. To be more definite let us write the evolution equation for the interface thickness $w^2(t) = \langle z^2(\vec{x}, t) \rangle$, starting from the evolution equation for $z(\vec{x}, t)$ [263]:

$$\frac{1}{2} \partial_t w^2(t) = \langle \vec{m} \cdot \vec{j}_{ES} \rangle - K \langle (\nabla^2 z)^2 \rangle \quad (\text{C4})$$

We have already argued that the two terms on the right hand side are of the same order of magnitude. Now their difference may be i) of the same order too [and therefore $\partial_t w^2(t) \sim \langle \vec{m} \cdot \vec{j}_{ES} \rangle$] or ii) it may be smaller. In the two cases we can write [263]:

$$\frac{1}{2} \partial_t w^2(t) \leq \langle \vec{m} \cdot \vec{j}_{ES} \rangle \quad (\text{C5})$$

In the same spirit as before, its qualitative evaluation gives:

$$\frac{m_0^2 L^2}{t} \leq t^{-\vartheta} \implies 2n \leq 1 - \vartheta \implies n \leq \frac{1}{4} \quad (\text{C6})$$

where the equal sign corresponds to the case (i) mentioned just above. The inequality $n \leq \frac{1}{4}$ applies to 2+1 as well as 1+1 dimensions: since our model gives $L(t) \sim \ln t$ in 1+1 dimensions (analytical result) and $L(t) \sim t^{1/4}$ in 2+1 dimensions (numerical result), the conclusion (C6) on one side supports these results, and on the other side emphasizes an important difference between one and two dimensions, due to topology: in 1+1 dimension the current \vec{j} which contributes to the evolution of the surface is vanishing small with respect to each term of the current itself.

APPENDIX D: NONLINEAR ANALYSIS OF THE DYNAMICS OF A SINGLE STEP, IN THE PRESENCE OF STEP-EDGE BARRIERS

We have to solve the differential equation:

$$D\nabla^2\rho - \rho/\tau + F_0 = 0 \quad (\text{D1})$$

in the (x, y) plane, with $y > \zeta(x, t)$ (one-sided model). Boundary conditions, if the step is locally in equilibrium, are:

$$\rho(x, \zeta(x, t), t) = \rho_{eq}^0(1 + \tilde{\Gamma}\kappa) \quad (\text{D2})$$

$$\rho(x, \infty, t) = \tau F_0 \quad (\text{D3})$$

where κ is the curvature: $\kappa = -\zeta_{xx}/[1 + \zeta_x^2]^{3/2}$.

The dynamics of the step is determined by the following relation:

$$v_n = \Omega D \partial_n \rho|_\zeta = \Omega D \vec{n} \cdot \nabla \rho|_\zeta \quad (\text{D4})$$

where v_n is the velocity normal to the step profile $\zeta(x, t)$:

$$v_n = (0, v_0 + \dot{\zeta}) \cdot \vec{n} = \frac{v_0 + \dot{\zeta}}{\sqrt{1 + \zeta_x^2}} \quad (\text{D5})$$

In the previous equations, v_0 is the velocity of the straight step and \vec{n} (the normal vector to the step) is:

$$\vec{n} = \frac{(-\zeta_x, 1)}{\sqrt{1 + \zeta_x^2}} \quad (\text{D6})$$

1. Dimensionless equation

By introducing a new variable $u = \rho - F_0\tau$ and by rescaling (x, y) with respect to x_s and t with respect to τ , Eqs. (D1,D2,D3,D4) read:

$$\nabla^2 u - u = 0 \quad (\text{D7})$$

$$u(x, \zeta, t) = -\frac{\Gamma}{\xi} - \frac{\Gamma \zeta_{xx}}{[1 + \zeta_x^2]^{3/2}} \quad (\text{D8})$$

$$u(x, \infty, t) = 0$$

$$\frac{\Omega\Gamma}{\xi} + \dot{\zeta} = \Omega(u_y - \zeta_x u_x) \quad (\text{D9})$$

where the quantities $\Gamma = \rho_{eq}^0 \tilde{\Gamma}/x_s$ and $\xi = \Gamma/\tau \Delta F$ had already been defined in the body of the article.

As explained in the main text, we introduce the small dimensionless parameter $\epsilon \equiv (1/2) - \xi$ and the new variables:

$$X = x\sqrt{\epsilon} \quad (\text{D10})$$

$$T = t\epsilon^2 \quad (\text{D11})$$

$$H(X, T) = \zeta(x, t)/\epsilon \quad (\text{D12})$$

through which Eqs. (D7,D8,D9) read:

$$\epsilon u_{XX} + u_{YY} - u = 0 \quad (\text{D13})$$

$$u(X, \epsilon H, T) = -\frac{\Gamma}{1/2 - \epsilon} - \epsilon^2 \frac{\Gamma H_{XX}}{[1 + \epsilon^3 H_X^2]^{3/2}} \quad (\text{D14})$$

$$\frac{\Omega\Gamma}{1/2 - \epsilon} + \epsilon^3 H_T = \Omega(u_Y - \epsilon^2 H_X u_X) \quad (\text{D15})$$

Now, u and H are expanded in powers of ϵ :

$$u = u_0 + \epsilon u_1 + \epsilon^2 u_2 + \epsilon^3 u_3 + \dots \quad (\text{D16})$$

$$H = H_0 + \epsilon H_1 + \epsilon^2 H_2 + \epsilon^3 H_3 + \dots \quad (\text{D17})$$

2. Differential equation and boundary conditions at different orders

Now the task is laborious, but straightforward: replace the expansions for u and H in Eqs. (D13,D14,D15), taking in mind that we must keep all the terms till order ϵ^3 . For the differential equation it is easy, and we obtain:

$$\begin{aligned} u_{0YY} - u_0 &= 0 \\ u_{0XX} + (u_{1YY} - u_1) &= 0 \\ u_{1XX} + (u_{2YY} - u_2) &= 0 \\ u_{2XX} + (u_{3YY} - u_3) &= 0 \end{aligned} \quad (D18)$$

For Eq. (D14), we start by rewriting the right-hand-side:

$$u(X, \epsilon H, T) = -2\Gamma(1 + 2\epsilon + 4\epsilon^2 + 8\epsilon^3) - \Gamma\epsilon^2(H_{0XX} + \epsilon H_{1XX}) \quad (D19)$$

The left-hand-side must be handled with care:

$$u(X, \epsilon H, T) = \sum_{n=0}^3 \epsilon^n u_n(X, \epsilon H, T) \quad (D20)$$

where:

$$u_n(X, \epsilon H, T) = u_n + u_{nY}\epsilon H + u_{nYY}\frac{\epsilon^2 H^2}{2} + u_{nYYY}\frac{\epsilon^3 H^3}{6} \quad (D21)$$

and H^n itself must be expanded, using Eq. (D17). So, at third order in ϵ , we obtain:

$$u_n(X, \epsilon H, T) = u_n + u_{nY}(\epsilon H_0 + \epsilon^2 H_1 + \epsilon^3 H_2) + \frac{u_{nYY}}{2}(\epsilon^2 H_0^2 + 2\epsilon^3 H_0 H_1) + \frac{u_{nYYY}}{6}\epsilon^3 H_0^3 \quad (D22)$$

where, here and in the future, an expression of the form $u_{nY..Y}$ must be evaluated in $Y = 0$.

By coming back to the expression of $u(X, \epsilon H, T)$ (see Eq. (D20)), we have:

$$u(X, \epsilon H, T) = u_0 + \epsilon(u_{0Y}H_0 + u_1) + \epsilon^2(u_{0Y}H_1 + u_{0YY}\frac{H_0^2}{2} + u_{1Y}H_0 + u_2) \quad (D23)$$

$$+ \epsilon^3(u_{0Y}H_2 + u_{0YY}H_0H_1 + u_{0YYY}\frac{H_0^3}{6} + u_{1Y}H_1 + u_{1YY}\frac{H_0^2}{2} + u_{2Y}H_0 + u_3) \quad (D24)$$

Comparing this expansion with the right-hand-side of Eq. (D19), the boundary condition (D14), at different orders in ϵ writes:

$$\begin{aligned} u_0 &= -2\Gamma \\ u_{0Y}H_0 + u_1 &= -4\Gamma \\ u_{0Y}H_1 + u_{0YY}\frac{H_0^2}{2} + u_{1Y}H_0 + u_2 &= -8\Gamma - H_{0XX}\Gamma \\ u_{0Y}H_2 + u_{0YY}H_0H_1 + u_{0YYY}\frac{H_0^3}{6} + u_{1Y}H_1 + u_{1YY}\frac{H_0^2}{2} + u_{2Y}H_0 + u_3 &= -16\Gamma - \Gamma H_{1XX} \end{aligned} \quad (D25)$$

Finally, we have to evaluate Eq. (D15) up to ϵ^3 . This requires to calculate u_Y at the order ϵ^3 and u_X at the order ϵ . Concerning $u_Y(X, \epsilon H, T)$, the result is identical to Eq. (D24), once that u_n is everywhere replaced by u_{nY} (and u_{nY} by u_{nYY}, \dots). Concerning $u_X(X, \epsilon H, T)$ at first order, since u_0 does not depend on X , the result is easily obtained:

$$u_X(X, \epsilon H, T) = \epsilon u_{1X}(X, 0, T) \quad (D26)$$

By using this expression, but not yet expanding u_Y , Eq. (D14) reads:

$$2\Gamma(1 + 2\epsilon + 4\epsilon^2 + 8\epsilon^3) + \Omega^{-1}\epsilon^3 H_{0T} = u_Y - \epsilon^3 H_{0X}u_{1X} \quad (D27)$$

If u_Y is expanded according to the criterion given above, the velocity of the step (Eq. (D15)) is determined at the various order in ϵ by the following relations:

$$\begin{aligned}
2\Gamma &= u_{0Y} \\
4\Gamma &= u_{0YY}H_0 + u_{1Y} \\
8\Gamma &= u_{0YY}H_1 + u_{0YYY}\frac{H_0^2}{2} + u_{1YY}H_0 + u_{2Y}
\end{aligned} \tag{D28}$$

$$16\Gamma + \Omega^{-1}H_{0T} = u_{0YY}H_2 + u_{0YYY}H_0H_1 + u_{0YYYY}\frac{H_0^3}{6} + u_{1YY}H_1 + u_{1YYY}\frac{H_0^2}{2} + u_{2YY}H_0 + u_{3Y} - u_{1X}H_{0X}$$

The next and final step is to solve, order by order, Eqs. (D18) with boundary conditions (D25) and (D28).

Zero order - We have to solve: $u_{0ZZ} - u_0 = 0$, with $u_0 = -2\Gamma$ and $u_{0Z} = 2\Gamma$ as boundary conditions. The solution is:

$$u_0(Z) = -2\Gamma \exp(-Z) \tag{D29}$$

We remark that the two boundary conditions are indeed equal, and this will be true also at the first and second order in ϵ ! This is not surprising, because H_{0T} –and therefore the motion of the step– enters at the third order of the boundary conditions (D28) only.

First order - The solution of the equation $u_{1ZZ} - u_1 = 0$ is:

$$u_1(X, Z, T) = A_1(X, T) \exp(-Z) \tag{D30}$$

and the boundary condition $u_{0Z}H_0 + u_1 = -4\Gamma$ implies:

$$2\Gamma H_0(X, T) + A_1(X, T) = -4\Gamma \tag{D31}$$

Second order - The differential equation $u_{1XX} + (u_{2ZZ} - u_2) = 0$ gives the solution:

$$u_2(X, Z, T) = A_2 \exp(-Z) + \frac{A_{1XX}}{2} Z \exp(-Z) \tag{D32}$$

where A_2 (as well A_1) is a function of X and T . The boundary condition $u_{0Z}H_1 + u_{0ZZ}\frac{H_0^2}{2} + u_{1Z}H_0 + u_2 = -8\Gamma - H_{0XX}$ gives:

$$\Gamma^{-1}A_2 = -8 - 2H_1 - H_0^2 - 4H_0 - H_{0XX} \tag{D33}$$

Third order - The differential equation $u_{2XX} + (u_{3ZZ} - u_3) = 0$ has the solution:

$$u_3(X, Z, T) = \left[A_3 + \left(\frac{A_{1XXXX}}{8} + \frac{A_{2XX}}{2} \right) Z + \frac{A_{1XXXX}}{8} Z^2 \right] \exp(-Z) \tag{D34}$$

This time the two boundary conditions (D25) and (D28) are not equivalent and this implies a condition on H_0 under the form of a differential equation which governs the dynamics of the step. In fact, Eq. (D25) gives:

$$\Gamma^{-1}A_3 + 16 + H_{1XX} + 2H_2 + 8H_0 + \frac{H_0^3}{3} + 2H_0^2 + 2H_0H_1 + 4H_1 = 0 \tag{D35}$$

and Eq. (D28) gives:

$$\begin{aligned}
&\Gamma^{-1}A_3 + 16 + H_{1XX} + 2H_2 + 8H_0 + \frac{H_0^3}{3} + 2H_0^2 + 2H_0H_1 \\
&+ 4H_1 + (\Omega\Gamma)^{-1}H_{0T} + (3/4)H_{0XXXX} - H_{0X}^2 + 2H_{0XX} = 0
\end{aligned} \tag{D36}$$

Their comparison provides the equation for H_0 we were looking for:

$$(\Omega\Gamma)^{-1}\partial_T H_0 = -2\partial_X^2 H_0 - (3/4)\partial_X^4 H_0 + (\partial_X H_0)^2 \tag{D37}$$

APPENDIX E: SCALING LAWS FOR COHERENT EPITAXIAL CLUSTERS

1. Scaling of the elastic free energy of a cluster with respect to the misfit

The first scaling law concerns the influence of the misfit for an adsorbate of fixed shape and volume and fixed elastic constants. The misfit can be represented by an external or force dipole density (or ‘stress’) acting inside the adsorbate. This stress will always be assumed weak enough, so that the response is linear, i.e. the strain at a given point is proportional to the misfit $\delta a/a$, so that the elastic energy density is proportional to $(\delta a/a)^2$. The total elastic energy is therefore also proportional to $(\delta a/a)^2$. The determination of the proportionality coefficient would be difficult. It is an integral which involves the elastic linear response functions (or ‘Green’s functions’) of the system, which are very complicated and depend on the adsorbate shape and elastic constants.

2. Scaling of the elastic free energy of a cluster with respect to its volume V

The second scaling law concerns the size dependence of the elastic free energy for an adsorbate of a particular shape, whose linear dimensions can be varied but keep fixed ratios. The elastic free energy is the sum of (149) and (152) and can be written as

$$\delta\mathcal{F}_{el}^{(a)} = \int d^3r \Phi(\vec{r}, \epsilon_{xx}(\vec{r}), \epsilon_{xy}(\vec{r}), \dots, \epsilon_{zz}(\vec{r})) \quad (\text{E1})$$

where the function Φ is defined by (149) and (152).

Expression (E1) is very general, and general expressions are sometimes brain-twisting. It may therefore be a helpful exercise to consider the example of a cluster which is a half-sphere of radius R . If the origin of the coordinates are chosen at the center of the sphere, the linear part of Φ can be written, according to (149), as

$$\Phi^{(lin)}(\vec{r}, \epsilon_{xx}, \epsilon_{xy}, \dots, \epsilon_{zz}) = \text{Const} \times \frac{\delta a}{a} [\epsilon_{xx} + \epsilon_{yy}] \theta(z) \theta(R - r) \quad (\text{E2})$$

where $\theta(z) = 0$ for $z < 0$ and $\theta(z) = 1$ for $z \geq 0$. The quadratic part $\Phi^{(quad)}$ can easily be written using (152).

Consider now (Fig. 45b) another structure of the adsorbate which is deduced from the first one (Fig. 45a) by the similarity transformation³⁶

$$\vec{r} \rightarrow \lambda \vec{r} \quad (\text{E3})$$

The elastic free energy of the new structure has the form

$$\delta\mathcal{F}_{el}^{(b)} = \int d^3r \Phi(\vec{r}/\lambda, \epsilon_{xx}(\vec{r}), \epsilon_{xy}(\vec{r}), \dots, \epsilon_{zz}(\vec{r})) \quad (\text{E4})$$

where the function Φ is just the same as before! The proof is easy and left to the reader, who can first treat the example of a half sphere. This property is true *even if anharmonicity is taken into account*. However, it would not be completely true if the atomic, discrete nature of matter were not disregarded.

Now, if one makes the change of variables

$$\epsilon_{\alpha,\gamma}(\vec{r}) = \eta_{\alpha,\gamma}(\vec{r}/\lambda) \quad , \quad \vec{r} = \lambda \vec{\rho}$$

formula (E4) reads

$$\delta\mathcal{F}_{el}^{(b)} = \lambda^3 \int d^3\rho \Phi(\rho, \eta_{xx}(\vec{\rho}), \eta_{xy}(\vec{\rho}), \dots, \eta_{zz}(\vec{\rho})) \quad (\text{E5})$$

which is identical to (E2) apart from the factor λ^3 and the different names of the variables. If (E2) is minimized by the strain $\epsilon_{\alpha,\gamma}(\vec{r}) = \epsilon_{\alpha,\gamma}^0(\vec{r})$, then (E5) is minimized by $\eta_{\alpha,\gamma}(\vec{\rho}) = \epsilon_{\alpha,\gamma}^0(\vec{\rho})$, and therefore (E4) is minimized by $\epsilon_{\alpha,\gamma}(\vec{r}) = \epsilon_{\alpha,\gamma}^0(\vec{r}/\lambda)$. And the minimum of (E4) or (E5) is equal to the minimum of (E2) multiplied by λ^3 . Since the volume of the transformed cluster is equal to the volume of the original cluster multiplied by λ^3 , *the elastic energy of a coherent, epitaxial cluster of a given shape is proportional to its volume V .*

3. Scaling of the strain at long distance \vec{r} of a cluster as a function of its volume V

The problem is analogous to the previous one but now we consider the elastic displacement $\vec{u}(\vec{r})$, at a fixed, large distance \vec{r} of the center of the cluster. In the special case of an isotropic elastic medium, the complete calculation has been done by Boussinesq [205].

³⁶The notation \vec{r} designates the points of the totally constrained adsorbate, so that the actual locations of the atoms are $\vec{r} + \vec{u}(\vec{r})$, where \vec{u} is the elastic displacement

The displacement at distance r turns out to be proportional to $1/r^2$, so that the strain is proportional to $1/r^3$. We shall argue here that this scaling is also true for an anisotropic elastic solid. As a lemma, we need to show first that, for fixed \vec{r} , the displacement and the strain are proportional to V .

Let us assume that the atomic displacements in a slab (S) just below the adsorbate are known. Its knowledge determines the displacement and strain in the remainder of the crystal through the equations of elasticity (154). Outside the slab (S), these equations are independent of the existence or non existence of the cluster. On the other hand, in the slab, the displacements \vec{u}_i are the same as those which would arise from external forces \vec{f}_i acting on the n atoms inside the slab in the absence of the adsorbed cluster. The forces \vec{f}_i can in principle be determined by solving the equations of elasticity which usually yield the \vec{u}_i 's when the forces \vec{f}_i are known, but can be used also to determine the \vec{f}_i 's if the \vec{u}_i 's are known, since there are $3n$ linear equations for $3n$ unknowns $f_{i\alpha}$. Since the total force must vanish, it may be preferable to introduce a force dipole density $\mu_{\gamma\xi}(\vec{r}')$.

The displacements $\vec{u}_i = \vec{u}(\vec{r})$ at distance \vec{r} are related to the forces by linear equations of the form

$$u_\alpha(\vec{r}) = \int_{(S)} d^3r' \sum_{\gamma\xi} \Gamma_{\alpha\gamma\xi}(\vec{r} - \vec{r}') \mu_{\gamma\xi}(\vec{r}') \quad (\text{E6})$$

where the response function $\Gamma_{\alpha\gamma\xi}(\vec{r} - \vec{r}')$ is independent of the size and shape of the cluster, since the cluster has been removed. It is also independent of the size and shape of the slab. Actually, $\Gamma_{\alpha\gamma\xi}(\vec{r} - \vec{r}')$ is a Green's function of an elastic solid limited by a plane, which can be found in textbooks... at least in the case of an isotropic solid or a cubic crystal limited by a (001) surface.

We now make the similarity transformation (E3). It can easily be shown that the term linear with respect to the fictitious forces satisfies (E4), so that the force or force dipole densities are the same in two corresponding points. Now, at a long distance, the dependence of $\Gamma_{\alpha\gamma\xi}(\vec{r} - \vec{r}')$ with respect to \vec{r}' can be ignored and, if the cluster is centered at the origin 0, (E6) reads, before the similarity transformation,

$$u_\alpha^{(1)}(\vec{r}) = \sum_{\gamma\xi} \Gamma_{\alpha\gamma\xi}(\vec{r}) \int_{(S)} d^3r' \mu_{\gamma\xi}(\vec{r}')$$

After the similarity transformation, if the transformed slab is called (S'), the displacement at the same point \vec{r} is

$$u_\alpha^{(2)}(\vec{r}) = \sum_{\gamma\xi} \Gamma_{\alpha\gamma\xi}(\vec{r}) \int_{(S')} d^3r' \mu_{\gamma\xi}(\vec{r}'/\lambda) = \lambda^3 \sum_{\gamma\xi} \Gamma_{\alpha\gamma\xi}(\vec{r}) \int_{(S)} d^3r'' \mu_{\gamma\xi}(\vec{r}'')$$

where $\vec{r}'' = \vec{r}'/\lambda$. Comparison of the last two formulae shows that $u^{(2)}(\vec{r}) = \lambda^3 u^{(1)}(\vec{r})$. *The elastic displacement and stress at a long, given distance r of a coherent, epitaxial cluster of a given shape is proportional to its volume.*

4. Scaling of the strain at long distance \vec{r} a cluster as a function of r

A consequence of the previous paragraph is that the strain on the adsorbate surface at a long distance r from the center of a cluster decays as r^{-3} . Indeed, the strain should be proportional to the volume, so that the strain $\epsilon_0(\vec{r})$ produced by the clusters (C) and (C') satisfies $\epsilon_1(\lambda\vec{r}) = \lambda^3 \epsilon_0(\lambda\vec{r})$. But we have seen that $\epsilon_1(\lambda\vec{r}) = \epsilon_0(\vec{r})$. Therefore $\epsilon_0(\lambda\vec{r}) = \lambda^{-3} \epsilon_0(\vec{r})$ in agreement with our statement. In particular, the strain produced by a single adsorbed atom at a distance r on the substrate surface is proportional to r^{-3} .

5. Elastic interactions at long distance \vec{r} between clusters or adatoms

One can deduce how the elastic interaction between two clusters at a long distance r behaves. Indeed, the energy change when depositing an adatom can be shown to be a linear function of the local strain. Therefore, there is an elastic interaction between adsorbed atoms

$$V_{el}(r) = \text{Const}/r^3 \quad (\text{E7})$$

The constant can be shown to be positive, so that the elastic interaction is repulsive [3,4]. There is no contradiction with the above statement that the *total* elastic energy is negative.

The elastic interaction between two adsorbed atoms at a long distance r is given by a formula analogous to (E7), which is (190).

The result (E7) can be used to determine the scaling of the interaction energy of a set of coherent clusters as a function of their average distance r or their average diameter R at constant coverage N/\mathcal{A} . The distance r will be assumed to be much longer than the average cluster diameter R . According to (190), the elastic interaction must be proportional to $1/r^3$ multiplied by the square of the average number n of adatom per clusters (proportional to R^3) and by the number of clusters \mathcal{N} which is proportional to $1/r^2$. Since the total adsorbed mass is proportional to $N = n\mathcal{N}$ and fixed, R^3 should be proportional to r^2 and the interaction energy between clusters is

$$\mathcal{F}_{inter} \approx \text{Const} \times \mathcal{N} n^2 / r^3 \sim \text{Const} \times R^6 / r^5 \sim \text{Const} / r \quad .$$

The constant is certainly positive since it is positive for a single atom. Thus, the ‘intercluster’ elastic energy \mathcal{F}_{inter} is a decreasing function of r and favours large clusters. In addition there is an ‘intracluster’ energy discussed earlier in this chapter. Since it is proportional to the cluster volume, i.e. to the number of atoms, the total intracluster energy is not affected by atom exchange, at least if the modification of the shape is ignored. A more detailed analysis taking shape modification into account does not modify the conclusion that the average cluster size should increase steadily with time, even if elasticity is taken into account. The possible reasons of the experimental facts which seem to contradict this conclusion are reviewed in paragraph XIII.

-
- [1] M.A. Herman, H. Sitter, *Molecular Beam Epitaxy* (Springer, Heidelberg, 1996).
 - [2] A. Valance, C. Misbah, D. Temkin, K. Kassner, Phys. Rev. E **48**, 1924 (1993). *Analytic theory for parity breaking in lamellar eutectic growth* and references therein.
 - [3] P. Nozières, in *Solids far from equilibrium*, ed. C. Godrèche (Cambridge University Press, Cambridge, 1991). *Shape and growth of crystals*.
 - [4] A. Pimpinelli, J. Villain, *Physics of Crystal Growth* (Cambridge University Press, Cambridge, 1998).
 - [5] A.L. Barabási and H.E. Stanley, *Fractals concepts in surface growth* (Cambridge University Press, Cambridge, 1995).
 - [6] L.H. Tang, T. Nattermann, Phys. Rev. Lett. **66**, 2899 (1991). *Kinetic roughening in molecular-beam epitaxy*.
 - [7] J.C. Heyraud, J.J. Métois, J.M. Bermond, Surf. Sci. **425**, 48 (1999). *The roughening transition of the Si(113) and Si(110) surfaces*.
 - [8] P.V. Hobbs, *Ice physics* (Clarendon Press, Oxford, 1974).
 - [9] D.P. Woodruff, *The solid-liquid interface* (Cambridge University Press, Cambridge, 1973).
 - [10] P. Pelcé, ed., *Dynamics of curved fronts* (Academic Press, New York 1988).
 - [11] J.S. Langer, Ann. Phys. **65**, 53-86 (1971). *Theory of spinodal decomposition in alloys*.
 - [12] Y. Pomeau, M. Ben Amar, in *Solids far from equilibrium*, ed. C. Godrèche (Cambridge Univ. Press, Cambridge, 1992). *Dendritic growth and related topics*.
 - [13] B. Caroli, C. Caroli, B. Roulet, in *Solids far from equilibrium*, ed. C. Godrèche (Cambridge Univ. Press, Cambridge, 1992). *Instabilities of planar solidification fronts*.
 - [14] T.A. Witten and L.M. Sander, Phys. Rev. Lett. **47**, 1400 (1981). *Diffusion-limited aggregation, a kinetic critical phenomenon*.
 - [15] T.A. Witten and L.M. Sander, Phys. Rev. B **27**, 5686 (1983). *Diffusion-limited aggregation*.
 - [16] B.J. Mason, Contemporary Physics **33**, 227 (1992). *Snow crystals, natural and man made*.
 - [17] W.W. Mullins, R.F. Sekerka, J. Appl. Phys. **34**, 323 (1963). *Morphological stability of a particle growing by diffusion or heat flow*.
 - [18] W.W. Mullins, R.F. Sekerka, J. Appl. Phys. **35**, 444 (1963). *Stability of a planar interface during solidification of a dilute binary alloy*.
 - [19] L. Pietronero, E. Tosatti, eds., *Fractals in Physics* (North Holland, Amsterdam 1986).
 - [20] P. Meakin, in Ref. [19], p. 205. *Some recent advances in the simulation of diffusion limited aggregation and related processes*.
 - [21] A. Arneodo, F. Argoul, Y. Couder, M. Rabaud, in *Growth and Form: Nonlinear aspects*, eds. M. Ben Amar, P. Pelcé, P. Tabeling (Plenum, New York 1991), p. 297. *Diffusion controlled growth phenomena: from smooth interfaces to fractal structures*.
 - [22] B.A. Joyce, D.D. Vvedensky, C.T. Foxon, "Handbook on semiconductors", Vol. 3, 275 (1994).
 - [23] A.F. Jankovski, J. Magn. Magn. Mater. **126**, 185 (1993). *Superhardness effect in Au/Ni multilayers*.
 - [24] P. Hermann, J.M. Guigner, B. Tardy, Y. Jugnet, D. Simon and J.C. Bertolini, Journal of Catalysis, **163**, 169 (1996). *The Pd/Ni(110) bi-metallic system. Surface characterization by LEED, AES, XPS and LEIS techniques. New insights on catalytic properties*.
 - [25] U. Gradmann, J. Magn. Magn. Mater. **54-57**, 733 (1986). *Magnetic surface anisotropies*.
 - [26] F.J.A. Den Broeder, W. Howings and P.J.H. Bloemen, J. Magn. Magn. Mater. **93**, 562 (1991). *Magnetic anisotropy of multilayers*.
 - [27] H. J. Hug, B. Steifel, A. Moser, I. Parashikov, A. Klicznik, D. Lipp, H.J. Guntherodt, G. Bochi, D.I. Paul, R.C. O'Handley, J. Appl. Phys. **79**, 5609 (1996). *Magnetic domain structure in ultrathin Cu/Ni/Cu/Si(001) films*.
 - [28] A. Cebollada, D. Weller, J. Sticht, G.R. Harp, R.F.C. Farrow, R.F. Marks, R. Savoy, J.C. Scott, Phys. Rev. B **50**, 3419 (1994). *Enhanced magneto-optical Kerr effect in spontaneously ordered FePt alloys: Quantitative agreement between theory and experiment*.
 - [29] V. Gehanno, A. Marty, B. Gilles, Y. Samson, Phys. Rev. B **55**, 12552 (1997). *Magnetic domains in epitaxial ordered FePd(001) thin films with perpendicular magnetic anisotropy*.
 - [30] S.S.P. Parkin, N. More, K.P. Roche, Phys. Rev. Lett. **64**, 2304 (1990). *Oscillations in exchange coupling and magnetoresistance in metallic superlattice structures: Co/Ru, Co/Cr, and Fe/Cr*.
 - [31] N.M. Baibich, J.M. Broto, A. Fert, F. Nguyen Van Dau, F. Petroff, P. Etienne, G. Creuset, A. Friederich, J. Chazelas, Phys. Rev. Lett. **61**, 2472 (1988). *Giant magnetoresistance of (001)Fe/(001)Cr magnetic superlattices*.
 - [32] P. Šmilauer and D.D. Vvedensky, Phys. Rev. B **48**, 17603-17606 (1993). *Step-edge barriers on GaAs(001)*.
 - [33] A. Zangwill, C.N. Luse, D.D. Vvedensky and M.R. Wilby, Surf. Sci. Lett. **274**, L529-L534 (1992). *Equations of motion for epitaxial growth*.
 - [34] A.K. Myers-Beaghton and D.D. Vvedensky, Phys. Rev. B **42**, 5544 (1990). *Nonlinear equation for diffusion and adatom*

interactions during epitaxial growth on vicinal surfaces.

- [35] J. Tersoff, M.D. Johnson, B.G. Orr, Phys. Rev. Lett. **78**, 282 (1997). *Adatom densities on GaAs: Evidence for Near-Equilibrium Growth.*
- [36] J.M. Moison, C. Guille, F. Houzay, F. Barthe, and M. Van Rompay, Phys. Rev. B **40**, 6149 (1989)
- [37] G. Ehrlich, F.G. Hudda, J. Chem. Phys. **44**, 1039 (1966). *Atomic view of surface diffusion: tungsten on tungsten.*
- [38] R.L. Schwoebel and E.J. Shipsey, J. Appl. Phys. **37**, 3682 (1966). *Step motion on crystal surfaces*; R.L. Schwoebel, J. Appl. Phys. **40**, 614 (1969). *Step motion on crystal surfaces II.*
- [39] J. Villain, J. de Physique I **1**, 19-42 (1991). *Continuum models for crystal growth from atomic beams with and without desorption.*
- [40] P. Stoltze, J. Phys.: Condens.Matter **6**, 9495 (1994). *Simulation of surface defects.*
- [41] R. Stumpf, M. Scheffler, Phys. Rev. Lett. **72**, 254 (1994). *Theory of self-diffusion and growth of Al(111).*
- [42] R. Ferrando and G. Tréglia, Phys. Rev. Lett. **76**, 2109-2112 (1996). *High-temperature study of the Schwoebel effect in Au(111).*
- [43] K. Kyuno and G. Ehrlich, Surf. Sci. **383**, L766-L774 (1997). *Step-edge barriers: truths and kinetic consequences.*
- [44] K. Bromann, H. Brune, H. Röder and K. Kern, Phys. Rev. Lett. **75**, 677-680 (1995). *Interlayer mass transport in homoepitaxial metal growth*; J.A. Meyer, J. Vrijmoeth, H.A. van der Vegt, E. Vlieg and R.J. Behm, Phys. Rev. B **51**, 14790-14793 (1995). *Importance of the additional step-edge barrier in determining film morphology during epitaxial growth*; P. Šmilauer and S. Harris, Phys. Rev. B **51**, 14798-14801 (1995). *Determination of step-edge barriers to interlayer transport from surface morphology during the initial stages of homoepitaxial growth*; I. Markov, Phys. Rev. B **54**, 17930-17937 (1996). *Method for evaluation of the Ehrlich-Schwoebel barrier to interlayer transport in metal homoepitaxy.*
- [45] K. Morgenstern, G. Rosenfeld, E. Laegsgaard, F. Besenbacher, G. Comsa, Phys. Rev. Lett. **80**, 556 (1998). *Measurement of energies controlling ripening and annealing on metal surfaces.*
- [46] D.J. Eaglesham, G.H. Gilmer, in *Surface disordering: growth, roughening and phase transition*, eds. R. Jullien, J. Kertész, P. Meakin and D.E. Wolf (Nova Science, New York, 1993). *Roughening during Si deposition at low temperature.*
- [47] C.J. Lanczycki, R. Kotlyar, E. Fu, Y.-N. Yang, E.D. Williams and S. Das Sarma, Phys. Rev. B **57**, 13132-13148 (1998). *Growth of Si on the Si(111) surface.*
- [48] S. Kodiyalam, K.E. Khor, S. Das Sarma, Phys. Rev. B **53**, 9913 (1996). *Calculated Schwoebel barriers on Si(111) steps using an empirical potential.*
- [49] M.C. Desjonquères, D. Spanjaard, *Concepts in Surface Physics*, Springer Series in Surface Science, Vol. 30 (Springer, Heidelberg, 1993).
- [50] J.E. Van Nostrand, S. Jay Chey, M.-A. Hasan, D.G. Cahill and J.E. Greene, Phys. Rev. Lett. **74**, 1127-1130 (1995). *Surface morphology during multilayer epitaxial growth of Ge(001).*
- [51] J.E. Van Nostrand, S. Jay Chey and D.G. Cahill, Phys. Rev. B **57**, 12536-12543 (1998). *Low-temperature growth morphology of singular and vicinal Ge(001).*
- [52] C. Orme, M.D. Johnson, J.L. Sudijono, K.T. Leung and B.G. Orr, Appl. Phys. Lett. **64**, 860-862 (1994). *Large scale surface structure formed during GaAs (001) homoepitaxy.*
- [53] M.D. Johnson, C. Orme, A.W. Hunt, D. Graff, J. Sudijono, L.M. Sander and B.G. Orr, Phys. Rev. Lett. **72**, 116-119 (1994). *Stable and unstable growth in molecular beam epitaxy.*
- [54] G.S. Bales and A. Zangwill, Phys. Rev. B **41**, 5500 (1990). *Morphological instability of a terrace edge during step flow growth.*
- [55] J.W. Cahn and J.E. Hilliard, J. Chem. Phys. **28**, 258 (1958). *Free energy of a nonuniform system. I. Interfacial free energy*; J.W. Cahn, J. Chem. Phys. **30**, 1121 (1959). *Free energy of a nonuniform system. II. Thermodynamic basis.*
- [56] I. Elkinani, J. Villain, J. de Physique I **1**, 1991 (1994). *Growth roughness and instability due to the Schwoebel effect: a one-dimensional model.*
- [57] D. Wolf, in *Scale invariance, interfaces, and non-equilibrium dynamics*, eds. A. McKane et al. (Plenum Press, New York, 1995). E. Somfai, D.E. Wolf and J. Kertész, J. de Physique I **6**, 393 (1996). *Correlated island nucleation in layer-by-layer growth.*
- [58] P. Politi, J. Villain, Phys. Rev B **54**, 5114 (1996). *The Ehrlich-Schwoebel instability in Molecular Beam Epitaxy: A minimal model.*
- [59] H. Kallabis, *Theoretical aspects of crystal growth*. Ph.D. Thesis (Jülich, December 1997). Jül-3483.
- [60] W.K. Burton, N. Cabrera, F. Frank, Phil. Trans. Roy. Soc. **243**, 299 (1951). *The growth of crystals and the equilibrium structure of their surfaces.*
- [61] M. Plischke, D. Liu and Z. Rácz, Phys. Rev. B **35**, 3485 (1987). *Time-reversal invariance and universality of two-dimensional growth models.*
- [62] D.D. Vvedensky, A. Zangwill, C.N. Luse and M.R. Wilby, Phys. Rev. E **48**, 852-862 (1993). *Stochastic equations of motion for epitaxial growth.*
- [63] M. Předota and M. Kotrla, Phys. Rev. E **54**, 3933 (1996). *Stochastic equations for simple discrete models of epitaxial growth.*
- [64] J. Krug, H.T. Dobbs and S. Majaniemi, Z. Phys. B **97**, 281-291 (1995). *Adatom mobility for the solid-in-solid model.*
- [65] J. Krug, Adv. Phys. **46**, 139-282 (1997). *Origins of scale invariance in growth processes.*

- [66] P. Politi, J. de Physique I **7**, 797-806 (1997). *Different regimes in the Ehrlich-Schwoebel instability.*
- [67] M. Siegert and M. Plischke, Phys. Rev. Lett. **73**, 1517 (1994). *Slope selection and coarsening in molecular beam epitaxy.*
- [68] M. Siegert, Physica A **239**, 420-427 (1997). *Ordering dynamics of surfaces in molecular beam epitaxy.*
- [69] J.A. Strosio D.T. Pierce, M.D. Stiles, A. Zangwill, L.M. Sander, Phys. Rev. Lett. **75**, 4246 (1995). *Coarsening of unstable surface features during Fe(001) homoepitaxy.*
- [70] J.W. Evans, Phys. Rev. B **43**, 3897-3905 (1991). *Factors mediating smoothness in epitaxial thin-film growth.*
- [71] A. Chame, S. Rousset, H.P. Bonzel and J. Villain, Bulg. Chem. Commun. **29**, 398 (1996/97). *Slow dynamics of step surfaces.*
- [72] W.W. Mullins, J. Appl. Phys. **28**, 333 (1957). *Theory of thermal grooving.*
- [73] J.A. Strosio and D.T. Pierce, Phys. Rev. B **49**, 8522-8525 (1994). *Scaling of diffusion-mediated island growth in iron-on-iron homoepitaxy.*
- [74] P. Politi and J. Villain, in *Surface diffusion: atomistic and collective processes*, eds. M. Scheffler and M. Tringides (Plenum Press, 1997). *Kinetic coefficient in a system far from equilibrium.*
- [75] J. Krug, in *Dynamics of fluctuating interfaces and related phenomena*, eds. D. Kim et al. (World Scientific, Singapore 1997). *Continuum equations for step flow growth.*
- [76] T. Sun, H. Guo and M. Grant, Phys. Rev. A **40**, 6763 (1989). *Dynamics of driven interfaces with a conservation law.*
- [77] H.J. Ernst, F. Fabre, R. Folkerts, J. Lapujoulade, Phys. Rev. Lett. **72**, 112 (1994). *Observation of a growth instability during low temperature molecular beam epitaxy.*
- [78] Louis C. Jorritsma, M. Bijmagne, G. Rosenfeld and B. Poelsema, Phys. Rev. Lett. **78**, 911-914 (1997). *Growth anisotropy and pattern formation in metal epitaxy.*
- [79] J.-K. Zuo and J.F. Wendelken, Phys. Rev. Lett. **78**, 2791-2794 (1997). *Evolution of mound morphology in reversible homoepitaxy on Cu(100).*
- [80] K. Thürmer, R. Koch, M. Weber and K.H. Rieder, Phys. Rev. Lett. **75**, 1767 (1995). *Dynamic evolution of pyramid structures during growth of epitaxial Fe(001) films.*
- [81] F. Tsui, J. Wellman, C. Uher and Roy Clarke, Phys. Rev. Lett. **76**, 3164-3167 (1996). *Morphology transition and layer-by-layer growth of Rh(111).*
- [82] E. Somfai and L.M. Sander, in *Dynamics of crystal surfaces and interfaces*, eds. P.M. Duxbury and T.J. Pence (Plenum Press, 1997). *Coarsening of MBE structures in 2+1 dimensions.*
- [83] A.W. Hunt, C. Orme, Williams, B. G. Orr, L.M. Sander, Europhys. Lett. **27**, 611 (1994). *Instabilities in MBE growth.*
- [84] P. Politi and A. Torcini, Preprint (1999). *Coarsening process in growth models without slope selection*
- [85] K. Kawasaki and T. Ohta, Physica **116A**, 573 (1982). *Kink dynamics in one-dimensional nonlinear systems.*
- [86] T. Kawakatsu and T. Munakata, Prog. Theo. Phys. **74**, 11 (1985). *Kink dynamics in a one-dimensional conserved TDGL system.*
- [87] M. Siegert and M. Plischke, Phys. Rev. E **53**, 307-318 (1996). *Formation of pyramids and mounds in molecular beam epitaxy.*
- [88] A.J. Bray, Adv. Phys. **43**, 357 (1994). *Theory of phase ordering kinetics.*
- [89] M. Siegert, M. Plischke and R.K.P. Zia, Phys. Rev. Lett. **78**, 3705-3708 (1997). *Contrasts between coarsening and relaxation dynamics of surfaces.*
- [90] Martin Rost, private communication.
- [91] M. Siegert, Phys. Rev. Lett. **81**, 5481-5484 (1998). *Coarsening dynamics of crystalline thin films.*
- [92] P. Politi, Phys. Rev. E **58**, 281 (1998). *Kink dynamics in a one-dimensional growing surface.*
- [93] Lei-Han Tang, P. Šmilauer and D.D. Vvedensky, Eur. Phys. J. B **2**, 409 (1998). *Noise-assisted mound coarsening in epitaxial growth.*
- [94] J. Krug, in *Nonequilibrium statistical mechanics in one dimension*, ed. V. Privman (Cambridge University Press, Cambridge, 1997). *Nonequilibrium surface dynamics with volume conservation.*
- [95] P. Šmilauer, D.D. Vvedensky, Phys. Rev. B **52** 14263 (1995). *Coarsening and slope evolution during unstable epitaxial growth.*
- [96] J.G. Amar and F. Family, Phys. Rev. B **54**, 14742-14753 (1996). *Effects of crystalline microstructure on epitaxial growth.*
- [97] K. Thürmer, R. Koch, P. Schilbe and K.H. Rieder, Surf. Sci. **395**, 12-22 (1998). *Pyramidal growth on bcc(001) stabilizes facets close to {012}: a Monte Carlo study.*
- [98] J.P. van der Eerden and H. Müller-Krumbhaar, Phys. Rev. Lett. **57**, 2431 (1986). *Dynamic coarsening of crystal surfaces by formation of macrosteps;* D. Kandel and J.D. Weeks, Phys. Rev. Lett. **72**, 1678 (1994). *Step motion, patterns, and kinetic instabilities on crystal surfaces;* Phys. Rev. Lett. **69**, 3758 (1992). *Step bunching as a chaotic pattern formation process.*
- [99] M. Uwaha and Y. Saito, Phys. Rev. Lett. **68**, 224-227 (1992). *Kinetic smoothing and roughening of a step with surface diffusion;* Y. Saito and M. Uwaha, Phys. Rev. B **49**, 10677-10692 (1994). *Fluctuation and instability of steps in a diffusion field.*
- [100] S. Stoyanov, Jap. J. Appl. Phys. **30**, 1 (1991). *Electromigration induced step bunching on Si surfaces - How does it depend on the temperature and heating current direction?;* H. Yasunaga and A. Natori, Surf. Sci. Rep. **15**, 207-80 (1992). *Electromigration on semiconductor surfaces.*

- [101] A. Pimpinelli, I. Elkinani, A. Karma, C. Misbah and J. Villain, J. Phys.: Condens. Matter **6**, 2661 (1994). *Step motions on high-temperature vicinal surfaces*.
- [102] I. Bena, C. Misbah and A. Valance, Phys. Rev. B **47**, 7408 (1993). *Nonlinear evolution of a terrace edge during step-flow growth*.
- [103] A. Karma and C. Misbah, Phys. Rev. Lett. **71**, 3810-3813 (1993). *Competition between noise and determinism in step flow growth*.
- [104] O. Pierre-Louis, C. Misbah, Y. Saito, J. Krug and P. Politi, Phys. Rev. Lett. **80**, 4221 (1998). *New nonlinear evolution equation for steps during MBE on vicinal surfaces*.
- [105] M. Rost, P. Šmilauer and J. Krug, Surf. Sci. **369**, 393-402 (1996). *Unstable epitaxy on vicinal surfaces*.
- [106] O. Pierre-Louis, *Instabilité, dynamique non-linéaire et fluctuations des surfaces vicinales hors de l'équilibre*. Ph.D. Thesis (Université de Grenoble I, 1997). Unpublished.
- [107] O. Pierre-Louis and C. Misbah, Phys. Rev. B **58**, 2259-2275 (1998). *Dynamics and fluctuations during M.B.E. on vicinal surfaces I: formalism and results of the linear theory; ibidem*, 2276-2288. *Dynamics and fluctuations during M.B.E. on vicinal surfaces II: non-linear analysis*.
- [108] J. Krug and M. Schimschak, J. de Physique I **5**, 1065-1086 (1996). *Metastability of step flow growth in 1+1 dimensions*.
- [109] Y. Kuramoto, *Chemical oscillations waves and turbulence* (Springer, Berlin, 1984).
- [110] Y. Saito and M. Uwaha, J. Phys. Soc. Japan **65**, 3576-3581 (1996). *Anisotropy effect on step morphology described by Kuramoto-Sivashinsky equation*.
- [111] O. Pierre-Louis and C. Misbah, Phys. Rev. Lett. **76**, 4761-4764 (1996). *Out-of-equilibrium step meandering on a vicinal surface*.
- [112] M. Rost and J. Krug, Phys. Rev. Lett. **75**, 3894-3897 (1995). *Anisotropic Kuramoto-Sivashinsky equation for surface growth and erosion*.
- [113] J.Y. Tsao, *Material fundamentals of molecular beam epitaxy* (Academic Press, Boston, 1993).
- [114] J. Krug, J. Stat. Phys. **87**, 505-518 (1997). *On the shape of wedding cakes*.
- [115] L. Schwenger, R.L. Folkerts and H.-J. Ernst, Phys. Rev. B **55**, R7406-R7409 (1997). *Bales-Zangwill meandering instability observed in homoepitaxial step-flow growth*.
- [116] R.T. Tung and F. Schrey, Phys. Rev. Lett. **63**, 1277-1280 (1989). *Topography of the Si(111) surface during silicon Molecular Beam Epitaxy*.
- [117] P. Tejedor, P. Šmilauer, C. Roberts and B.A. Joyce, Phys. Rev. B **59**, 2341-2345 (1999). *Surface morphology evolution during unstable homoepitaxial growth of GaAs(110)*.
- [118] R.P.U. Karunasiri, R. Bruinsma, J. Rudnick, Phys. Rev. Lett. **62** 788 (1989). *Thin film Growth and the shadow instability*.
- [119] R. Bruinsma, R.P.U. Karunasiri, J. Rudnick, in *Kinetics of Ordering and Growth at Surfaces*, ed. M.G. Lagally (Plenum, New York, 1990). *Growth and erosion of thin solid films*.
- [120] H.J. Leamy, G.A. Gilmer, A.G. Dirks (1980) in *Current topics in Materials Science*, ed. E. Kaldis (North-Holland, Amsterdam, 1980). *The microstructure of vapor deposited films*.
- [121] I.J. Hodgkinson, P.W. Wilson, CRC Crit. Rev. Solid State and Mater. Sci. **15**, 27-61 (1988). *Microstructural-induced anisotropy in thin films for optical applications*.
- [122] J.S. Gau, J. Magn. Mat. **80** 290-298 (1989). *Magnetic properties of oblique-evaporated Co-Ni thin films*.
- [123] J.M. Nieuwenhuizen, H.B. Hanstra, Philips Technische Rundschau **27**, 177-181 (1966). *Mikrofraktographie dünner Schichten*.
- [124] S. Lichter, H. Chen, Phys. Rev. Lett. **56**, 1396-99 (1986). *Model for columnar microstructure of thin solid films*.
- [125] J. Krug, P. Meakin, Phys. Rev. A **43**, 900-919 (1991). *Columnar growth in oblique incidence ballistic deposition: Faceting, noise reduction and mean-field theory*.
- [126] J. Krug, Materialwissenschaft und Werkstofftechnik **26** 22 (1995). *The columnar growth angle in obliquely evaporated thin films*.
- [127] A. Chamberod and J. Hillairet, eds., *Metallic Multilayers*, Materials Science Forum **59-60** (Transtech Publications, Aedermannsdorf, 1990).
- [128] B.K. Chakraverty, J. Phys. Chem. Sol. **28**, 2401 and 2413 (1967). *Grain size distribution in thin films*.
- [129] M. Avignon, B.K. Chakraverty, Proc. Roy. Soc. A **310**, 277 (1969). *Morphological stability of two-dimensional nucleus*.
- [130] M. Avignon, J. Cryst. Growth **11**, 265 (1971). *Role of interface kinetics on the shape stability of a two-dimensional nucleus on a substrate*.
- [131] F.C. Frank, J.H. van der Merve, Proc. Roy. Soc. A **189**, 205-225 (1949). *One-dimensional dislocations. I. Static theory*.
- [132] D.C. Houghton, Appl. Phys. Lett. **57**, 2124 (1990). *Nucleation rate and glide velocity of misfit dislocations in $Ge_xSi_{1-x}/(100)Si$ heterostructures*.
- [133] D.D. Perovic, D.C. Houghton, Mechanisms of Heteroepitaxy and Growth symposium. Mater. Res. Soc., Pittsburgh, Pa, USA, **514**, 391 (1992). *Barrierless misfit dislocation nucleation in SiGe/Si strained layer epitaxy*.
- [134] R. Hull, J.C. Bean, J. Vac. Sci. Technol. **A7**, 2580 (1989). *Nucleation of misfit dislocations in strained layer epitaxy in Ge_xSi_{1-x}/Si system*.
- [135] J. W. Matthews, J. Vac. Sci. Technol. **12**, 126 (1975). *Defects associated with the accommodation of misfit between crystals*.
- [136] L.B. Freund, J. Appl. Phys. **68**, 2073 (1990). *A criterion for arrest of a threading dislocation in a strained epitaxial layer*

due to an interface misfit dislocation in its path.

- [137] A. Bourret, J. Desseaux-Thibault, F. Lançon, J. de Phys. Colloque C4, **44** C4.15-C4.24 (1983). *La structure du coeur des dislocations dans le silicium CZ étudié par microscopie électronique.*
- [138] A.S. Nandedkar, J. Narayan, Phil. Mag. **A61** 873 (1990). *Atomic structure of dislocations in silicon, germanium and diamond.*
- [139] M.A. Hermann and H. Sitter, Springer Series in Materials Science 7, ed. Morton B. Panish (Springer-Verlag, Berlin, Heidelberg, 2nd Ed., 1996) p. 290. *Molecular Beam Epitaxy.*
- [140] J.P. Hirth and J. Lothe, *Theory of Dislocations* (McGraw-Hill, New York, 1982).
- [141] P.M.J. Maree, J.C. Barbour, J.F. Van der Veen, K.L. Kavanagh, C.W.T. Bule-Lieuwma, M.P.A. Vieggers, J. Appl. Phys. **62**, 4413 (1987). *Generation of misfit dislocations in semiconductors.*
- [142] M. Dynna, A. Marty, B. Gilles, G. Patrat, Acta Materialia **44**, 4417 (1996). *Ordering and the relaxation of elastic strain in thin Au-Ni films grown on Au(001).*
- [143] J.R. Willis, S.C. Jain, and R. Bullough, Philos. Mag. **A62**, 115 (1990). *The energy of an array of dislocations: implications for strain relaxation in semiconductor heterostructures.*
- [144] S.C. Jain, T.J. Gosling, J.R. Willis D.H.J. Totterdell and R. Bullough, Philos. Mag. **A65**, 1151 (1992). *A new study of critical layer thickness, stability and strain relaxation in pseudomorphic Ge_xSi_{1-x} strained epilayers.*
- [145] M. Dynna, T. Okada and G.C. Weatherly, Acta metall. mater. **42**, 1661 (1994). *The nature of dislocation sources and strain relief in $InAs_yP_{1-y}$ films grown on (100) InP substrates.*
- [146] A.K. Head, Proc. Phys. Soc. **66B**, 793 (1953).
- [147] C.A.B. Ball, J.H. van der Merwe, in *Dislocations in solids*, ed. F.R.N. Nabarro, **6** (North-Holland, Amsterdam, 1983), chap. 27 *The growth of dislocation-free layers.*
- [148] E. Kasper, Surface Science **174**, 630 (1986). *Growth and properties of Si/SiGe Superlattices.*
- [149] J.L. Vassent, M. Dynna, A. Marty, B. Gilles, G. Patrat, J. Appl. Phys. **80**, 5727-35 (1996). *A study of growth and the relaxation of elastic strain in MgO on Fe(001).*
- [150] T.J. Gosling, S.C. Jain, J.R. Willis, A. Atkinson, R. Bullough, Philos. Mag. **66**, 119 (1992). *Stable configurations in strained epitaxial layers.*
- [151] V. T. Gillard and W. D. Nix, J. Appl. Phys. **76**, 7280 (1994). *Role of dislocation blocking in limiting strain relaxation in heteroepitaxial films.*
- [152] B. A. Fox and W. A. Jesser, J. Appl. Phys. **68**, 2801 (1990). *The effect of frictional stress on the calculation of critical thickness in epitaxy.*
- [153] R. Beanland, J. Appl. Phys. **77**, 62171 (1995). *Dislocation multiplication mechanisms in low-misfit strained epitaxial layers.*
- [154] A. Ponchet, A. Le Corre, A. Godefroy, S. Salaün, A. Poudoulec, J. Cryst. Growth, **153**, 71 (1995). *Influence of stress and surface reconstruction on the morphology of tensile GaInAs grown on InP(001) by gas source molecular beam epitaxy.*
- [155] R. Nötzel, J. Temmyo, and T. Tamamura, Nature **369**, 131 (1994). *Self-organized growth of strained InGaAs quantum disks.*
- [156] R. Nötzel, J. Temmyo, A. Kozen, T. Tamamura, T. Fukui, and H. Hasegawa, Appl. Phys. Lett. **66**, 2525 (1995). *Self-organization of strained GaInAs microstructures on InP(311) substrates grown by metalorganic vapor-phase epitaxy.*
- [157] K. Nishi, R. Mirin, D. Leonard, G. Medeiro-Ribeiro, P. M. Petroff, and A. C. Gossard, J. Appl. Phys. **80**, 3466 (1996). *Structural and optical characterization of InAs/InGaAs self-assembled quantum dots grown on (311)B GaAs.*
- [158] B.A. Joyce, J.L. Sudijono, J.G. Belk, H. Yamaguchi, X.M. Zhang, H.T. Dobbs, A. Zangwill, D.D. Vvedensky, T.S. Jones, Jpn J. Appl. Phys. **36**, 4111 (1997). *A scanning tunneling microscopy-reflection high energy electron diffraction-rate equation study of the molecular beam epitaxial growth of InAs on GaAs(001),(110) and (111)A-Quantum dots and two-dimensional modes.*
- [159] I. Goldfarb, P.T. Hayden, J.H.G. Owen, G.A.D. Briggs, Phys. Rev. B **56**, 10459 (1997). *Competing growth mechanisms of Ge/Si(001) coherent clusters .*
- [160] A. Madhukar, Q. Xie, P. Chen, A. Konkar, Appl. Phys. Lett. **64**, 2727 (1994) *Nature of strained InAs three-dimensional islands formation and distribution on GaAs(100).*
- [161] Y.Chen and J. Washburn, Phys. Rev. Lett. **77**, 4046 (1996). *Structural transition in Large-Lattice-Mismatch Heteroepitaxy.*
- [162] A. Ponchet, A. Le Corre, M. L'Haridon, B. Lambert, S. Salaün, D. Alquier, D. Lacombe, L. Durand, Appl. Surface Sci. **123**, 751 (1998). *The effect of the growth procedure and the InAs amount on the formation of strain induced islands in the InAs/InP(001) system.*
- [163] H.T. Johnson, L.B. Freund, J. Appl. Phys. **81**, 6081 (1997). *The mechanics of coherent and dislocated island morphologies in strained epitaxial material systems.*
- [164] N.P. Kobayashi, T.R. Ramachandran, P. Chen, A. Madhukar, App. Phys. Lett. **68**, 3299-3301 (1996). *In situ, atomic force microscope studies of the evolution of InAs three-dimensional islands on GaAs(001).*
- [165] H.T. Dobbs, D.D. Vvedensky, A. Zangwill, J. Johansson, N. Calsson, W. Seifert, Phys. Rev. Lett. **79**, 897 (1997). *Mean Field Theory of Quantum Dot formation.*
- [166] R.J. Asaro, W.A. Tiller, Metall.Trans. **3**, 1789 (1972). *Interface morphology development during stress corrosion cracking.*
- [167] M.Ya. Grinfeld, Dokl. Akad. Nauk SSSR **290**, 1358 (1986) [Sov. Phys. Dokl. **31**, 831 (1986)]. *Instability of the separation*

boundary between a nonhydrostatically stressed elastic body and a melt.

- [168] J.E. Hack, S.P. Chen, D.J. Srolovitz, *Acta metall.* **37**, 1957-70 (1989). *A kinetic criterion for quasi-brittle fracture.*
- [169] W.H. Yang and D.J. Srolovitz, *Phys. Rev. Lett.* **71**, 1593 (1993). *Cracklike surface instabilities in stressed solids.*
- [170] K. Portz and A.A. Maradudin, *Phys. Rev. B* **16**, 3535 (1977). *Surface contribution to the low-temperature specific heat of a cubic crystal.*
- [171] L. Landau, E. Lifshitz, *Theory of Elasticity* (Pergamon Press, London 1959).
- [172] P. Nozières, *J. de Physique I* **3**, 681 (1993). *Amplitude expansion for the Grinfeld instability due to uniaxial stress at a solid surface.*
- [173] J. Grilhé, *Europhys. Lett.* **23**, 141 (1993). *Surface instabilities and dislocation formation at free surfaces of stressed solids.*
- [174] K. Kassner, C. Misbah, *Europhys. Lett.* **28**, 245 (1994). *Nonlinear development of a uniaxially stressed solid: a route to fracture?*
- [175] M. Thiel, A. Willibald, P. Evers, A. Levchenko, P. Leiderer, S. Balibar, *Europhys. Lett.* **20**, 707 (1992). *Stress-induced melting and surface instability of the crystals.*
- [176] D.S. Spencer, P.W. Vorhees, S.H. Davis, *Phys. Rev. Lett.* **67**, 3696 (1991). *Morphological instability in epitaxially strained dislocations-free solid films.*
- [177] D.S. Spencer, P.W. Vorhees, S.H. Davis, *J. Appl. Phys.* **73**, 4955 (1993). *Morphological instability in epitaxially strained dislocation-free solid films: Linear stability theory.*
- [178] L. Landau, E. Lifshitz, *Statistical Physics* (Pergamon Press, London 1959).
- [179] J.A. Venables, G.D. Spiller and M. Hanbücken, *Rep. Prog. Phys.* **47**, 399 (1984). *Nucleation and growth of thin films.*
- [180] S. Stoyanov and D. Kashchiev, in *Current topics in material science* Vol. 7, ed. E. Kaldis (North Holland, 1981), p. 69. *Thin film nucleation and growth theories: a confrontation with experiment.*
- [181] C. Duport, P. Politi, J. Villain, *J. de Physique I* **5**, 1317-1350 (1995) *Growth instabilities induced by elasticity in a vicinal surface.*
- [182] B. Voigtländer, A. Zinner, *Appl. Phys. Lett.* **63**, 3055 (1993). *Simultaneous molecular beam epitaxy growth and scanning tunneling microscopy imaging during Ge/Si epitaxy.*
- [183] A.J. Pidduck, D.J. Robbins, A.G. Cullis, W.Y. Leong, A.M. Pitt, *Thin Solid Films* **222** 78 (1992). *Evolution of surface morphology and strain during SiGe epitaxy.*
- [184] D. Dutartre, F. Warren, F. Chollet, F. Gisbert, M. Bérenguer, I. Berbézier, *J. Cryst. Growth* **142**, 78 (1994). *Defect-free Stranski-Krastanov growth of strained Si_{1-x}Ge_x layers on Si.*
- [185] I. Berbézier, B. Gallas, B. Ronda, J. Derrien, *Surf. Sci.* **412/413**, 415 (1998). *Dependence of SiGe growth instability on Si surface orientation.*
- [186] J.E. Guyer, P.W. Vorhees, *Phys. Rev. B* **54**, 11710 (1996). *Morphological stability of alloys thin films.*
- [187] F. Glas, *Phys. Rev. B* **55**, 11277 (1997). *Thermodynamics of a stressed alloy with a free surface: Coupling between the morphological and compositional stability.*
- [188] J. Tersoff, *Phys. Rev. Lett.* **43**, 9377 (1991). *Stress-induced layer-by-layer growth of Ge on Si(100).*
- [189] J.M. Moison, F. Houzay, F. Barthe, L. Leprince, E. André, O. Vatel, *Appl. Phys. Lett.* **64**, 196 (1994). *Self-organized growth of regular nanometer-scale InAs dots on GaAs.*
- [190] M. Grinfeld, *Phys. Rev. B* **49**, 8310 (1994). *Two-dimensional islanding atop stressed solid helium and epitaxial films.*
- [191] M. Grinfeld, *Scanning microscopy* **8**, 869 (1994). *Stress corrosion and stress induced surface morphology of epitaxial films.*
- [192] N. Junqua, J. Grilhé, *J. de Physique III* **3**, 1589 (1993). *Surface instability of epitaxial films on a substrate.*
- [193] C.W. Snyder, J.F. Mansfield, B.G. Orr, *Phys. Rev. B* **46**, 9551 (1992). *Kinetically controlled critical thickness for coherent islanding and thick highly strained polymorphic films of In_xGa_{1-x}As on GaAs(100).*
- [194] A. Ponchet, A. Le Corre, M. L'Haridon, B. Lambert, S. Salaün, *Appl. Phys. Lett.* **67** 1850 (1995). *Relationship between self-organization and size of InAs islands on InP(001) grown by gas source molecular beam epitaxy.*
- [195] A. Ponchet, A. Le Corre, M. L'Haridon, B. Lambert, S. Salaün, J. Goeren, R. Carles, *Solid State Electronics* **40**, 615 (1996). *Structural aspects of the growth of InAs islands on InP substrate.*
- [196] J.M. Gérard, J.Y. Marzin, G. Zimmermann, A. Ponchet, O. Cabrol, D. Barrier, B. Jusserand, B. Sermage, *Solid State Electronics* **40**, 807 (1996). *InAs/GaAs quantum boxes obtained by self-organized growth: intrinsic electronic properties and applications.*
- [197] J.M. Gérard, O. Cabrol, J.Y. Marzin, N. Lebouché, J.M. Moison, *Materials Science and Engineering B* **37** 8-16 (1996). *Optical investigation of some statistic and kinetic aspects of the nucleation and growth of InAs islands on GaAs.*
- [198] C. Priester, M. Lannoo, *Phys. Rev. Lett.* **75**, 93 (1995). *On the origin of self-assembled quantum dots in highly mismatched heteroepitaxy.*
- [199] N. Junqua, J. Grilhé, *Phil. Mag. Letters* **69**, 61 (1994). *Instability of planar interfaces between two stressed materials.*
- [200] N. Sridhar, J.M. Rickman and D.J. Srolovitz, *J. Appl. Phys.* **82**, 4852 (1997). *Multilayer film stability.*
- [201] D. Leonard, M. Krishnamurthy, C.M. Reaves, S.P. DenBaars, P.M. Petroff, *Appl. Phys. Lett.* **63**, 3203 (1993). *Direct formation of quantum-sized dots from uniform coherent islands of InGaAs on GaAs surfaces.*
- [202] J.Y. Marzin, J.M. Gérard, A. Izraël, D. Barrier, G. Bastard, *Phys. Rev. Lett.* **73**, 716 (1994). *Photoluminescence of single InAs quantum dots obtained by self-organized growth on GaAs.*
- [203] V.A. Shchukin, N.N. Ledentsov, P.S. Kop'ev, D. Bimberg, *Phys. Rev. Lett.* **75**, 2968 (1995). *Spontaneous ordering of*

arrays of coherent strained islands.

- [204] R. Kern, P. Müller, Surf. Sci. **392**, 103-133 (1997). *Elastic relaxation of coherent epitaxial deposits.*
- [205] J.V. Boussinesq, *Applications des potentiels à l'étude de l'équilibre et du mouvement des corps élastiques* (Gauthier-Villars, Paris, 1885).
- [206] J. Tersoff and F.K. LeGoues, Phys. Rev. Lett. **72**, 3570 (1994). *Competing relaxation mechanisms in strained layers.*
- [207] J. Tersoff and R.M. Tromp, Phys. Rev. Lett. **70**, 2782 (1993). *Shape transition in growth of strained islands: spontaneous formation of quantum wires.*
- [208] C. Duport, C. Priester, J. Villain, in *Morphological Organization in Epitaxial Growth and Removal*, eds. Zh. Zhang and M. Lagally (World Scientific Series on Directions in Condensed Matter Physics, 1997). *Equilibrium shapes of a coherent epitaxial cluster.*
- [209] C. Duport, *Élasticité et croissance cristalline*, Ph.D. Thesis (Université de Grenoble, 1996).
- [210] A. Ponchet, L. Durand, J.M. Cardona, unpublished (1998).
- [211] L.B. Freund, H.T. Johnson, R.V. Kukta, Proceedings of the Materials Research Society Fall Meeting (Boston, 1995). *Observations on the mechanics of strained epitaxial island growth.*
- [212] N. Moll, M. Scheffler, E. Pehlke, Phys. Rev. B **58**, 4566 (1998). *The influence of surface stress on the equilibrium shape of strained quantum dots.*
- [213] C.B. Ling, J. Math. and Phys. **26**, 284 (1948). *On the stresses in a notched plate under tension.*
- [214] E. Weinel, Z. ang. Math und Mech. **21**, 228-230 (1941). *Die Spannungserhöhung durch Kreisbogenkerben.*
- [215] Isibasi, Memoirs of the Faculty of Engineering, Kyushu Imperial University, Fukuoka, Japan, IX, 131-143 (1940). *Stresses in a semi-infinite plate with a circular notch under uniform tension.*
- [216] Y. Androussi, P. François, A. Lefebvre, C. Priester, I. Lefebvre, G. Allan, M. Lannoo, J.M. Moison, N. Lebouche, F. Barthe, Mat. Res. Soc. Symp. Proc. **355**, 569 (1995). *Evolution of thin film and surface : structure and morphology.*
- [217] E. Pehlke, N. Moll and M. Scheffler, Proc. 23rd Int. Conf. on the Physics of Semiconductors, eds M. Scheffler and R. Zimmermann (World Scientific, Singapore, 1996) p.301. *The equilibrium shape of Quantum dots.*
- [218] Y.W. Mo, D.E. Savage, B.S. Schwartzengruber, M.G. Lagally, Phys. Rev. Lett. **65**, 1020 (1990). *Kinetic pathway in Stranski-Krastanov Growth of Ge on Si(001).*
- [219] G. Medeiros-Ribeiro, T.I Kamins, D.A.A. Ohlberg, R. Stanley Williams, Phys. Rev. B **58**, 3533 (1998). *Annealing of Ge nanocrystals on Si(001) at 550°C: Metastability of huts and the stability of pyramids and domes.*
- [220] J. A. Floro, G. A. Lucadamo, E. Chason, L. B. Freund, M. Sinclair, R. D. Twisten, and R. Q. Hwang, Phys. Rev. Lett. **80** (1998) 4717. *SiGe island shape transitions induced by elastic repulsion.*
- [221] A. Rudra, R. Houdré, J. F. Carlin, and M. Ilegems, J. Crys. Growth, **136**, 278 (1994). *Dynamics of island formation in the growth of InAs/InP quantum well.*
- [222] R. Houdré, J. F. Carlin, A. Rudra, J. Ling and M. Ilegems, Superlattices and Microstructures, **13**, 67 (1993). *Formation and optical properties of islands in ultra-thin InAs/InP quantum wells grown by chemical beam epitaxy.*
- [223] B. Lambert, A. LeCorre, V. Drouot, H. L'Haridon, S. Loualiche, Semicond. Sci. Technol. **13**, 143 (1998). *High photoluminescence efficiency of InAs/InP self-assembled quantum dots emitting at 1.5-1.6 μ m.*
- [224] M. Colocci, F. Bogani, L. Carraresi, M. Mattolini, A. Bosacchi, S. Franchi, P. Frigeri, M. Rosa-Clot, S. Taddei, Appl. Phys. Lett. **70**, 3140 (1997). *Growth patterns of self-assembled quantum dots near the two-dimensional to three-dimensional transition.*
- [225] M. Zinke-Allmang et al., Phys. Rev. Lett. **68**, 2782 (1992). *Experimental Study of Self-similarity in the coalescence growth regime.*
- [226] G. Zinnmeister, Thin solid films **2**, 497 (1968). *Theory of thin film condensation. Part B: solution of the simplified condensation equation; ibidem, 7, 51 (1971). *Theory of thin film condensation. Part D: influence of a variable collision factor.**
- [227] G.S. Bales, D.C. Chrzan, Phys. Rev. B **50**, 6057 (1994). *Dynamics of irreversible island growth during submonolayer epitaxy.*
- [228] M.C. Bartelt, J.W. Evans, Phys. Rev. B **46**, 12675 (1992). *Scaling analysis of diffusion-mediated island growth in surface adsorption processes.*
- [229] H.T. Dobbs, A. Zangwill, D.D. Vvedensky, in *Diffusion : Atomistic and collective processes*, eds. M.C. Tringides, M. Scheffler (Plenum, New York, 1997). *Nucleation and growth of coherent quantum dots: a mean field theory.*
- [230] W. Ostwald, *Foundation of Analytical Chemistry* (Mc Millan, London, 1908), p. 22.
- [231] I.M. Lifshitz, V.V. Slyozov, J. Phys. Chem. Solids **19**, 35 (1961). *The kinetics of precipitation from supersaturated solid solutions.*
- [232] J. Villain, Europhys. Lett. **2**, 531 (1986). *Healing of a rough surface.*
- [233] F. M. Ross, J. Tersoff, R. M. Tromp, Phys. Rev. Lett. **80**, 984 (1998). *Coarsening of self-assembled Ge quantum dots on Si(001).*
- [234] C. Duport, Ph. Nozières, J. Villain, Phys. Rev. Lett. **74**, 134 (1995). *New instability in molecular beam epitaxy.*
- [235] A. L. Barabási, Appl. Phys. Lett. **70**, 2565 (1997). *Self assembled island formation in heteroepitaxial growth.*
- [236] J. F. Carlin, A. Rudra, R. Houdré, P. Ruterana, and M. Ilegems, J. of Crys. growth. **120**, 155-156 (1992). *Effect of growth interruptions on ultra-thin InAs/InP quantum well grown by CBE.*

- [237] C. Ratsch, P. Šmilauer, D.D. Vvedensky, A. Zangwill, J. Physique I **6**, 575 (1996). *Mechanism for coherent island formation during heteroepitaxy.*
- [238] M. Schroeder, D.E. Wolf, Surface Sci. **375**, 129-140 (1997). *Diffusion on strained surfaces.*
- [239] J. Tersoff, Phys. Rev. Lett. **81**, 3183 (1998). *Enhanced nucleation and enrichment of strained-alloy quantum dots.*
- [240] C. Priester, M. Lannoo, Appl. Surf. Sc. **123** 658 (1998). *Enhancement of alloy segregation due to strain assisted atomic diffusion in heteroepitaxy.*
- [241] K. Tilmann, A. Thust, M. Lentzen, P. Swiatek, A. Förster, K. Urban, W. Laufs, D. Gerthsen, T. Remmele, A. Rosenauer, Phil. Mag. Lett. **74**, 309 (1996). *Determination of segregation, elastic strain and thin-foil relaxation in InGaAs islands on GaAs(001) by HRTEM.*
- [242] N. Grandjean, J. Massies, and O. Tottereau, Phys. Rev. B **55**, 10189 (1997). *Surface segregation in GaInAs/GaAs quantum boxes.*
- [243] G. Medeiros-Ribeiro, P.T. Hayden, J.H.G. Owen, G.A.D. Briggs, Science **279**, 353 (1998). *Shape transition of Germanium nanocrystals on a Silicon(001) surface from pyramids to domes.*
- [244] D. E. Jesson, K. M. Chen, and S. J. Pennycook, Phys. Rev. Lett. **80**, 5156 (1998). *Self-limiting growth of strained faceted islands.*
- [245] D. E. Jesson, G. Chen, K. M. Chen, and S. J. Pennycook, MRS Bulletin **21**, 31 (1996). *Kinetic pathways to strain relaxation in the SiGe system.*
- [246] B. Gallas, I. Berb  zier, J. Chevrier, J. Derrien, Phys. Rev. B **54**, 4919 (1996). *Gallium-mediated homoepitaxial growth of silicon at low temperature.*
- [247] B. Voigtl  nder, A. Zinner, T. Weber, H.P. Bonzel, Phys. Rev. B **51**, 7583 (1995). *Modification of growth kinetics in surfactant-mediated epitaxy.*
- [248] M. Copel, M.C. Reuter, E. Kaxiras, R.M. Tromp, Phys. Rev. Lett. **63**, 632 (1989). *Surfactants in epitaxial growth.*
- [249] M. Copel, M.C. Reuter, M. Horn von Hoegen, R.M. Tromp, Phys. Rev. B **42**, 11682 (1990). *Influence of surfactants in Ge and Si epitaxy on Si(001).*
- [250] D.J. Eaglesham, F.C. Unterwald, D.C. Jacobson, Phys. Rev. Lett. **70**, 966 (1993). *Growth morphology and the equilibrium shape: the role of "surfactants" in Ge/Si island formation.*
- [251] M.C. Reuter, R.M. Tromp, Phys. Rev. Lett. **67**, 1130 (1991). *Defect self-annihilation in surfactant-mediated epitaxial growth.*
- [252] G. Rosenfeld, R. Servaty, C. Teichert, B. Poelsema, G. Comsa, Phys. Rev. Lett. **71**, 895 (1993). *Layer-by-layer growth of Ag on Ag(111) induced by enhanced nucleation: a model study for surfactant-mediated growth.*
- [253] D. Kandel, E. Kaxiras, Phys. Rev. Lett. **75**, 2742 (1995). *Surfactant mediated crystal growth of semiconductors.*
- [254] K. Schroeder, B. Engels, P. Richard, S. Bl  gel, Phys. Rev. Lett. **80**, 2873 (1998). *Reexchange controlled diffusion in surfactant-mediated epitaxial growth: Si on As-terminated Si(111).*
- [255] I. Markov, Phys. Rev. B **50**, 11271 (1994). *Kinetics of surfactant-mediated epitaxial growth .*
- [256] G. Rosenfeld, B. Poelsema, G. Comsa, J. Crys. Growth, **151**, 230 (1995) *The concept of two mobilities in homoepitaxial growth.*
- [257] N. Grandjean, J. Massies, V.H. Etgens, Phys. Rev. Lett. **69**, 796 (1992). *Delayed relaxation by surfactant action in highly strained III-V semiconductor epitaxial layers.*
- [258] J. Massies, N. Grandjean, V.H. Etgens, Appl. Phys. Lett. **61**, 99 (1992). *Surfactant mediated epitaxial growth of $In_xGa_{1-x}As$ on $GaAs(001)$.*
- [259] H.N. Davidson, W.E. Pickett, Phys. Rev. B **49**, 14770 (1994). *Graphite layer formation at a diamond (111) surface step.*
- [260] J. Villain, A. Pimpinelli and D. Wolf, Comm. Cond. Matter Phys. **16**, 1-18 (1992). *Layer by layer growth in molecular beam epitaxy.*
- [261] H. Kallabis, P.L. Krapivsky and D.E. Wolf, Eur. Phys. J. B **5**, 801 (1998). *Island Distance in One-Dimensional Epitaxial Growth.*
- [262] L. Golubovi  , Phys. Rev. Lett. **78**, 90-93 (1997). *Interfacial coarsening in epitaxial growth models without slope selection.*
- [263] M. Rost and J. Krug, Phys. Rev. E **55**, 3952 (1997). *Coarsening of surface structures in unstable epitaxial growth.*

	$T < T_R$	$T > T_R$
Step free energy per unit length γ	finite	$\gamma = 0$
Typical radius of thermal fluctuations (bumps and valleys)	$R \approx k_B T / \gamma$ finite	$R = \infty$
Typical height δh of thermal fluctuations	finite	infinite
Excess free energy density of a height modulation of small amplitude δh and wave vector q	$\delta \mathcal{F} / \mathcal{A} = 2\gamma q \delta h / (\pi c)$ +...	$\delta \mathcal{F} / \mathcal{A} = \bar{\sigma} q^2 \delta h^2 / 4$ +...
Variation of the free energy density resulting from a rotation of the surface of small amplitude $\delta \theta$ around a high symmetry orientation	$\delta \mathcal{F} / \mathcal{A} = \gamma \delta \theta / c$ +...	$\delta \mathcal{F} / \mathcal{A} = \bar{\sigma} \delta \theta^2 / 2$ +...
Continuous changes of surface height	impossible	possible

TABLE I. Some typical properties of an infinite, plane crystal surface above and below T_R . The step free energy per unit length γ is assumed to be isotropic, and therefore equal to the step stiffness. The infinite value of δh above T_R is an intuitive consequence of the property $R = \infty$, which in turn results from the formula $R \approx k_B T / \gamma$ since $\gamma = 0$ above T_R . c is the monolayer thickness.

Exp. system	$T(K)$	n	L (nm)	Slope ^a	N (ML)	Flux (ML/min)	Exp. technique ^f	Ref.
GaAs(001)	830/900		$< 10^3$	$1^\circ / 2^\circ$	540 ^e	10	AFM,STM	[52,53]
Ge(001)	330/500	0.4	< 200	$2^\circ / 3^\circ$ ^b	$1 \mu\text{m}$	40	STM	[50,51]
Cu(100)	160	0.26		(113)	100	0.5	TEAS	[77]
	200	0.56		(115)				
Cu(100)	< 180			(113)	150	0.6	TEAS,SPALEED	[78]
	180/280			(115)				
	280/300			(117)				
Cu(100)	300	0.25(1)	$12.5 \div 25$ ^d	5.6° ^c	$1 \div 20$	1.2	LEED	[79]
		0.23(1)	$10 \div 35$		$1 \div 150$		STM	
Fe(001)	290	0.16(4)	$4 \div 9$	$13^\circ \pm 3^\circ$	$20 \div 600$	1.5/30	STM,RHEED	[69]
Fe/Mg(001)	400/450	0.23(2)	$20 \div 60$	30° (012)	$30 \div 2000$	3	STM,LEED	[80]
Rh(111)/mica	725	0.33(3)	$10 \div 100$	1°	$1 \div 300$	2	STM,RHEED	[81]

TABLE II. Details on the table are given in the main text. When a box is empty, it means that the datum is not available. ^a The slope is given in degrees and/or through the orientation of the corresponding facet. The notation $1^\circ / 2^\circ$ means that the slope is in between one and two degrees. ^b Authors study the distribution of the local slope and find that it is peaked at 2° after $0.5 \mu\text{m}$ have been deposited, and at 3° after $1 \mu\text{m}$. ^c The experimental finding of a slope corresponding to 2.4° is modified to 5.6° , because the former value is considered an ‘average’ one. ^d The values of L correspond to $2\pi/L^*$, L^* being ‘the diameter of the diffraction ring’ in the SPA-LEED angular profiles. ^e In the case of GaAs, 1 ML means one ML of gallium and one ML of arsenic. ^f AFM = Atomic force microscopy; STM = Scanning tunneling microscopy; TEAS = Thermal energy atom beam scattering; LEED = Low energy electron diffraction; SPALEED = Spot profile analysis LEED; RHEED = Reflection high energy electron diffraction.

FIG. 1. Cross-section of a ZnTe/CdTe multilayer seen by low resolution (a) and high resolution (b) electron microscopy. Narrow white stripes in (a) are two monolayer thick ZnTe inclusions. Since the lattice parameter of both components is quite different, phase separation into ZnTe and CdTe would presumably lower the free energy. Thus, the system is in principle unstable or metastable. Courtesy of N. Magnéa and J.L. Pautrat, C.E.A. Grenoble.

FIG. 2. Four mechanisms which can produce a growth instability. (a) Diffusion instability. (b) Kinetic instability due to step-edge barriers. (c) Thermodynamic instability due to different lattice constants, a and $a + \delta a$, of the substrate and the adsorbate. In the present case $\delta a > 0$. (d) Geometric, shadowing instability.

FIG. 3. (a) Principle of a diffusion instability. If a small bump tends to form on a solid nucleus growing in a supersaturated solution, diffusing atoms (circles) tend to go to the bump which thus grows more rapidly than the rest of the nucleus. Matter diffusion on the solid (dashed arrows) has a stabilizing effect, i.e. tends to destroy the bump. (b) A snowflake. (c) The Mullins-Sekerka instability in directional solidification. The initially plane solid-liquid interface takes a wavy shape which can reach a stable shape if the velocity v of the interface is low enough.

FIG. 4. A two-dimensional DLA pattern from the computer (a) and its experimental realization by electrodeposition of Zn in the electrolysis of a quasi-two-dimensional solution of ZnSO_4 (b). Courtesy of S. Bodea and P. Molho, Laboratoire Louis Néel, CNRS, Grenoble.

FIG. 5. Schematic description of MBE growth in the case of a III-V semiconductor, e.g., GaAs. Each cube represents a cubic unit cell. Note that a large proportion of As atoms evaporate, while Ga atoms do not.

FIG. 6. Energy gap and lattice constant for a few III-V compound semiconductors.

FIG. 7. Transmission electron microscopy image of $\text{Al}_{0.48}\text{In}_{0.52}\text{As}$ lattice matched grown on $\text{InP}(001)$ by MBE (V/III BEP ratio equal 20, growth rate equal to $1 \mu\text{m/h}$ and growth temperature equal to 450°C) revealing a fine quasi-periodic contrast due to the presence of In-rich and Al-rich clusters : (a) plane view, (b) cross section . Courtesy of O. Marty, Univ. Lyon I.

FIG. 8. TEM image of $\text{Ga}_{0.47}\text{In}_{0.53}\text{As}$ grown by MOCVD showing CuPt ordering along (111) and (11-1). Courtesy of O. Marty and C. Pautet, Univ. Lyon I.

FIG. 9. Two examples of carrier confinement (a) in a $\text{Ga}_{0.43}\text{In}_{0.57}\text{As}$ quantum well between $\text{Al}_{0.48}\text{In}_{0.52}\text{As}$ barriers; (b) in a heterojunction between highly n-type AlInAs and lightly n-type doped GaAs.

FIG. 10. Surface profile with top, bottom and vicinal terraces. D is the diffusion constant and k_{\pm} are the sticking coefficients from above and below (see the main text).

FIG. 11. The adatom uses its condensation heat (a) to look for a high-coordination site or (b) to knock-out and replace an edge atom. Except for simple cubic structures, the solid-on-solid constraint implies (c) that the capture area of a higher coordination site is larger. Dotted circles are newly incorporated atoms, directly from the flux (a,c) or after a knock-out process (b).

FIG. 12. Profiles for the different potentials $V(m)$. Full line: model I, Eq. (44). Short-dashed: model II with $\gamma = 1$, Eq. (45). Long-dashed: model II with $\gamma = 2$, Eq. (46). The behaviour at small m is the same in all the cases: $V(m) \simeq \alpha m^2/2$.

FIG. 13. (a) Numerical solutions of the four-state clock model (66) and the surface growth model with (b) four-fold in-plane symmetry (67) and with (c) in-plane invariance (68). Figures (a) and (b) are taken from Ref. [68] and are courtesy of Martin Siegert. White, light and dark grey, and black domains correspond respectively to the orientations (1,1), (1,-1), (-1,1) and (-1,-1). Figure (c) is unpublished and is courtesy of Martin Rost.

FIG. 14. Example of a mound structure obtained with the Zeno model.

FIG. 15. Surface morphology in kinetic Monte Carlo simulations of a vicinal surface in presence of ES barriers. The steps become wavy (a) due to the Bales and Zangwill instability [54]. Subsequently, the ripples break down starting at the defects of the ripple pattern, and three-dimensional features appear on the surface (b). The figure is taken from Ref. [117] and it is courtesy of Pavel Šmilauer.

FIG. 16. Columnar growth.

FIG. 17. Droplets of the Volmer-Weber type (above) and of the Stranski-Krastanov type (below). The shape, and particularly the angle θ , is independent of the size.

FIG. 18. $[\bar{1}\bar{1}0]_{Au}$ zone axis Fourier Filtered HREM image showing a misfit dislocation at an Au/AuNi(001) interface with a Burgers vector $(1/2) < 10\bar{1} >$. The arrow shows only the projection of the Burgers vector in the $(1\bar{1}0)$ observation plane. The dashed line is the Burgers circuit around the dislocation core. The excess plane is also shown in black dashed line. Courtesy of C. Dressler and J. Thibault, DRFMC/SP2M, CEA-Grenoble.

FIG. 19. Schematic cross-sectional view of a Shockley partial dislocation of Burgers vector $(1/6)[112]$ which has glided in a (111) plane from the surface to the interface. A stacking fault appears in the glide plane between the dislocation and the surface, so that lattice planes have a discontinuity when crossing the glide plane.

FIG. 20. Schematic cross-sectional view of a dislocation of Burgers vector $(1/2)[110]$ which has climbed from the surface to the interface with the introduction of two supplementary planes (atoms in grey). The arrows represent the displacement field in the epilayer.

FIG. 21. Schematic cross-sectional view of a perfect dislocation $(1/2)[101]$ which has glided in a (111) plane from the surface to the interface. The arrows represent the displacement field in the epilayer. There is no lattice discontinuity at the glide plane.

FIG. 22. A dislocation of Burgers vector \vec{b} moving in its glide plane.

FIG. 23. Critical thickness versus misfit for the glide system of Burgers vector $(1/2)[101]$ and glide plane (111) in the FCC lattice of lattice parameter a_0 for two values of the core parameter α (Dashed curve: $\alpha=2$, continuous curve: $\alpha=4$).

FIG. 24. A dislocation loop nucleating at the surface. An atomic step appears at the intersection of the glide plane with the surface.

FIG. 25. Total energy of a half-loop vs radius for 90° partial and 60° perfect dislocation in $Au_{80}Ni_{20}/Au(001)$.

FIG. 26. Schematic representation of 2 arrays of orthogonal alternating dislocations.

FIG. 27. Curves showing the total energy density of dislocations versus the residual elastic strain in the epilayer (lower axis) or versus the dislocation density (upper axis).

FIG. 28. Blocking mechanism for the relaxation of MgO grown on Fe(001). Circles: experimental data from RHEED measurements. Continuous lines : equilibrium and blocking models.

FIG. 29. Blocking mechanism : the progression of a threading dislocation \mathcal{D}_1 may be disturbed by the stress field of a perpendicular dislocation \mathcal{D}_2 lying at the interface, so that it bypasses this obstacle at a depth h^* .

FIG. 30. Residual strain needed to overcome the line tension (ϵ_{line}), the orthogonal dislocation stress field (ϵ_D) and both retaining forces (ϵ_{tot}) as functions of the channel width h^* . The value ϵ_{min} corresponds to the possible residual strain before blocking of further moving dislocations.

FIG. 31. Two ways of relaxing the stress in an adsorbate. (a) Creation of a misfit dislocation D by a microscopic motion of atoms in a ‘glide plane’ inside the material. (b) Creation of waves at the surface by atom diffusion on the surface on long distances.

FIG. 32. Experimental image of a modulation arising from the misfit in a $\text{Ga}_{1-x}\text{In}_x\text{As}$ multilayer on an $\text{InP}(001)$ substrate ($x \approx 0.28$), from Ref. [154]. The dark layers are under tensile stress ($\delta a/a \approx -1.7\%$). The bright layers are lattice matched to InP and are used as growth markers. Although the quantitative theory can be different in a multilayer, the mechanism is probably the same as described for a single adsorbed layer in paragraph IX B.

FIG. 33. Experimental images of clusters of InAs on an $\text{InP}(001)$ substrate: (a) plane view and (b) cross-sectional observations. The adsorbate (InAs) has a lattice constant 3.2 % greater than the substrate (InP). Small clusters are dislocation-free while bigger ones are not, as most clearly seen from the lower picture

FIG. 34. Schematic representation of clusters of increasing size which arise from elasticity in coherent, epitaxial growth. The shape and the contact angle depend on the size. Small clusters are one monolayer thick while bigger ones are ‘three-dimensional’ with an increasing contact angle when the size increases. The spherical shape assumed for three-dimensional clusters is not realistic. In practice, almost detached clusters such as the right hand one have never been observed in the dislocation-free state.

FIG. 35. Sinusoidal modulation of a surface (a) under the influence of an anisotropic, mechanical stress and (b) under the influence of an adsorbate.

FIG. 36. A slab and a truncated pyramidal cluster.

FIG. 37. A Ge cluster arising from the deposition of Ge on $\text{Si}(001)$. STM image kindly communicated by Max Lagally.

FIG. 38. The function $G(x)$.

FIG. 39. Growth of a submonolayer.

FIG. 40. The Lifshitz-Slyozov mechanism. Atoms leave the small clusters to go to the big ones where the free energy per atom (i.e. the chemical potential) is lower.

FIG. 41. Microscopic twins in $\text{Au}_{0.5}\text{Ni}_{0.5}$ layers grown epitaxially on $\text{Au}(001)$. High resolution electron microscopy cross-section image, the beam direction is $[110]$.

FIG. 42. AFM image of the surface of a FePd epilayer deposited on $\text{Pd}(001)$. The steps oriented at about 45° with respect to the edges of the figure correspond to the emergence of the microscopic twins at the surface.

FIG. 43. Schematic representation of a microscopic twin due to the gliding of several Shockley partial dislocations on successive (111) atomic planes.

FIG. 44. Nucleation lengths (ℓ_n) for the different kinds of terraces in a 1+1 dimensional model, as a function of the ES length (ℓ_{ES}). All the lengths are expressed in units of the diffusion length ℓ_D . Starting from the top, we have ℓ_n^B (which does not depend on ℓ_{ES}), ℓ_n^V (which goes to the constant value $1/\sqrt{2}$) and ℓ_n^T (which slowly goes to zero). The behaviour of ℓ_n^T at large ℓ_{ES} can be directly found from Eq. (B4): $\ell_n^T \simeq (1/6\ell_{ES})^{1/3}$. The small exponent $(1/3)$ explains the slow decrease of ℓ_n^T .

FIG. 45. (a) and (b) represent two similar adsorbed clusters (C), (C'). The strain in two corresponding points is identical. (c) Appropriate external forces within a thin slab (L) just below the surface produce the same elastic displacements and strains in the substrate as the cluster (a). (d) The slab (L') deduced from (L) by the similarity transformation produces the same effect as the cluster (C'). On the other hand, the strain at long distance \vec{r} is multiplied by λ^3 .

This figure "fig1a.jpg" is available in "jpg" format from:

<http://arxiv.org/ps/cond-mat/9906289v1>

This figure "fig1b.jpg" is available in "jpg" format from:

<http://arxiv.org/ps/cond-mat/9906289v1>

This figure "fig2.gif" is available in "gif" format from:

<http://arxiv.org/ps/cond-mat/9906289v1>

This figure "fig3.gif" is available in "gif" format from:

<http://arxiv.org/ps/cond-mat/9906289v1>

This figure "fig4a.gif" is available in "gif" format from:

<http://arxiv.org/ps/cond-mat/9906289v1>

This figure "fig4b.gif" is available in "gif" format from:

<http://arxiv.org/ps/cond-mat/9906289v1>

This figure "fig5.gif" is available in "gif" format from:

<http://arxiv.org/ps/cond-mat/9906289v1>

This figure "fig6.gif" is available in "gif" format from:

<http://arxiv.org/ps/cond-mat/9906289v1>

This figure "fig7a.gif" is available in "gif" format from:

<http://arxiv.org/ps/cond-mat/9906289v1>

This figure "fig7b.gif" is available in "gif" format from:

<http://arxiv.org/ps/cond-mat/9906289v1>

This figure "fig8.gif" is available in "gif" format from:

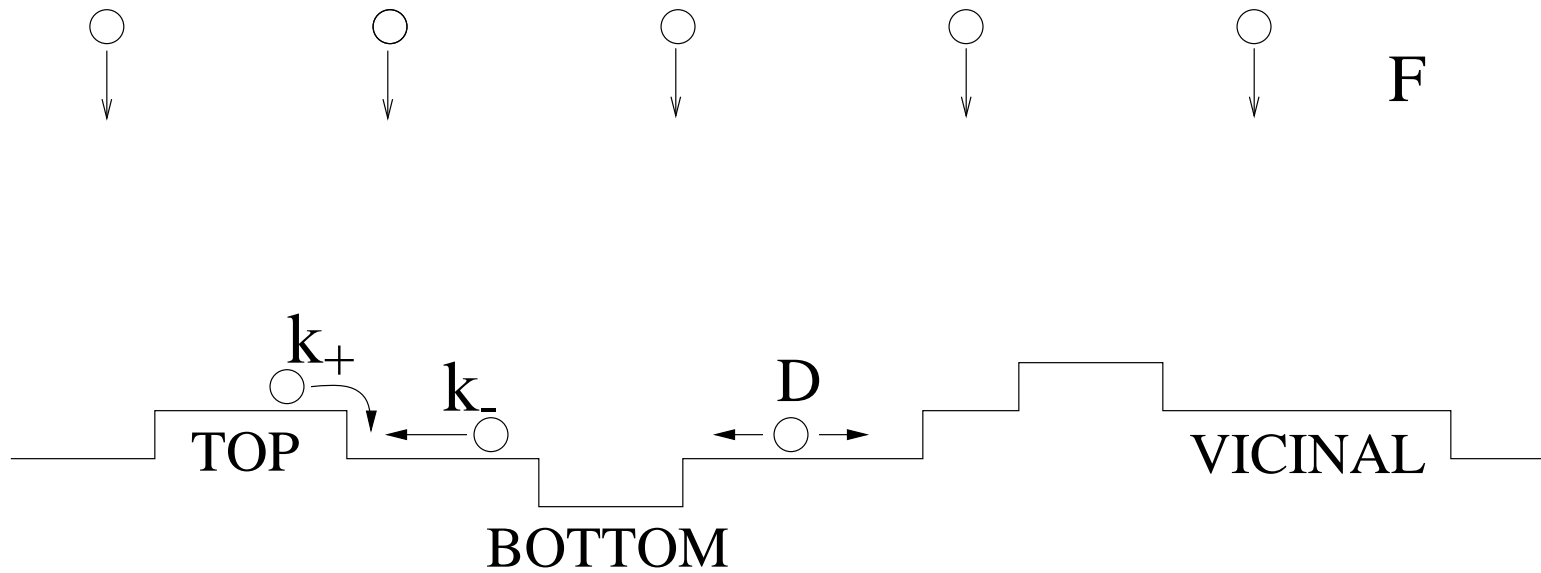
<http://arxiv.org/ps/cond-mat/9906289v1>

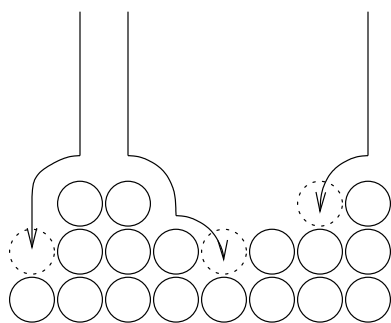
This figure "fig9a.gif" is available in "gif" format from:

<http://arxiv.org/ps/cond-mat/9906289v1>

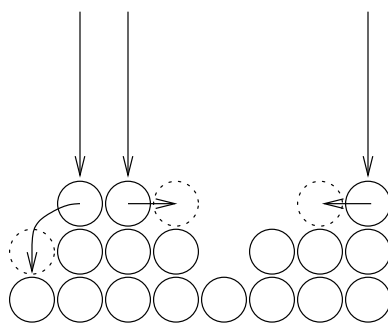
This figure "fig9b.gif" is available in "gif" format from:

<http://arxiv.org/ps/cond-mat/9906289v1>

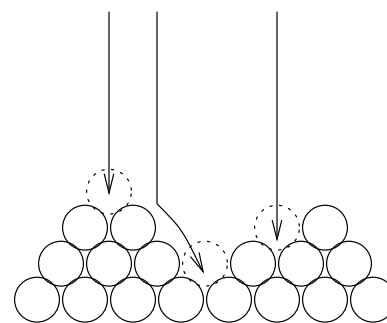




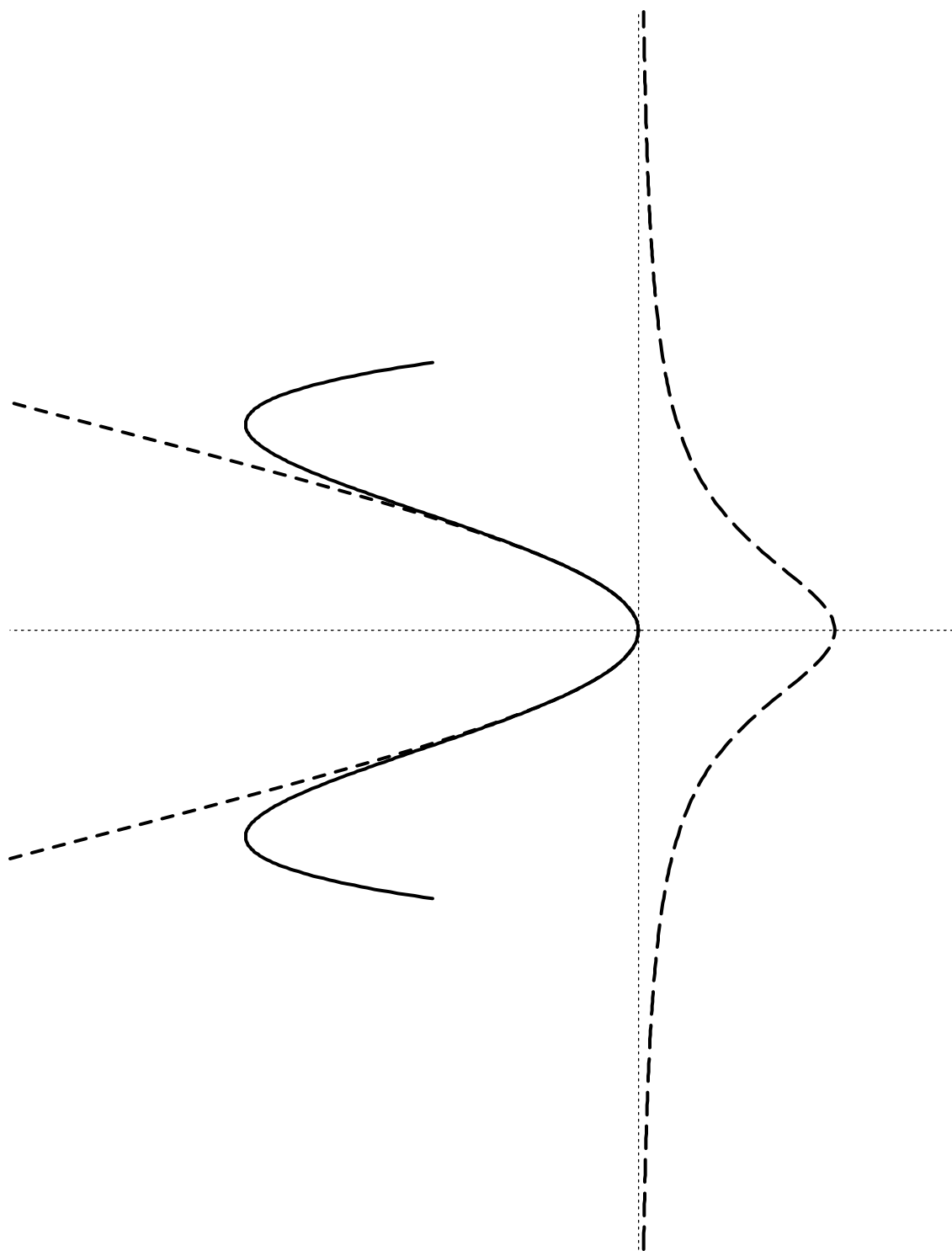
a



b



c



This figure "fig13a.gif" is available in "gif" format from:

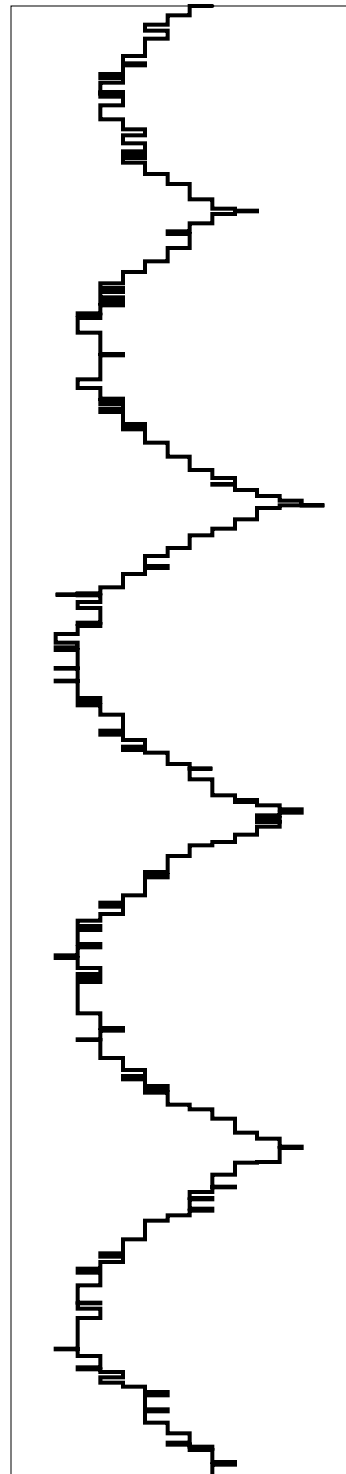
<http://arxiv.org/ps/cond-mat/9906289v1>

This figure "fig13b.gif" is available in "gif" format from:

<http://arxiv.org/ps/cond-mat/9906289v1>

This figure "fig13c.gif" is available in "gif" format from:

<http://arxiv.org/ps/cond-mat/9906289v1>



This figure "fig15.gif" is available in "gif" format from:

<http://arxiv.org/ps/cond-mat/9906289v1>

This figure "fig16.gif" is available in "gif" format from:

<http://arxiv.org/ps/cond-mat/9906289v1>

This figure "fig17.gif" is available in "gif" format from:

<http://arxiv.org/ps/cond-mat/9906289v1>

This figure "fig18.gif" is available in "gif" format from:

<http://arxiv.org/ps/cond-mat/9906289v1>

This figure "fig19.gif" is available in "gif" format from:

<http://arxiv.org/ps/cond-mat/9906289v1>

This figure "fig20.gif" is available in "gif" format from:

<http://arxiv.org/ps/cond-mat/9906289v1>

This figure "fig21.gif" is available in "gif" format from:

<http://arxiv.org/ps/cond-mat/9906289v1>

This figure "fig22.gif" is available in "gif" format from:

<http://arxiv.org/ps/cond-mat/9906289v1>

This figure "fig23.gif" is available in "gif" format from:

<http://arxiv.org/ps/cond-mat/9906289v1>

This figure "fig24.gif" is available in "gif" format from:

<http://arxiv.org/ps/cond-mat/9906289v1>

This figure "fig25.gif" is available in "gif" format from:

<http://arxiv.org/ps/cond-mat/9906289v1>

This figure "fig26.gif" is available in "gif" format from:

<http://arxiv.org/ps/cond-mat/9906289v1>

This figure "fig27.gif" is available in "gif" format from:

<http://arxiv.org/ps/cond-mat/9906289v1>

This figure "fig28.gif" is available in "gif" format from:

<http://arxiv.org/ps/cond-mat/9906289v1>

This figure "fig29.gif" is available in "gif" format from:

<http://arxiv.org/ps/cond-mat/9906289v1>

This figure "fig30.gif" is available in "gif" format from:

<http://arxiv.org/ps/cond-mat/9906289v1>

This figure "fig31.gif" is available in "gif" format from:

<http://arxiv.org/ps/cond-mat/9906289v1>

This figure "fig32.gif" is available in "gif" format from:

<http://arxiv.org/ps/cond-mat/9906289v1>

This figure "fig33a.gif" is available in "gif" format from:

<http://arxiv.org/ps/cond-mat/9906289v1>

This figure "fig33b.gif" is available in "gif" format from:

<http://arxiv.org/ps/cond-mat/9906289v1>

This figure "fig34.gif" is available in "gif" format from:

<http://arxiv.org/ps/cond-mat/9906289v1>

This figure "fig35.gif" is available in "gif" format from:

<http://arxiv.org/ps/cond-mat/9906289v1>

This figure "fig36.gif" is available in "gif" format from:

<http://arxiv.org/ps/cond-mat/9906289v1>

This figure "fig37.gif" is available in "gif" format from:

<http://arxiv.org/ps/cond-mat/9906289v1>

This figure "fig38.gif" is available in "gif" format from:

<http://arxiv.org/ps/cond-mat/9906289v1>

This figure "fig39.gif" is available in "gif" format from:

<http://arxiv.org/ps/cond-mat/9906289v1>

This figure "fig40.gif" is available in "gif" format from:

<http://arxiv.org/ps/cond-mat/9906289v1>

This figure "fig41.gif" is available in "gif" format from:

<http://arxiv.org/ps/cond-mat/9906289v1>

This figure "fig42.gif" is available in "gif" format from:

<http://arxiv.org/ps/cond-mat/9906289v1>

This figure "fig43.gif" is available in "gif" format from:

<http://arxiv.org/ps/cond-mat/9906289v1>

This figure "fig44.gif" is available in "gif" format from:

<http://arxiv.org/ps/cond-mat/9906289v1>

This figure "fig45.gif" is available in "gif" format from:

<http://arxiv.org/ps/cond-mat/9906289v1>